

Dissertation zur Erlangung des Doktorgrades  
der Fakultät Chemie und Pharmazie  
der Ludwig-Maximilians-Universität München

# High Pressure and Microwave Based Synthesis of Transition Metal Pnictides

Roman Rupert Pobel

aus

Dachau

2016









Erklärung:

Diese Dissertation wurde im Sinne von § 7 der Promotionsordnung vom 28. November 2011 von Herrn Prof. Dr. Dirk Johrendt betreut.

Eidesstattlich Versicherung

Diese Dissertation wurde eigenständig und ohne unerlaubte Hilfe erarbeitet.

München, 18. April 2016

.....  
Roman Pobel

Dissertation eingereicht am: 10.03.2016

1. Gutachter: Prof. Dr. Dirk Johrendt

2. Gutachter Prof. Dr. Hubert Huppertz

Mündliche Prüfung am: 11.04.2016



## DANKSAGUNG

Ich möchte mich zuerst bei Prof. Dr. Dirk Johrendt für die Aufnahme in seinen Arbeitskreis und die Freiheiten bei der Wahl meiner Forschungsschwerpunkte und -orte mit denen ich diese Dissertation anfertigen konnte bedanken.

Mein Dank gilt weiterhin Herrn Prof. Dr. Wolfgang Schnick für das *know how* und die Erlaubnis seine 1000 t Pressen für meine Forschung zu nutzen.

Prof. Dr. Hubert Huppertz danke ich für die Bereitschaft das Zweitgutachten zu Übernehmen und für die Prüfung aus Innsbruck anzureisen.

Zusätzlich danke ich auch dem Rest meines Prüfungskomitees bestehend aus Prof. Dr. Constantin Karaghiosoff, Prof. Dr. Achim Hartschuh, Prof. Dr. Hans-Christian Böttcher und Herrn Prof. Dr. Wolfgang Schnick für die Bereitschaft mein Rigorosum durchzuführen.

Vielen Dank auch an alle aktuellen und ehemaligen Kollegen im AK Johrendt: Daniel Bichler, Lars Bulthaupt, Rainer Frankovsky, Gina Friederichs, Arthur Haffner, Franziska Hummel, Michelle Klein, Lola Lilensten, Katarina Marković, Marianne Martin, Fabian Nitsche, Ursula Pachmayr, Simon Peschke, Tobias Rackl, Constantin Frhr. Schirndinger von Schirnding, Anne Schulz, Juliane Stahl, Christine Stürzer, Tobias Stürzer, Marcus Tegel, Erwin Wiesenmayer, Veronika Zinth und *last but not least* der AK Muddi Catrin Löhnert die es doch immer wieder schafft den ganzen Haufen irgendwie unter Kontrolle zu behalten.

Im Besonderen geht mein Dank an die wechselnde Besetzung des Labors D2.061 für eine großartige Arbeitsatmosphäre zu praktisch jeder Zeit.

Ein spezieller Dank geht an Rainer der mich durch das Praktikum bei ihm in den AK geführt und neben einem Gefühl für abwegige Synthesemethoden, schon frühzeitig essentielle aber lautstarke Techniken zur Frustrbewältigung gelehrt hat.

Vielen Dank auch an Franziska, die mir als meine Büro-Mitbewohnerin durch jedwede Ausbrüche an akutem Wahnsinn geholfen und sämtliche noch so dummen Fragen mit bewundernswerter Geduld beantwortet hat.

An Simi meinen VSM-/SQUID-Buddy vielen Dank für die geile Zeit im/am/ums Labor, sei es Grillen, nationale & internationale Konferenzen oder wenn mal (in den Augen anderer) „merkwürdige“ Essmuster anstanden. Herz!

Vielen Dank auch an die Uschi für das bisschen Vernunft, das sie im Raum D2.061 gegen erbitterten Widerstand hochhalten konnte, auch wenn sie das mit dem Feuerlöscher vielleicht doch nochmal üben sollte. Zur Sicherheit.

Danke an Alexey Marchuk, den König der Affen, für die mentale Unterstützung bei Spätschichten und allem was sonst zur Endphase einer Promotion dazu gehört. Am Ende ist es doch noch „nur“ ein Unentschieden geworden.

Natürlich danke ich auch meinen Praktikanten Mirella Brugger, Christian Maak, Katharina Strobl, Lars Bulthaupt, Philipp Angloher und Sebastian Wendl ohne die diese Arbeit in dieser Form mit Sicherheit nicht zu Stande gekommen wäre.

Vielen Dank auch an Prof. Dr. Ram Seshadri und seine Gruppe am MRL der UC Santa Barbara Kalifornien, für die Gelegenheit Forschung in der wohl angenehmsten Umgebung betreiben zu dürfen, die man sich vorstellen kann. Speziell bei Dr. Moureen Kemei, Dr. Kim See und Prof. Dr. Jakoah Brgoch möchte ich mich für die Betreuung auch jenseits des Campus bedanken.

Bei Thomas Miller und Wolfgang Wunschheim bedanke ich mich für die zu allen Zeiten offenen Ohren bei verschiedensten Problemchen und die stete Bereitschaft bei der Behebung derselben zu helfen.

Ganz besonders bedanken möchte ich mich auch bei Herrn Dipl.-Ing. Johannes Köppern. Natürlich für alle konstruktiven, aber vor allem für die übrigen Diskussionen, die meistens viel lustiger sind. Vielen Dank auch an Peter Lübke der immer für den gemeinsamen virtuellen Stressabbau zur Stelle ist und auf den ich mich auch im echten Leben immer verlassen kann.

Meiner Familie danke ich für die immerwährende Unterstützung und die daraus erwachsende Möglichkeit das zu tun was mich glücklich macht. Meinem Bruder Christoph danke ich für das Korrekturlesen dieser Arbeit und die mal mehr, mal weniger konstruktiven Gestaltungsvorschläge.

Zu guter Letzt ein besonderes Danke an die wunderbare Agnieszka. Du machst einfach alles noch besser.

*„Build a man a fire and he'll be warm for a day.  
Set a man on fire and he'll be warm for the rest of his life.”*  
Terry Pratchett



## TABLE OF CONTENTS

1 Introduction.....	1
1.1 Synthetic Methods in Materials Chemistry.....	1
1.2 Transition Metals, Pnictides and Superconductivity.....	2
1.3 The Goal of this Thesis.....	3
1.4 References.....	4
2 High Pressure Synthesis Of Iron Pnictides.....	5
2.1 Materials & Methods.....	8
2.1.1 Sample Preparation.....	8
2.1.2 Sample Characterization.....	8
2.1.3 References.....	10
2.2 Absence of Superconductivity in Metastable $\text{Ca}_{1-x}\text{Pr}_x\text{Fe}_2\text{As}_2$ ( $0 \leq x \leq 1$ ) Synthesized under Hydrostatic High Pressure Conditions.....	11
2.2.1 Introduction.....	11
2.2.2 Sample Preparation.....	12
2.2.3 The Solid Solution $\text{Ca}_{1-x}\text{Pr}_x\text{Fe}_2\text{As}_2$ and the New $\text{ThCr}_2\text{Si}_2$ -type Compound $\text{PrFe}_2\text{As}_2$ ....	12
2.2.4 The Metastability of <i>hp</i> - $\text{Ca}_{1-x}\text{Pr}_x\text{Fe}_2\text{As}_2$ .....	15
2.2.5 Absence of Superconductivity in <i>hp</i> - $(\text{Ca},\text{Pr})\text{Fe}_2\text{As}_2$ .....	18
2.2.6 Conclusions.....	19
2.2.7 References.....	20
2.3 Properties and High Pressure Synthesis of $\text{Sr}_{0.3}\text{La}_{0.7}\text{Fe}_2\text{As}_2$ and $\text{LaFe}_2\text{As}_2$ .....	23
2.3.1 Introduction.....	23
2.3.2 Sample Preparation.....	24
2.3.3 High Pressure Synthesis of $\text{Sr}_{1-x}\text{La}_x\text{Fe}_2\text{As}_2$ ( $x = 0.3, 1$ ).....	24
2.3.4 Structural and Physical Properties of $\text{LaFe}_2\text{As}_2$ .....	25
2.3.5 Conclusions.....	28
2.3.6 References.....	28
2.4 High Pressure Synthesis, Structural and Physical Properties of Rare Earth doped $\alpha$ - $\text{CaFe}_5\text{As}_3$ .....	31
2.4.1 Introduction.....	31

2.4.2 Sample Preparation .....	32
2.4.3 Structural Properties of $\text{Ca}_{1-x}\text{Pr}_x\text{Fe}_5\text{As}_3$ ( $0 \leq x \leq 1$ ) .....	32
2.4.4 Structural Changes in $\text{Ca}_{1-x}\text{Pr}_x\text{Fe}_5\text{As}_3$ ( $0 \leq x \leq 1$ ) at Low Temperatures.....	34
2.4.5 Physical Properties of $\text{Ca}_{1-x}\text{Pr}_x\text{Fe}_5\text{As}_3$ ( $0 \leq x \leq 1$ ) at Low Temperatures.....	36
2.4.6 Conclusions .....	37
2.4.7 References .....	39
2.5 Details of the High Pressure Synthesis of Pr-doped $\text{CaFe}_2\text{As}_2$ and other Iron Pnictides.....	40
2.5.1 Introduction .....	40
2.5.2 Sample Preparation .....	40
2.5.3 Influence of Pressure During Synthesis.....	40
2.5.4 Influence of Crucible Treatment .....	41
2.5.5 Conductivity Measurements on Unrefined Samples.....	41
2.5.6 Crystal Growth from FeAs Flux under High Pressure .....	42
2.5.7 Conclusions .....	43
2.5.8 Reference.....	43
3 Microwave based synthesis of transition metal pnictides and chalcogenides.....	45
3.1 Introduction.....	45
3.1.1 The History of Microwaves .....	45
3.1.2 Physical Principles of Microwave Radiation.....	45
3.1.3 Practical aspects of microwave heating.....	47
3.1.4 Chemical application of microwave heating.....	47
3.1.5 Microwaves and materials chemistry.....	47
3.1.6 Microwave based synthesis of pnictides and chalcogenides.....	48
3.1.7 References .....	49
3.2 Materials and Methods.....	52
3.2.1 Sample preparation.....	52
3.2.2 Sample characterization.....	52
3.2.3 Microwave based synthesis.....	54
3.2.4 References .....	56
3.3 Superfast Microwave Based Synthesis of Binary Transition Metal Compounds .....	59
3.3.1 Introduction .....	59

---



---

3.3.2 Synthesis of binary iron arsenides FeAs and Fe <sub>2</sub> As.....	59
3.3.3 Synthesis of FeSe.....	60
3.3.4 Synthesis of CaCu.....	62
3.3.5 Summary.....	64
3.3.6 References.....	65
3.4 Development and Application of a Fast Microwave Based Dopant Screening Procedure for Ca <sub>2</sub> Cu <sub>6</sub> P <sub>5</sub> and the Physical and Structural Properties of Ca <sub>2</sub> Cu <sub>6</sub> P <sub>5-x</sub> As <sub>x</sub> (0 ≤ x < 2).....	67
3.4.1 Introduction.....	67
3.4.2 Synthesis optimization.....	68
3.4.3 Screening for potential transition metal dopants.....	71
3.4.4 Screening for potential pnictogen/chalcogen dopants.....	72
3.4.5 The physical and structural properties of Ca <sub>2</sub> Cu <sub>6</sub> P <sub>5-x</sub> As <sub>x</sub> (0 ≤ x < 2).....	72
3.4.6 Summary.....	76
3.4.7 References.....	77
4 Summary.....	79
4.1 High Pressure Synthesis of Iron Pnictides.....	79
4.2 Microwave Based Synthesis of Transition Metal Pnictides.....	79
4.3 Final remarks.....	81
Scientific Contributions.....	82
Full List of Publications.....	82
Conference Contributions.....	82
Talks.....	82
Posters.....	82
Curriculum Vitae.....	83
Personal Details.....	83
Education.....	83

---



## 1 INTRODUCTION

According to the chemistry dictionary of *Pierre-Joseph Macquer*, “all the chemistry operations could be reduced to decomposition and combination; hence, the fire appears as a universal agent in chemistry as in nature.”<sup>[1]</sup> This basic principle is still true today, even though technological progress has equipped chemists with very elaborate kinds of “fire” over the years. Today the range of applied heat sources stretches from the classical Bunsen burner, which is mostly used in undergraduate chemistry lab courses, to spark plasma sintering devices which are used to achieve nearly ideal densities in ceramic materials.<sup>[2]</sup> Modern synthetic methods have opened a wide array of accessible compounds that could not be obtained otherwise and tweaking synthetic conditions remains the main challenge for chemists of all fields.

### 1.1 Synthetic Methods in Materials Chemistry

Synthesis of new materials has always been a driving force in the history of mankind. The significance of a particular material for a specific time period is even reflected in its name. From the Stone Age, to the Iron Age, to the age of plastics, the method of preparation always played a major role in the applicability of a material. But only when a certain material can be obtained reproducibly and in large quantities is there a chance for it to really impact a society. Understanding the properties of a material on a deep level thus is indispensable. Materials chemists are needed to achieve just that.

During the 20<sup>th</sup> century there were several major discoveries in materials sciences that led to significant technological progress and almost all of them were achieved by using previously non-existent synthesis techniques. In the 1910s Bakelite, one of the first plastics, was made commercially available when *Baekeland* invented the “Bakelizer” to apply pressure during the final heating step of the synthesis.<sup>[3]</sup> During the 1950s a reliable way for the production of artificial diamonds was found via high pressure/high temperature synthesis<sup>[4]</sup> which led to the widespread availability of diamond cutting tools. This in turn enabled previously unattainable precision in the manufacturing of parts for engineering applications. Later, the discovery of the ceramic high temperature superconductors during the 1980s by *Bednorz* and *Müller*<sup>[5]</sup> increasingly blurred the line between physics and solid state chemistry. Ever new and different approaches were taken to find new compounds with higher and higher critical temperatures in hopes to revolutionize the way electrical energy is transported.

Superconductivity was thought to be a well understood phenomenon at the time. It is characterized by zero resistivity and a strong diamagnetism, both of which appear rather suddenly when the temperature falls below the critical temperature  $T_c$ . It was discovered by *Onnes* in 1911<sup>[6]</sup> and a theoretical description was introduced in 1957 by *Bardeen*, *Cooper* and *Shrieffer*.<sup>[7]</sup> The theory explains the phenomenon through the pairing of electrons mediated by lattice vibrations (phonons) into Cooper pairs. These Cooper pairs behave as Bosons and can thus travel the material without experiencing electrical resistivity. This model however predicts a maximum of the critical temperature at ~40 K above which the phonons become too strong for the electrons to

---

form Cooper pairs. Realistically these conventional metallic superconductors exhibit critical temperatures below 30 K. Because of this theoretical limit, superconductivity in the ceramic cuprates with critical temperatures of more than 35 K with subsequent reports of  $T_c$  reaching more than 100 K sparked such enthusiasm. It seemed like lossless energy transport and the cost-efficient generation of large magnetic fields was only a few steps away. As it turns out these materials suffer from many problems making their commercial application very costly and consequently interest in high temperature superconductivity died down quite a bit.

## 1.2 Transition Metals, Pnictides and Superconductivity

The discovery of superconductivity in iron pnictide compounds in 2008 has revived the interest of the materials science community in this complex physical behavior.<sup>[8]</sup> The observation of superconductivity and magnetism in materials and the interplay and sometimes even coexistence of these phenomena remains an extensively researched topic for physicists and chemists alike.

A common feature of all iron based superconductors is a layered structure that consists of  $\text{FeX}_{4/4}$  ( $X = \text{As}, \text{Se}$ ) edge sharing tetrahedral layers. These alternate with layers that can show many different structural features. These can range from alkali and alkaline earth metal atoms in  $\text{NaFeAs}$ <sup>[9]</sup> or  $\text{BaFe}_2\text{As}_2$ <sup>[10]</sup> to very complex motifs as observed in  $\text{Sr}_2\text{VO}_3\text{FeAs}$ <sup>[11]</sup> or  $(\text{CaFe}_{1-x}\text{Pt}_x\text{As})_{10}\text{Pt}_{4-y}\text{As}_8$ .<sup>[12]</sup>

An essential way of inducing superconductivity or influencing the critical temperatures of these compounds is substituting some of the atoms with others. This process is called doping and is considered isovalent if the element has the same oxidation state as the replaced one, otherwise it is called aliovalent. Doping means that additional negative charges (electron doping) or positive charges (hole doping) are introduced into the host structure. It usually cannot be reliably predicted which kind of doping is beneficial for superconductivity. In some cases both lead to superconductivity as observed in hole doped  $\text{Ba}_{1-x}\text{K}_x\text{Fe}_2\text{As}_2$  with a  $T_c$  of up to 38 K<sup>[13]</sup> and electron doped  $\text{BaFe}_{2-x}\text{Co}_x\text{As}_2$  with a  $T_c$  of up to 22 K<sup>[14]</sup> or  $\text{BaFe}_2\text{As}_{2-x}\text{P}_x$  with a  $T_c$  of up to 30 K.<sup>[15]</sup> The  $\text{BaFe}_2\text{As}_2$ -system also illustrates that doping of any crystallographic site may be able to induce superconductivity in a suitable host structure.

While the investigation of doped variants of an established system poses its own challenges, the search for new host systems still remains the main task for materials chemists. Several new members have been added to the class of known transition metal pnictides since 2008. While many of them are not superconductors, they still add to the fundamental understanding of this compound class and may thus pave the way for other important discoveries. Optimizing the energy consumption during preparation of those compounds that are well understood on the other hand may be the key to making them commercially available.

The use of synthetic approaches that go beyond traditional solid state synthesis at high temperatures from the elements has already proven to be a valuable tool in this regard.<sup>[16]</sup> Going one step further, this thesis will explore other synthetic approaches to advance the toolset of

---

materials chemists in the ongoing exploration of the physical properties of transition metal compounds as well as superconductivity.

### 1.3 The Goal of this Thesis

The goal of this thesis was to explore the possibilities of synthetic methods that are not very common in current transition metal pnictide research. By straying from the path of common solid state synthesis a wide range of unknown compounds may be accessible and explorative research of these systems may be significantly accelerated.

The substitution of the Ca-site in  $\text{CaFe}_2\text{As}_2$  with rare earth elements such as Pr has been reported to induce superconductivity.<sup>[17]</sup> However, some inconsistencies in the data suggested a non-intrinsic origin of the observed diamagnetic signal. Furthermore a solubility limit of 13% was found when prepared in an electrical furnace thus leaving a huge part of the physical phase diagram inaccessible. A high pressure/high temperature synthesis was developed to allow access to the whole doping range and an in-depth characterization of this compound was carried out.

During the experiments concerning the high pressure synthesis of  $\text{Ca}_{1-x}\text{Pr}_x\text{Fe}_2\text{As}_2$  the new ternary iron arsenide  $\text{CaFe}_5\text{As}_3$  was identified and classified as a member of the  $\text{Ca}_{n(n+1)/2}(\text{Fe}_{1-x}\text{M}_x)_{(2+3n)}\text{M}'_{n(n-1)/2}\text{As}_{(n+1)(n+2)/2}$  ( $n = 1-3$ ;  $M = \text{Nb, Pd, Pt}$ ;  $M' = \square, \text{Pd, Pt}$ ) family. The complete solid solution  $\text{Ca}_{1-x}\text{Pr}_x\text{Fe}_5\text{As}_3$  ( $0 \leq x \leq 1$ ) was prepared and physically characterized. Furthermore, several useful techniques were developed to aid in future high pressure based investigations of transition metal pnictides.

The second part of this thesis concerns a completely different, but equally promising synthetic approach. Microwave based synthesis is a well-established technique in many solution based fields, such as organic, medicinal or nano chemistry.<sup>[18]</sup> For solid state and materials research several parameters and particularities have to be considered. But when successful, it allows for the reduction of reaction time by several orders of magnitude. It has very rarely been applied in the preparation of pnictides and only once in the context of pnictide superconductor research.<sup>[19]</sup> The possibilities of this method were explored and employed in the preparation of several binary starting materials some of which are superconductors themselves.

To really take advantage of the quickness this method offers, a dopant screening strategy was developed and applied to  $\text{Ca}_2\text{Cu}_6\text{P}_5$ , a very poorly investigated system that shares many features with 122-type pnictide superconductors.<sup>[20]</sup> Arsenic was identified as a suitable dopant, the solid solution  $\text{Ca}_2\text{Cu}_6\text{P}_{5-x}\text{As}_x$  ( $0 \leq x < 2$ ) was prepared and its structural behavior as well as its physical properties were characterized.

## 1.4 References

- [1] P.-J. Macquer, *Dictionnaire de Chymie contenant la théorie et la pratique de cette science, Vol. II*, Lacombe, Paris, **1766**.
  - [2] K. Sairam, J. K. Sonber, T. S. R. C. Murthy, C. Subramanian, R. K. Fotedar, P. Nanekar, R. C. Hubli, *Int. J. Refract. Met. Hard Mater.* **2014**, *42*, 185-192.
  - [3] L. H. Baekeland, *J. Ind. Eng. Chem. (Washington, D. C.)* **1909**, *1*, 149-161.
  - [4] F. P. Bundy, H. T. Hall, H. M. Strong, R. H. Wentorf, Jr., *Nature (London, U. K.)* **1955**, *176*, 51-55.
  - [5] J. G. Bednorz, K. A. Müller, *Z. Phys. B: Condens. Matter* **1986**, *64*, 189.
  - [6] H. K. Onnes, *Commun. Phys. Lab. Univ. Leiden* **1911**, *12*.
  - [7] J. Bardeen, L. N. Cooper, J. R. Schrieffer, *Phys. Rev. B: Condens. Matter Mater. Phys.* **1957**, *108*, 1175.
  - [8] Y. Kamihara, T. Watanabe, M. Hirano, H. Hosono, *J. Am. Chem. Soc.* **2008**, *130*, 3296.
  - [9] C. W. Chu, F. Chen, M. Gooch, A. M. Guloy, B. Lorenz, B. Lv, K. Sasmal, Z. J. Tang, J. H. Tapp, Y. Y. Xue, *Phys. C (Amsterdam, Neth.)* **2009**, *469*, 326-331.
  - [10] M. Rotter, M. Tegel, I. Schellenberg, W. Hermes, R. Pöttgen, D. Johrendt, *Phys. Rev. B: Condens. Matter Mater. Phys.* **2008**, *78*, 020503.
  - [11] X. Zhu, F. Han, G. Mu, P. Cheng, B. Shen, B. Zeng, H.-H. Wen, *Phys. Rev. B: Condens. Matter Mater. Phys.* **2009**, *79*, 220512.
  - [12] C. Löhnert, T. Stürzer, M. Tegel, R. Frankovsky, G. Friederichs, D. Johrendt, *Angew. Chem., Int. Ed.* **2011**, *50*, 9195-9199.
  - [13] M. Rotter, M. Tegel, D. Johrendt, *Phys. Rev. Lett.* **2008**, *101*, 107006.
  - [14] A. S. Sefat, R. Y. Jin, M. A. McGuire, B. C. Sales, D. J. Singh, D. Mandrus, *Phys. Rev. Lett.* **2008**, *101*, 117004.
  - [15] J. Shuai, X. Hui, X. Guofang, W. Cao, R. Zhi, F. Chunmu, D. Jianhui, X. Zhu'an, C. Guanghan, *Journal of Physics: Condensed Matter* **2009**, *21*, 382203.
  - [16] R. Frankovsky, A. Marchuk, R. Pobel, D. Johrendt, *Solid State Commun.* **2012**, *152*, 632-634.
  - [17] S. R. Saha, N. P. Butch, T. Drye, J. Magill, S. Ziemak, K. Kirshenbaum, P. Y. Zavalij, J. W. Lynn, J. Paglione, *Physical Review B* **2012**, *85*, 024525.
  - [18] C. O. Kappe, A. Stadler, D. Dallinger, *Microwaves in Organic and Medicinal Chemistry, Vol. 52*, 2nd ed., Wiley-VCH, Weinheim, **2012**.
  - [19] S. W. Muir, O. D. Rachdi, M. A. Subramanian, *Mater. Res. Bull.* **2012**, *47*, 798-800.
  - [20] I. Pilchowski, A. Mewis, *Z. Anorg. Allg. Chem.* **1990**, *581*, 173-182.
-

## 2 HIGH PRESSURE SYNTHESIS OF IRON PNICTIDES

For many years the application of high pressure during synthesis has steadily led to great accomplishments in materials research. Initially developed for geological investigations of inaccessible region in the earth crust, it has since become a valuable tool for the preparation and exploration of new materials. The discovery of a reproducible process to obtain synthetic diamonds in 1955 and the subsequent commercial availability of high pressure systems sparked the interest of chemists for this type of synthesis.<sup>[1]</sup> Since then many different materials have been subjected to high pressure not only during synthesis but also to study its influence on the physical properties. Naturally superconductors are among them.

### HIGH PRESSURE AND ITS APPLICATIONS IN SUPERCONDUCTOR RESEARCH

High pressure and superconductor research have had an intimate relationship for many years as the effect of external pressure, mainly on the critical temperature of a substance was extensively studied from very early on. These measurements especially gained fame when the highest critical temperature of a cuprate-superconductor to date was observed in  $\text{HgBa}_2\text{Ca}_2\text{Cu}_3\text{O}_{8+\delta}$  at 15 GPa ( $T_c = 150$  K).<sup>[2]</sup> Beyond that, physical measurements under high pressure conditions also contributed a lot to the general understanding of superconductivity. Most recently one of the highest critical temperatures ever recorded was observed in a high pressure phase of the  $\text{H}_2\text{S}$  system.<sup>[3]</sup> At pressures of approximately 90 GPa the system had transitioned to a metallic state and exhibited superconductivity with a  $T_c$  of 203 K. While this finding may not have a direct technical application, it will most likely lead to a deeper understanding of the phenomenon from a physical point of view. This makes high pressure studies an indispensable tool in the investigation of new materials.

Naturally almost all classes of FeAs-based superconductors have been extensively investigated by means of high pressure studies as well, provided they can be grown as single crystals of sufficient size. For example, the magnetic phase diagram of  $\beta$ -FeSe was explored through high pressure measurements and found that the critical temperature can be raised from 8 K at ambient pressure up to 36 K at 8.9 GPa.<sup>[4]</sup> Further high pressure studies investigated, among others, 111-type compounds like  $\text{LiFeAs}$ <sup>[5]</sup> and  $\text{NaFeAs}$ <sup>[6]</sup> as well as 122-type compounds such as  $\text{CaFe}_2\text{As}_2$ .<sup>[7-9]</sup> The latter sparked quite a controversy as it turned out that its behavior depends on whether the pressure distribution is hydrostatic or uniaxial.

### HIGH PRESSURE SYNTHESIS AND IRON ARSENIDE SUPERCONDUCTORS

Even though the application of pressure plays such an important role in their physical characterization, the application of high pressure synthesis has only been reported for relatively few different classes of iron pnictide compounds so far. Since 2008 there have been reports on the high pressure synthesis of  $RE\text{FeAsO}$  ( $RE = \text{La, Nd, Pr, Sm, Gd, Tb, Dy}$ ) with various dopants and/or oxygen deficiency.<sup>[10-15]</sup> Even doping of the O-site with H is possible under high pressure conditions.<sup>[16]</sup> The growth of single crystals up to 300-650  $\mu\text{m}$  in size was also successful in many cases and greatly aided the understanding of this type of superconductor.<sup>[17-21]</sup>

The synthesis of  $\text{Ca}_2\text{AlO}_{3-y}\text{FePn}$  ( $\text{Pn} = \text{As}, \text{P}$ ) at 4.5 GPa in a cubic anvil cell ( $\text{Sr}_2\text{GaO}_3\text{CuS}$ -type,<sup>[22]</sup> space group  $P4/nmm$ ) has first been reported in 2010,<sup>[23]</sup> closely followed by the discovery of  $\text{Ca}_3\text{Al}_2\text{O}_{5-y}\text{Fe}_2\text{Pn}_2$  ( $\text{Pn} = \text{As}, \text{P}$ ) by the same group ( $\text{Sr}_3\text{Fe}_2\text{O}_5\text{Cu}_2\text{S}_2$ -type,<sup>[24]</sup> space group  $I4/mmm$ ).<sup>[25]</sup> All four compounds become superconducting between 15-30 K but the small shielding fractions found in the magnetic measurements suggest that this may not be an intrinsic property of these compounds. The discovery of non-superconducting  $\text{LaTM}_2\text{AsN}$  ( $\text{TM} = \text{Fe}, \text{Co}, \text{Ni}$ ) crystallizing in a so far unknown structure type (space group  $\text{Cmcm}$ ), was reported by Jeong *et al* in 2015.<sup>[26]</sup> These new arsenides are initial antiferromagnets but exhibit parasitic ferromagnetism at temperatures ranging from 260 K to 560 K. Even though these new compounds are not numerous they highlight the diversity of accessible substances that cannot be obtained via conventional solid state synthesis. Besides superconductor research, high pressure/high temperature thus also has the potential to broaden the knowledge of the transition metal pnictides from a structural point of view.

Taking all this into account, it is unexpected that the preparation of a 122-type superconductor has only been reported very rarely. One example is an isotope effect study of  $(\text{Ba},\text{K})\text{Fe}_2\text{As}_2$  which was reported in 2010 that highlights some advantages of this technique.<sup>[27]</sup> Another publication from the same year by Muraba *et al.* reported the high pressure synthesis of La-doped  $\text{SrFe}_2\text{As}_2$  in a Belt-type high pressure setup. Under pressures of 2-4 GPa samples exhibiting superconductivity at 22 K were obtained. This served as the primary inspiration for the high pressure experiments presented in this thesis. Chapter 0 will discuss the differences and similarities to their results.

## REFERENCES

- [1] F. P. Bundy, H. T. Hall, H. M. Strong, R. H. Wentorf, Jr., *Nature (London, U. K.)* **1955**, 176, 51-55.
- [2] C. W. Chu, L. Gao, F. Chen, Z. J. Huang, R. L. Meng, Y. Y. Xue, *Nature* **1993**, 365, 323-325.
- [3] A. P. Drozdov, M. I. Eremets, I. A. Troyan, V. Ksenofontov, S. I. Shylin, *Nature* **2015**, 525, 73-76.
- [4] S. Medvedev, T. M. McQueen, I. A. Troyan, T. Palasyuk, M. I. Eremets, R. J. Cava, S. Naghavi, F. Casper, V. Ksenofontov, G. Wortmann, C. Felser, *Nat. Mater.* **2009**, 8, 630-633.
- [5] M. Gooch, B. Lv, J. H. Tapp, Z. Tang, B. Lorenz, A. M. Guloy, P. C. W. Chu, *EPL* **2009**, 85, 27005.
- [6] S. J. Zhang, X. C. Wang, Q. Q. Liu, Y. X. Lv, X. H. Yu, Z. J. Lin, Y. S. Zhao, L. Wang, Y. Ding, H. K. Mao, C. Q. Jin, *EPL (Europhysics Letters)* **2009**, 88, 47008.
- [7] A. Kreyssig, M. A. Green, Y. Lee, G. D. Samolyuk, P. Zajdel, J. W. Lynn, S. L. Bud'ko, M. S. Torikachvili, N. Ni, S. Nandi, J. B. Leao, S. J. Poulton, D. N. Argyriou, B. N. Harmon, R. J. McQueeney, P. C. Canfield, A. I. Goldman, *Phys. Rev. B: Condens. Matter Mater. Phys.* **2008**, 78, 184517.
- [8] M. S. Torikachvili, S. L. Bud'ko, N. Ni, P. C. Canfield, *Physical review letters* **2008**, 101.
- [9] W. Yu, A. A. Aczel, T. J. Williams, S. L. Bud'ko, N. Ni, P. C. Canfield, G. M. Luke, *Physical Review B* **2009**, 79.



- 
- [10] Z. A. Ren, J. Yang, W. Lu, W. Yi, G. C. Che, X. L. Dong, L. L. Sun, Z. X. Zhao, *Mater. Res. Innovations* **2008**, *12*, 105-106.
- [11] Z.-A. Ren, J. Yang, W. Lu, W. Yi, X.-L. Shen, Z.-C. Li, G.-C. Che, X.-L. Dong, L.-L. Sun, F. Zhou, *EPL (Europhysics Letters)* **2008**, *82*, 57002.
- [12] Z.-A. Ren, W. Lu, J. Yang, W. Yi, X.-L. Shen, Z.-C. Li, G.-C. Che, X.-L. Dong, L.-L. Sun, F. Zhou, Z.-X. Zhao, *Chin. Phys. Lett.* **2008**, *25*, 2215.
- [13] E. P. Khlybov, O. E. Omelyanovsky, A. Zaleski, A. V. Sadakov, D. R. Gizatulin, L. F. Kulikova, I. E. Kostuleva, V. M. Pudalov, *Jetp Lett.* **2009**, *90*, 387-390.
- [14] J.-W. G. Bos, G. B. S. Penny, J. A. Rodgers, D. A. Sokolov, A. D. Huxley, J. P. Attfield, *Chem. Commun. (Cambridge, U. K.)* **2008**, 3634-3635.
- [15] K. A. Yates, K. Morrison, J. A. Rodgers, G. B. S. Penny, J. W. G. Bos, J. P. Attfield, L. F. Cohen, *New Journal of Physics* **2009**, *11*, 025015.
- [16] H. Hosono, S. Matsuishi, *Curr. Opin. Solid State Mater. Sci.* **2013**, *17*, 49-58.
- [17] J. Karpinski, N. D. Zhigadlo, S. Katrych, Z. Bukowski, P. Moll, S. Weyeneth, H. Keller, R. Puzniak, M. Tortello, D. Daghero, R. Gonnelli, I. Maggio-Aprile, Y. Fasano, O. Fischer, K. Rogacki, B. Batlogg, *Phys. C (Amsterdam, Neth.)* **2009**, *469*, 370-380.
- [18] T. Kondo, A. F. Santander-Syro, O. Copie, C. Liu, M. E. Tillman, E. D. Mun, J. Schmalian, S. L. Bud'ko, M. A. Tanatar, P. C. Canfield, A. Kaminski, *Phys. Rev. Lett.* **2008**, *101*, 147003.
- [19] T. Ito, A. Iyo, H. Eisaki, H. Kito, K. Kihou, R. Kumai, N. Takeshita, Y. Tomioka, H. Matsuhata, K. Miyazawa, C.-H. Lee, P. M. Shirage, M. Ishikado, *Kotai Butsuri* **2008**, *43*, 651-663.
- [20] S. K. Kim, M. E. Tillman, H. Kim, A. Kracher, S. L. Bud'ko, R. Prozorov, P. C. Canfield, *Superconductor Science and Technology* **2010**, *23*, 054008.
- [21] K. Miyazawa, K. Kihou, P. M. Shirage, C.-H. Lee, H. Kito, H. Eisaki, A. Iyo, *J. Phys. Soc. Jpn.* **2009**, *78*, 034712.
- [22] W. Zhu, P. Hor, *Inorganic chemistry* **1997**, *36*, 3576-3577.
- [23] P. M. Shirage, K. Kihou, C.-H. Lee, H. Kito, H. Eisaki, A. Iyo, *Applied Physics Letters* **2010**, *97*, 172506.
- [24] W. J. Zhu, P. H. Hor, *Journal of Solid State Chemistry* **1997**, *134*, 128-131.
- [25] P. M. Shirage, K. Kihou, C.-H. Lee, H. Kito, H. Eisaki, A. Iyo, *Journal of the American Chemical Society* **2011**, *133*, 9630-9633.
- [26] S. Jeong, S. Matsuishi, J. Bang, H. Hosono, *APL Mater.* **2015**, *3*, 041509.
- [27] P. M. Shirage, K. Kihou, K. Miyazawa, C. H. Lee, H. Kito, Y. Yoshida, H. Eisaki, Y. Tanaka, A. Iyo, *Phys. C (Amsterdam, Neth.)* **2010**, *470*, 986-988.
-

## 2.1 Materials & Methods

### 2.1.1 Sample Preparation

The samples were prepared under high pressure/high temperature conditions in a modified Walker-type module in combination with a 1000 t press (Voggenreiter, Mainleus, Germany). The technique used in these experiments was developed by Prof. Dr. Wolfgang Schnick, Prof. Dr. Hubert Huppertz and their coworkers. As pressure medium, Cr<sub>2</sub>O<sub>3</sub> doped (5%) MgO-octahedra (Ceramic Substrates & Components, Isle of Wight, UK) with an edge length of 18 mm or 25 mm were employed. Eight tungsten carbide cubes (Hawedia, Marklkofen, Germany) with truncation edge lengths of 11 mm or 17 mm compressed the octahedron (18/11 and 25/17 assembly, respectively). Handling of all samples as well as the preparation of the octahedra was conducted in a glove box under purified argon atmosphere (Unilab, MBraun, Garching; O<sub>2</sub> < 1 ppm, H<sub>2</sub>O < 1 ppm). Table 2.1-1 gives an overview of the starting materials that were used.

Table 2.1-1: Substances used in the experiments.

Substance	Purity	Molar weight (g/mol)	Appearance	Supplier
As	99.95 %	74.9216	Powder	Sigma-Aldrich
Ca	99.99 %	40.078	Dendritic pieces	Sigma-Aldrich
Fe	99.90 %	55.845	Powder	Chempur
La	99.9 %	138.9055	Ingot	Smart Elements
Pr	99.90 %	140.907	Ingot	Alfa Aesar
Sr	99.95 %	87.62	Pieces	Alfa Aesar

The corresponding mixtures of starting materials were carefully ground in an agate mortar, filled into a cylindrical *h*-BN (hexagonal boron nitride) crucible (Henze BNP GmbH, Kempten, Germany), and sealed with a *h*-BN disc. Details of the setup are described in the literature.<sup>[1-5]</sup>The specific synthesis parameters are detailed for each compound in its respective chapter. Additional details on the synthesis can be found in chapter 2.5.

### 2.1.2 Sample Characterization

#### X-RAY DIFFRACTION

The sample composition was analyzed via powder X-ray diffraction (PXRD) on a STOE Stadi P diffractometer (Mo-K $\alpha_1$  radiation, Ge[111] monochromator) and a Huber G670 Guinier imaging plate diffractometer (Cu-K $\alpha_1$  radiation, Ge[111] monochromator), respectively. Low temperature PXRD was performed using the same setup with Ge[111] monochromated Co-K $\alpha_1$  radiation instead. Temperatures between 300 K and 8 K were achieved using a cryostat (CTI-Cryogenics, Model 22 CP) controlled by a Si-diode sensor (Lakeshore, model 331). Diffractograms over a range of  $6.5^\circ \leq 2\theta \leq 100^\circ$  were recorded at temperatures from 10 K to 300 K.

For high-temperature PXRD, the samples were loaded into silica capillaries (Hilgenberg, Malsfeld, Germany) with a diameter of 0.3 mm and sealed under argon. Data was recorded on the STOE Stadi P diffractometer. Temperature was regulated by a computer-controlled STOE resistance

graphite furnace. The samples were heated up to 773 K or 973 K respectively and then cooled to room temperature. Heating and cooling were each conducted at a rate of 5 K/min. in steps of 25 K. At each step two diffraction patterns in the range of  $2^\circ \leq 2\theta \leq 80^\circ$  were recorded and later added to improve the signal to noise ratio. Data acquisition in all cases was done using the STOE software (WinX<sup>POW</sup>), Rietveld refinements were performed with the TOPAS package.<sup>[6]</sup> Data measured on the Huber G670 devices were per-processed with a custom script.<sup>[7]</sup>

### SCANNING ELECTRON MICROSCOPY (SEM) AND ENERGY DISPERSIVE X-RAY ANALYSIS (EDX)

Verification of the chemical composition as well as analysis of the morphology were performed in a Carl Zeiss EVO-MA 10 SEM with SE (secondary electrons), BSE (back scattered electrons) detectors as well as a Bruker Nano EDX (X-Flash 420-M) detector. Samples were fixed with an adhesive conducting carbon film on an Al sample holder. The elements C and Al thus were excluded from the measurement. The composition of a particular crystallite was determined by averaging 10-20 individual spectra taken from different locations.

### DIFFERENTIAL THERMAL ANALYSIS (DTA)

Differential thermal analysis was done on a Netzsch STA 409C with a retrofitted electronic scale. The sample was placed in an alumina crucible ( $\phi = 1$  mm) which was closed by an alumina disc. Heat flow and mass loss were measured over a temperature range from 298 K to 873 K.

### MEASUREMENT OF MAGNETIC PROPERTIES

AC-Susceptibility was measured on a custom setup. This employs a differential dual-coil setup at an applied field of 3 Oe over a temperature range from 3.5 K to 300 K. A detailed description of this setup can be found in the literature.<sup>[8]</sup>

Further Susceptibility measurements as well as magnetization measurements were carried out using a MPM-XL (Quantum Design) SQUID magnetometer which allowed for measurements at fields between -50 kOe and 50 kOe and temperatures between 1.8 K and 400 K.

All magnetic were done on on 20-50 mg of each respective sample. The data were processed using an automated script.<sup>[9, 10]</sup> Magnetic measurements were evaluated by fitting the inverse molar susceptibility in CGS units employing the extended Curie-Weiss law (1). The definition of magnetic quantities as well as details on the method can be found elsewhere.<sup>[11, 12]</sup>

$$\chi = \frac{C}{T - \theta} + \chi_0 \quad (1)$$

$$\text{with } C = \frac{\mu_0 N_A \mu_B n_{eff}^2}{3k_B}$$

### ELECTRICAL RESISTIVITY

Resistivity measurements were carried out using a custom built setup employing the *van-der-Pauw* method at temperatures between 3.5 K and 300 K. Samples were cold pressed into pellets at 10 kN beforehand (4 mm diameter, ca 0.8 mm thickness).

## DFT CALCULATIONS

Self-consistent DFT band structure calculations were performed using the LMTO-method in its scalar relativistic version as implemented in the TB-LMTO-ASA program.<sup>[13-15]</sup> Reciprocal space integrations were performed with the tetrahedron method using 16x16x16 irreducible  $k$ -points in the tetragonal Brillouin zone. The basis sets were Sr-5s/[5p]/4d/[3f], La-6s/[6p]/5d/4f, Fe-4s/4p/3d and As-4s/4p/[4d], orbitals in brackets were downfolded.

### 2.1.3 References

- [1] D. Walker, M. A. Carpenter, C. M. Hitch, *American Mineralogist* **1990**, 75, 1020-1028.
  - [2] D. Walker, *American Mineralogist* **1991**, 76, 1092-1100.
  - [3] H. Huppertz, *Zeitschrift fuer Kristallographie* **2004**, 219, 330-338.
  - [4] D. C. Rubie, *Phase Transitions* **1999**, 68.
  - [5] N. Kawai, S. Endo, *Rev. Sci. Instrum.* **1970**, 8.
  - [6] A. Coelho, 4.1 ed., Coelho Software, Brisbane, **2007**.
  - [7] M. Tegel, 0.7 ed., unpublished, **2010**.
  - [8] M. C. Tegel, Dissertation thesis, Ludwig-Maximilians-Universität München (München), **2011**.
  - [9] M. Tegel, 0.2 ed., LMU München, **2010**.
  - [10] M. Tegel, LMU, München, **2010**.
  - [11] M. Tegel, Diploma thesis, Ludwig-Maximilians-Universität München (München), **2007**.
  - [12] D. Bichler, Dissertation thesis, Ludwig-Maximilians-Universität München (München), **2010**.
  - [13] H. L. Skriver, *The LMTO method - muffin tin orbitals and electronic structure*, Springer Verlag, Berlin, **1984**.
  - [14] O. K. Andersen, O. Jepsen, M. Sob, in *Electronic Band Structure and its Applications, Lecture Notes in Physics, Vol. 283* (Ed.: M. Yussouff), Springer Verlag, Berlin, **1987**, pp. 1-57.
  - [15] O. K. Andersen, O. Jepsen, 47c ed., Tight-Binding LMTO, Max-Planck-Institut für Festkörperforschung, Stuttgart, **1998**.
-

## 2.2 Absence of Superconductivity in Metastable $\text{Ca}_{1-x}\text{Pr}_x\text{Fe}_2\text{As}_2$ ( $0 \leq x \leq 1$ ) Synthesized under Hydrostatic High Pressure Conditions

Roman Pobel, Katharina Strobl, Christian Maak and Dirk Johrendt

*In preparation for publication*

### ABSTRACT

Samples of  $\text{Ca}_{1-x}\text{Pr}_x\text{Fe}_2\text{As}_2$  covering the full range of  $0 \leq x \leq 1$  have been prepared by means of high pressure synthesis thus overcoming the claimed solubility limit of  $x = 0.13$  for Pr in this system. Samples adopted a new metastable high pressure phase at Pr-contents between 30 and 80%. High temperature PXRD and DTA measurements revealed that at temperatures above 723 K an irreversible structural transition to a phase with a  $c$ -axis closer to the values found in undoped Ca-122 occurs. The transition temperature increases linearly with  $x$ , heat treatment of samples with Pr-contents of  $x \geq 0.8$  results in decomposition. None of the samples showed indications for superconductivity, neither when measured as synthesized nor after heat treatment.

### 2.2.1 Introduction

Ever since the discovery of superconductivity in  $\text{Ba}_{1-x}\text{K}_x\text{Fe}_2\text{As}_2$  in 2008<sup>[1]</sup> the so called 122 iron-arsenides (corresponding to their stoichiometry of  $\text{XFe}_2\text{As}_2$  with  $X =$  alkali- or alkaline earth metal), have been in the focus of materials chemists and physicists alike. Members of this family of compounds share a  $\text{ThCr}_2\text{Si}_2$  or  $\text{BaZn}_2\text{P}_2$ -type structure (space group  $I4/mmm$ ) and exhibit a remarkable flexibility in incorporating various dopants. Over the last years several groups could show that many of these compounds are able to incorporate almost any kind of alkali, alkaline earth, transition metal, pnictide, chalcogenide and rare earth metal with varying effects on their magnetic and superconducting properties. Because of its unique behavior, especially  $\text{CaFe}_2\text{As}_2$  has drawn a lot of attention. The parent compound crystallizes in the tetragonal  $\text{BaZn}_2\text{P}_2$ -type structure [ $a = 3.879(3)$  Å and  $c = 11.740(3)$  Å] and is non-magnetic at ambient conditions. Below approximately 170 K it shows a transition into an orthorhombic structure [ $a = 5.531(1)$  Å,  $b = 5.457(1)$  Å and  $c = 11.683(1)$  Å] along with antiferromagnetic ordering.<sup>[2-4]</sup> Remarkably the effects of applying pressure on this compound seem to be different for non-hydrostatic<sup>[5]</sup> and hydrostatic<sup>[6]</sup> pressure, leading to superconducting or non-superconducting properties, respectively. At pressures above 0.35 GPa, the structure “collapses” into a *collapsed tetragonal* ( $cT$ ) phase [ $a = 3.979(1)$  Å and  $c = 10.637(1)$  Å] resulting in a drastic shortening of the  $c$ -axis and the appearance of interlayer As-As dimers indicated by an interatomic distance below 3 Å.<sup>[7]</sup> This and the accompanying changes in the electronic structure are believed to suppress superconductivity.<sup>[8, 9]</sup> The question arises in which way controlled chemical pressure and/or electron doping, which has similar effects,<sup>[10]</sup> may enable superconducting properties in  $\text{CaFe}_2\text{As}_2$  without the need for external pressure.

Especially rare earth elements of the 6<sup>th</sup> period have attracted a lot of interest in this regard since their radii for six-fold coordination are in many cases very close to that of Ca.<sup>[11]</sup> Indeed superconductivity has been found to arise in single crystals of  $\text{RE}_x\text{Ca}_{1-x}\text{Fe}_2\text{As}_2$  for different dopants

with the highest critical temperatures reported for  $RE = \text{Pr}$  at 47 K.<sup>[12-14]</sup> However, the superconducting volume fractions in these samples are very small especially in the case of  $RE = \text{Pr}$ . Thus it is not clear whether these properties are intrinsic or rather stem from other physical phenomena.<sup>[15, 16]</sup> Additionally the solubility limit of rare earth elements in the host compound, which was usually reported to be at around  $x = 13$ , hinders a thorough investigation of the physical phase diagrams of these systems. In the preparation of bulk superconducting La-doped Sr-122, the solubility limit of that system could be overcome when moderate pressure was applied during synthesis in a Belt-type setup.<sup>[17]</sup> Taking this into account we wanted to expand the accessible range of Pr substitution in  $\text{CaFe}_2\text{As}_2$ . We further set out to elucidate the effects of rare earth doping on the properties of bulk samples of Ca-122 by applying high pressure during synthesis. This way we shed some light on the behavior of this still not very well understood system while establishing a methodology for the investigation of physical phase diagrams in doping ranges not accessible via common solid state synthesis.

### 2.2.2 Sample Preparation

The binary starting materials  $\text{CaAs}$ ,<sup>[18]</sup>  $\text{Fe}_2\text{As}$ <sup>[19]</sup> and  $\text{PrAs}$ <sup>[20]</sup> were prepared from the elements as described in the literature. Some of the temperature profiles had to be slightly modified in order to obtain starting materials of increased purity.

The 18/11 assembly as described in chapter 2.1 was compressed up to 6 GPa at room temperature within 213 min, then heated to 1273 K within 60 min, kept at this temperature for 120 min, and cooled to room temperature in 360 min. Subsequently, the pressure was released over a period of 420 min. The recovered MgO octahedron was cracked open in a glove box, and the sample was isolated from the surrounding BN crucible. The pellet was then ground in an agate mortar and kept inside the glove box for storage and preparation of the physical measurements.

### 2.2.3 The Solid Solution $\text{Ca}_{1-x}\text{Pr}_x\text{Fe}_2\text{As}_2$ and the New $\text{ThCr}_2\text{Si}_2$ -type Compound $\text{PrFe}_2\text{As}_2$

In order to determine the effect of Pr doping on the structure of  $\text{Ca}_{1-x}\text{Pr}_x\text{Fe}_2\text{As}_2$ , samples with the nominal composition  $0 \leq x \leq 1$  have been synthesized. Figure 2.2-1 shows the PXRD data obtained from our purest sample of  $\text{PrFe}_2\text{As}_2$  along with the results of Rietveld refinement. A full comparison of the structural properties obtained from PXRD with those of Ca-122 prepared under ambient pressure<sup>[21]</sup> is given in Table 2.2-1.

---

Table 2.2-1: Comparison of the structural data of the newly synthesized compounds with published data of Ca-122.

	Ambient pressure phase <sup>[21]</sup>	<i>cT</i> phase (T = 50 K, p = 0.63 GPa) <sup>[7]</sup>	High pressure phase	PrFe <sub>2</sub> As <sub>2</sub>
<b>Formula</b>	CaFe <sub>2</sub> As <sub>2</sub>	CaFe <sub>2</sub> As <sub>2</sub>	CaFe <sub>2</sub> As <sub>2</sub>	PrFe <sub>2</sub> As <sub>2</sub>
<b>Synth. method</b>	Sn flux	Sn flux	High pressure	High pressure
<b>Label</b>	Ca-122	<i>cT</i> Ca-122	<i>hp</i> Ca-122	<i>hp</i> Pr-122
<b>Structure type</b>	BaZn <sub>2</sub> P <sub>2</sub>	ThCr <sub>2</sub> Si <sub>2</sub>	BaZn <sub>2</sub> P <sub>2</sub>	ThCr <sub>2</sub> Si <sub>2</sub>
<b>Space group</b>	<i>I4/mmm</i> (139)	<i>I4/mmm</i> (139)	<i>I4/mmm</i> (139)	<i>I4/mmm</i> (139)
<b><i>a</i> (Å)</b>	3.872(9)	3.978(1)	3.911(1)	4.000(1)
<b><i>c</i> (Å)</b>	11.730(2)	10.607(1)	11.479(1)	10.531(1)
<b><i>V</i> (Å<sup>3</sup>)</b>	175.94(5)	167.85(1)	175.65(1)	168.55(1)
<b><i>c/a</i></b>	3.03	2.67	2.93	2.63
<b><i>z</i><sub>As</sub></b>	0.3665(9)	0.3663(5)	0.3672(1)	0.3626(1)
<b><i>d</i><sub>As-As</sub> (Å)</b>	3.129(9)	2.836(1)	3.047(1)	2.893(1)

When comparing the *c/a* ratio and the interlayer distances *d*<sub>As-As</sub> it is apparent that *hp* CaFe<sub>2</sub>As<sub>2</sub> shows higher similarity to the ambient pressure phase than to *cT* CaFe<sub>2</sub>As<sub>2</sub>. Despite a shorter *c*-axis however, there seem to be no significant interlayer bonding interactions, which would be indicated by an interlayer distance below 3 Å.

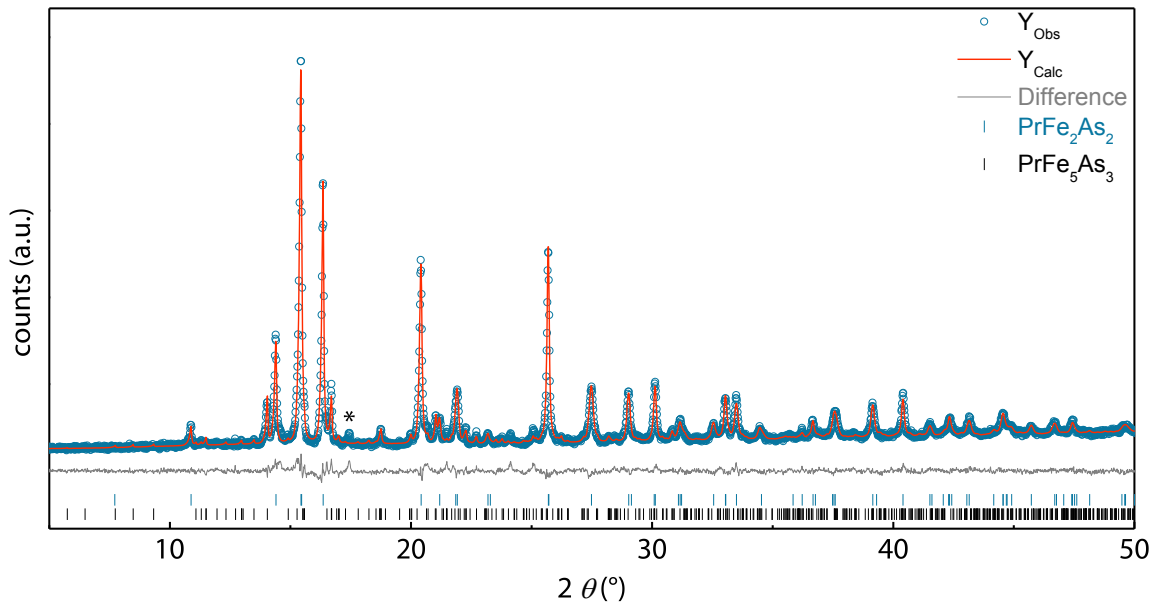


Figure 2.2-1: PXRD data (blue circles) and Rietveld refinement (red line) of the new ThCr<sub>2</sub>Si<sub>2</sub>-type compound PrFe<sub>2</sub>As<sub>2</sub>. An unidentified impurity phase reflection is marked with an asterisk; Indices of the main phases are shown as blue ticks.

PrFe<sub>2</sub>As<sub>2</sub> on the other hand shows a striking structural similarity to *cT* CaFe<sub>2</sub>As<sub>2</sub> in both its interlayer distance of 2.89 Å, which shows substantial bonding interactions, as well as in its lattice parameters. Besides the stabilization of the *cT* phase at ambient conditions, the complete substitution of Ca<sup>II</sup> with Pr<sup>III</sup> in this compound does not seem to have any further effect on the structure. There was no indication of deficiency on either, the Fe- or the Pr-position in any of our measurements. Thus it will be interesting to see the changes that the introduction of an additional

charge from Pr has on the electronic structure of this compound, as the *collapsed tetragonal* form has recently been studied extensively via optical spectroscopy and theoretical calculations.<sup>[8, 9, 22]</sup>

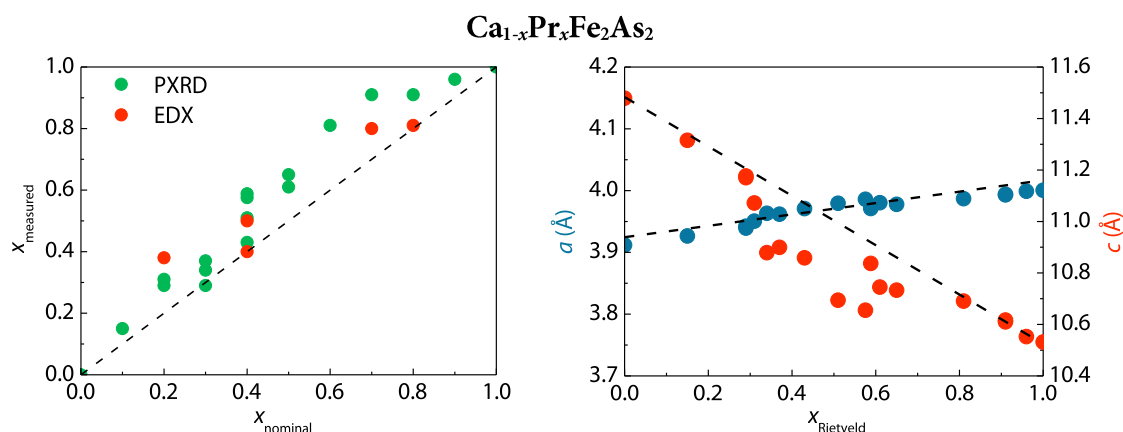


Figure 2.2-2: Left side: Composition of the various samples analyzed via PXR/Rietveld and EDX methods respectively. Right side: Lattice parameters of the solid solution Ca<sub>1-x</sub>Pr<sub>x</sub>Fe<sub>2</sub>As<sub>2</sub> ( $0 \leq x \leq 1$ ) as synthesized.

The left side of Figure 2.2-2 shows the correlation of the nominal Pr-content with the Pr-contents determined via Rietveld refinement and EDX respectively. It shows that the Pr content of all samples, albeit slightly higher than the nominal value, increases continuously and without apparent gaps. It thereby proves the existence of the solid solution Ca<sub>1-x</sub>Pr<sub>x</sub>Fe<sub>2</sub>As<sub>2</sub> for all values of  $x$  without the occurrence of intermediate phases or major structural transitions. The close proximity of the Pr-contents obtained via EDX and Rietveld refinement further shows that a discussion based on the data obtained by PXR measurements/Rietveld refinements is justified. To verify homogenous dopant distribution in the samples we carried out EDX mapping experiments shown in Figure 2.2-3. They indicate an homogenous concentration of Pr across the measured area, which at this scale, is in agreement with previously published results.<sup>[23]</sup>

Taking a look at the solid solution Ca<sub>1-x</sub>Pr<sub>x</sub>Fe<sub>2</sub>As<sub>2</sub>, one can also see a similarity to the transition of undoped CaFe<sub>2</sub>As<sub>2</sub> into the  $cT$  phase. The right side of Figure 2.2-2 shows the development of the cell parameters with increasing Pr content  $x$ . The most drastic changes in  $c$  appear up to  $x = 0.5$  followed by a plateau with a small decrease at very high values of  $x$ . Both lattice parameters behave generally as expected from previous studies.<sup>[10]</sup> However it is noteworthy that they show linear behavior which is intermitted by a region between  $x = 0.3$  and  $x = 0.8$  in which especially  $c$  seems to shrink a lot faster than  $a$ . This is reminiscent of the structural transition of undoped CaFe<sub>2</sub>As<sub>2</sub> under pressure.



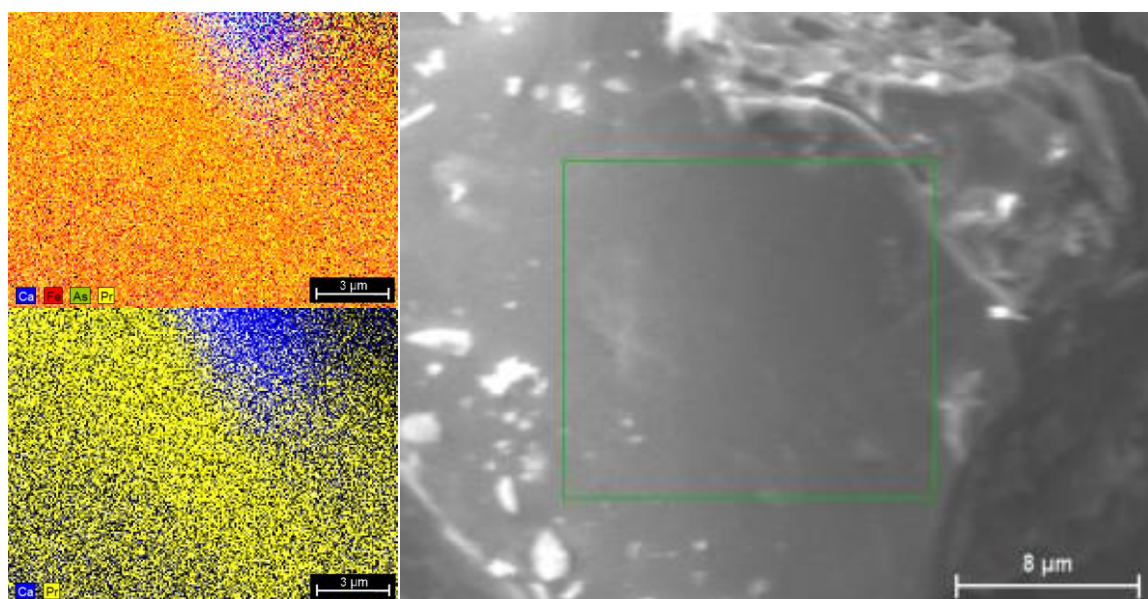


Figure 2.2-3: SEM picture of a sample with the composition  $\text{Ca}_{0.6}\text{Pr}_{0.4}\text{Fe}_2\text{As}_2$ . Insets (Ca in blue, Pr in yellow, Fe in red, As in green) show the results of EDX mapping which indicate homogenous distribution of the dopant.

#### 2.2.4 The Metastability of $hp\text{-Ca}_{1-x}\text{Pr}_x\text{Fe}_2\text{As}_2$

The most interesting feature of  $hp\text{-Ca}_{1-x}\text{Pr}_x\text{Fe}_2\text{As}_2$  is its metastability. This metastable phase is very similar to the *collapsed phase* of  $\text{CaFe}_2\text{As}_2$  over a wide range of Pr-contents. The compressed phase exhibits lattice parameters as well as interlayer As-As distances very close to those reported for  $cT$   $\text{CaFe}_2\text{As}_2$  but does so under ambient conditions and without post-annealing or other treatment. This enables us to study the properties of the different modifications of this compound at ambient conditions.

Figure 2.2-4 shows the development of lattice parameters  $a$  and  $c$  with increasing temperature in a sample containing 60% Praseodymium. The behavior is exemplary for all samples up to a Pr-content of about 75%. The most important feature is the hysteretic behavior of the lattice parameters indicating the existence of a metastable compressed phase  $c\text{-}hp\text{-Ca}_{1-x}\text{Pr}_x\text{Fe}_2\text{As}_2$  that is able to relax at relatively moderate temperatures. We define the temperature at which this relaxation occurs (relaxation temperature  $T_r$ ) as the peak of the first derivative of  $c$  ( $dc/dT$ ), i.e. the data point marking the steepest slope in the heating curve of  $c$  in a HT-PXRD data set. We conducted DTA measurements in order to justify this approach as shown in the lower row of Figure 2.2-4. Since the usual sample size is rather small due to the limitations of the high pressure setup, we used the HT-PXRD measurements to obtain  $T_r$  in most of the samples. The results are also shown in Figure 2.2-4 and show a strictly linear behavior of  $T_r$  with increasing Pr-content  $x$ . Rietveld refinements also proved that there is no loss of Pr during the transition.

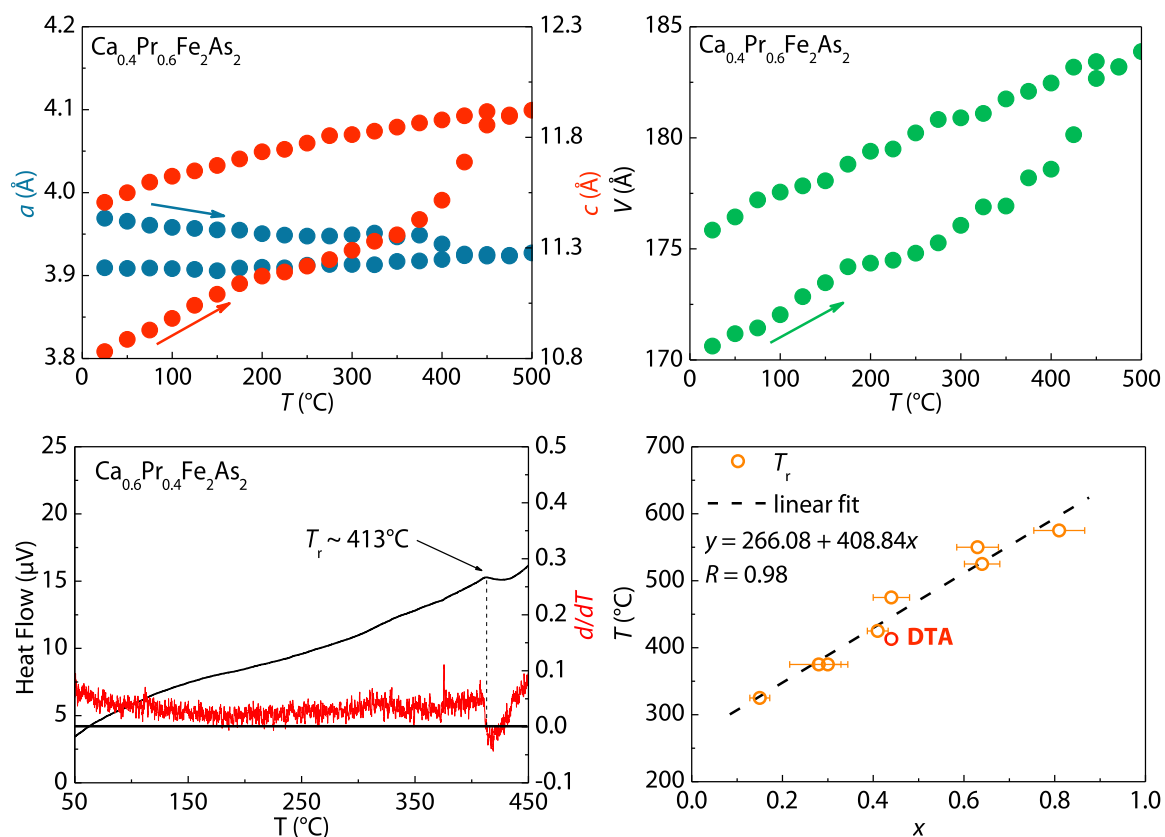


Figure 2.2-4: *Upper row*: Progression of the lattice parameters (left) and cell volume (right) obtained from HT-PXRD measurements with a refined Pr-content of  $x = 0.6$ . *Lower row*: Results of the DTA measurements (left) on the same sample and overall development of  $T_r$  with increasing Pr-content (right). The result of the DTA measurement is highlighted in red.

Starting from  $x = 0.5$  on significant decomposition of the samples occurs at elevated temperatures. At  $x = 0.8$  a transition can be observed in the HTPXRD data but the sample decomposes during the measurement which makes the extraction of the “relaxed” lattice parameters impossible. Above  $x = 0.8$  the compounds decompose before relaxation can take place. This renders the determination of reasonable values for  $T_r$  impossible. The closer the composition approaches  $\text{PrFe}_2\text{As}_2$ , the more sensitive the compound becomes to heat treatment. The absence of any sign of a transition and its decomposition at elevated temperatures could imply that  $\text{PrFe}_2\text{As}_2$  itself may not be a thermodynamically stable compound at ambient pressure.

It should be noted that *hp*- $\text{CaFe}_2\text{As}_2$ , albeit slightly “compressed” along its  $c$ -axis in comparison to its ambient pressure form, does not show a comparable jump in the behavior of its structural parameters upon heating but rather appears to expand continuously. This expansion however is irreversible as well.

Since samples with higher Pr contents than  $x = 0.13$  remain stable after heat treatment, this means that they must be a thermodynamically stable phase. This in turn means that Pr contents of more than  $x = 0.13$  should be accessible via regular high temperature solid state synthesis without the application of pressure, which does not seem to be the case. A possible explanation may be that the high temperature which is necessary to obtain these compounds via solid state synthesis results in the presence of too much thermal energy for the system to be stable at ambient pressure.

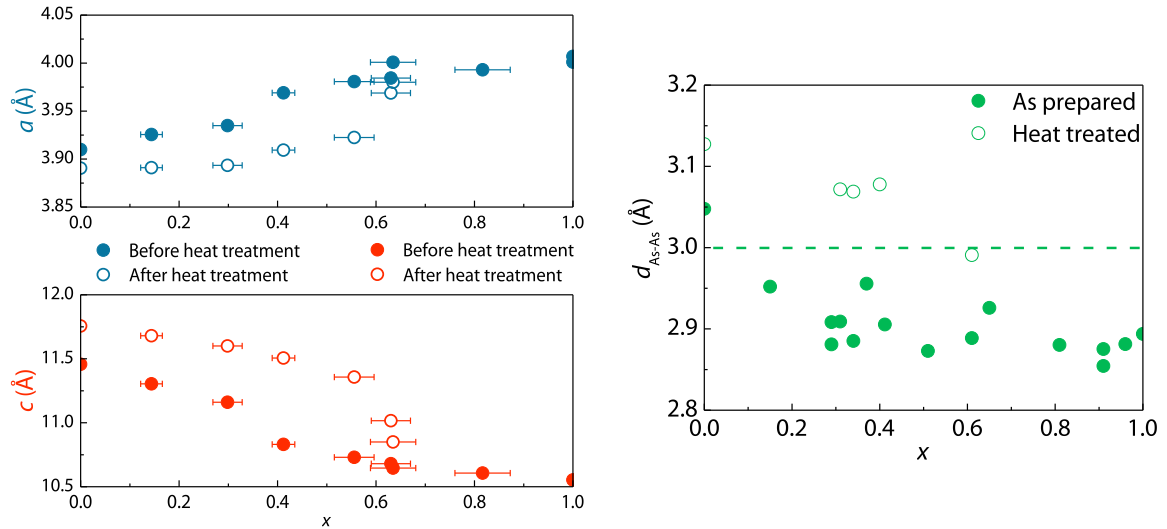


Figure 2.2-5: Comparison of the lattice parameters and interlayer distance  $d_{\text{As-As}}$  of the samples before and after heat treatment.

When studying the interlayer As-As distance  $d_{\text{As-As}}$  (see Figure 2.2-5) it becomes apparent that there is a maximum Pr-content of around  $x = 0.6$  above which the compound cannot transition into a relaxed state. The interlayer distance is indicative of interlayer-bonding interactions that have been shown to correlate with an absence of superconductivity in  $\text{CaFe}_2\text{As}_2$  and related compounds. This means that only samples with Pr-contents below  $x = 0.6$  may be able to show superconducting behavior at all.

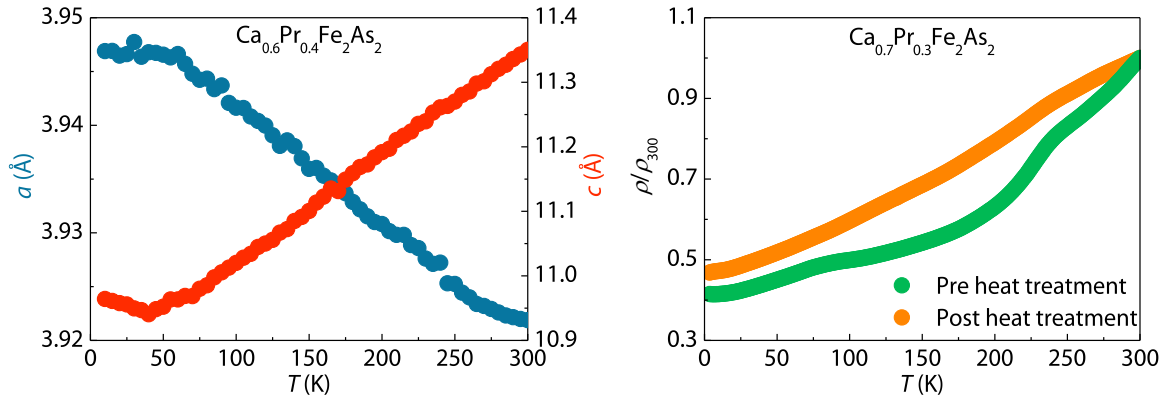


Figure 2.2-6: Left side: Behavior of the lattice parameters during cooling as observed via low temperature PXRD. Right side: Resistivity measurements showing the regular metallic behavior of the electrical resistivity in samples of hp (Ca,Pr)-122 before and after heat treatment.

Furthermore these findings allow for the direct observation of the influence of structural stress on the properties of this compound. We found that heat-treatment of the samples at temperatures close to  $T_{\text{r}}$  for 24 h is sufficient to achieve a complete structural relaxation of the bulk sample. The irreversibility of the relaxation could be proven via low temperature XRD measurements which showed no spontaneous contraction of  $c$  upon cooling. Rather the cell appears to linearly contract along the  $c$ -axis while expanding along  $a$  (Figure 2.2-6).

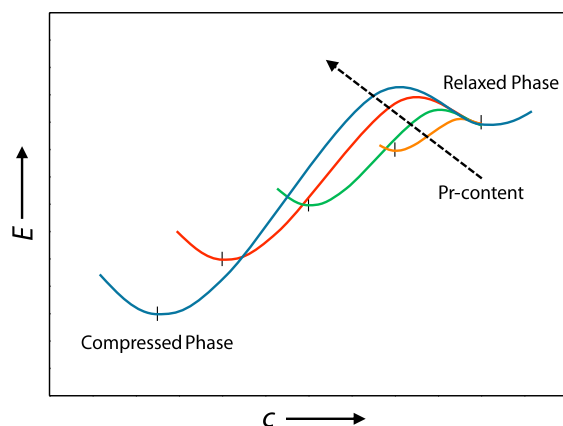


Figure 2.2-7: Qualitative illustration of the stability of highly Pr-doped  $(Ca,Pr)Fe_2As_2$ .

A qualitative model for the behavior of  $(Ca,Pr)Fe_2As_2$  is given in Figure 2.2-7. In this model, there is a relaxed state and a compressed state indicated by two local minima for every Pr-content  $x = 0-1$ . The Pr-content on the other hand has a direct correlation to the structural parameter  $c$ . In order to transition from the compressed state, which is characterized by a shorter  $c$ -axis, to the relaxed state with a longer  $c$ -axis, a certain amount of activation energy is required. The amount of energy, i.e.  $T_b$ , increases for increasing Pr-contents, which in turn leads to shorter  $c$ -axes. At extremely high Pr-contents the amount of energy required for a transition is high enough to lead to decomposition of the compound. At very low Pr-contents on the other hand, the compressed phase cannot be stabilized at ambient conditions at all, which is exactly what is observed for the  $cT$ -phase of  $CaFe_2As_2$ .

### 2.2.5 Absence of Superconductivity in $hp$ - $(Ca,Pr)Fe_2As_2$

The magnetic properties of  $(Ca,Pr)Fe_2As_2$  are still not fully understood and especially the low superconducting volume fraction in single crystals of this compound indicates that superconductivity might not be an intrinsic property of this system. In fact many recent findings point towards a domain wall induced form of filamentary superconductivity.<sup>[15, 16, 23]</sup> To shed some light on the influence of the Pr-concentration we carried out susceptibility measurements on all samples. Due to the presence of  $(CaPr)Fe_5As_3$  with strong magnetic ordering at lower temperatures further investigations of the magnetic behavior were impossible. Details on this impurity phase and its magnetic properties will be published elsewhere.

However, it is apparent that none of the samples show any sign of behavior one would expect from a superconductor. At weight fractions of about 70-80% even partial superconductivity of the main phase should give a clearly visible signal in susceptibility measurements. As mentioned before this might be due to the stabilized *collapsed tetragonal* phase of  $hp$ - $(Ca,Pr)Fe_2As_2$ .

To avoid the influence of the structural collapse we heat treated samples for 24 h at 723 K for  $x = 0.1-0.5$  and 773 K for samples with higher Pr-contents, following the findings we detailed above. The investigation of these structurally relaxed samples showed no interfering signals of the magnetic impurity phase, as this compound already seems to decompose at lower temperatures. None of the samples showed any sign of diamagnetism after heat treatment as well.

The resistivity of all samples behaves as expected from a bad metal at low temperatures (see Figure 2.2-6). Pr doping is known to suppress the tetragonal to orthorhombic transition in  $\text{CaFe}_2\text{As}_2$  which would be visible as an anomaly in the resistivity curve. The absence of any steps further confirms the absence of a superconducting phase.

Due to the presence of impurity phases in all samples it is not possible to study the magnetic behavior of *hp*-(Ca,Pr) $\text{Fe}_2\text{As}_2$  in depth. The total absence of any diamagnetism and zero-resistivity in all samples across the whole doping range proves that despite many other claims, (Ca,Pr) $\text{Fe}_2\text{As}_2$  is not an intrinsically superconducting compound. The superconductivity observed in single crystals obviously must arise from non-intrinsic origins. This is in agreement with findings on the Pr-distribution<sup>[23]</sup> and the suggestion of an antiphase domain wall induced mechanism of superconductivity in single crystalline (Ca,Pr) $\text{Fe}_2\text{As}_2$ .<sup>[16]</sup>

### 2.2.6 Conclusions

In this contribution we report on our findings on the high pressure synthesis of Pr-doped  $\text{CaFe}_2\text{As}_2$ . We could show that by using pressures of 6 GPa and temperatures of 1273 K during synthesis, the solid solution  $\text{Ca}_{1-x}\text{Pr}_x\text{Fe}_2\text{As}_2$  can be obtained for  $0 \leq x \leq 1$ . The samples exhibit structural parameters resembling those of the so called *collapsed tetragonal phase* of  $\text{CaFe}_2\text{As}_2$  but at ambient conditions. This provides a method for future investigations on compounds exhibiting similar structural instabilities.

We found that all samples exhibit a rapid, endothermic and irreversible expansion of the *c*-axis upon heating to 723 K - 773 K which is visible via HT-PXRD and DTA measurements alike. We thereby were able to prove that this new found high pressure form of (Ca,Pr)-122 is metastable. Our investigation of the physical properties of all samples did not show any signs of superconductivity. Since we could rule out the presence of interlayer bonding by heat treatment of our samples, we were thereby able to conclusively show that Pr-doped Ca-122 is not an intrinsically superconducting compound. Our findings contradict previous reports on the superconducting properties of these compounds but point toward the presence of a different mechanism that gives rise to traces of superconductivity in single crystals, which has been discussed in recent publications.

Our findings show that by applying synthetic methods that go beyond conventional synthesis one can find completely new and unexpected properties in otherwise seemingly well investigated compounds. We are convinced that high pressure synthesis holds great potential for the further investigation of the sometimes still mysterious superconducting properties in the family of iron arsenide compounds.

### ACKNOWLEDGEMENTS

We would like to thank Wolfgang Schnick for courteously allowing us to use his 1000t press. We would also like to thank Alexey Marchuk and Florian Pucher for their helpful advice on the use of the multi anvil assembly. This work was financially supported by the German Research Foundation (DFG) within the priority program SPP1458, Project No. JO257/6-2.

### 2.2.7 References

- [1] M. Rotter, M. Pangerl, M. Tegel, D. Johrendt, *Angew. Chem. Int. Ed.* **2008**, 47.
  - [2] N. Ni, S. Nandi, A. Kreyssig, A. I. Goldman, E. D. Mun, S. L. Bud'ko, P. C. Canfield, *Physical Review B* **2008**, 78.
  - [3] A. I. Goldman, D. N. Argyriou, B. Ouladdiaf, T. Chatterji, A. Kreyssig, S. Nandi, N. Ni, S. L. Bud'ko, P. C. Canfield, R. J. McQueeney, *Physical Review B* **2008**, 78.
  - [4] F. Ronning, T. Klimczuk, E. D. Bauer, H. Volz, J. D. Thompson, *J. Phys.: Condens. Matter* **2008**, 20, 322201.
  - [5] M. S. Torikachvili, S. L. Bud'ko, N. Ni, P. C. Canfield, *Physical review letters* **2008**, 101.
  - [6] W. Yu, A. A. Aczel, T. J. Williams, S. L. Bud'ko, N. Ni, P. C. Canfield, G. M. Luke, *Physical Review B* **2009**, 79.
  - [7] A. Kreyssig, M. A. Green, Y. Lee, G. D. Samolyuk, P. Zajdel, J. W. Lynn, S. L. Bud'ko, M. S. Torikachvili, N. Ni, S. Nandi, J. B. Leao, S. J. Poulton, D. N. Argyriou, B. N. Harmon, R. J. McQueeney, P. C. Canfield, A. I. Goldman, *Phys. Rev. B: Condens. Matter Mater. Phys.* **2008**, 78, 184517.
  - [8] R. S. Dhaka, R. Jiang, S. Ran, S. L. Bud'ko, P. C. Canfield, B. N. Harmon, A. Kaminski, M. Tomic, R. Valenti, Y. Lee, *Phys. Rev. B: Condens. Matter Mater. Phys.* **2014**, 89, 020511.
  - [9] R. Yang, C. Le, L. Zhang, B. Xu, W. Zhang, K. Nadeem, H. Xiao, J. Hu, X. Qiu, *Phys. Rev. B: Condens. Matter Mater. Phys.* **2015**, 91, 1-6.
  - [10] R. Pobel, R. Frankovsky, D. Johrendt, *Z. Naturforsch., B: J. Chem. Sci.* **2013**, 68, 581-586.
  - [11] R. D. Shannon, *Acta Crystallographica Section A* **1976**, 32, 751-767.
  - [12] Z. Gao, Y. Qi, L. Wang, D. Wang, X. Zhang, C. Yao, C. Wang, Y. Ma, *EPL* **2011**, 95, 67002.
  - [13] Y. Qi, Z. Gao, L. Wang, D. Wang, X. Zhang, C. Yao, C. Wang, C. Wang, Y. Ma, *Supercond. Sci. Technol.* **2012**, 25, 045007.
  - [14] S. R. Saha, N. P. Butch, T. Drye, J. Magill, S. Ziemak, K. Kirshenbaum, P. Y. Zavalij, J. W. Lynn, J. Paglione, *Physical Review B* **2012**, 85, 024525.
  - [15] B. Lv, F. Y. Wei, L. Z. Deng, Y. Y. Xue, C. W. Chu, *arXiv.org, e-Print Arch., Condens. Matter* **2013**, 1-9, arXiv:1308.3129v1301 [cond-mat.supr-con].
  - [16] H. Xiao, T. Hu, A. P. Dioguardi, N. apRoberts-Warren, A. C. Shockley, J. Crocker, D. M. Nisson, Z. Viskadourakis, X. Tee, I. Radulov, C. C. Almasan, N. J. Curro, C. Panagopoulos, *Phys. Rev. B.* **2012**, 85.
  - [17] Y. Muraba, S. Matsuishi, S.-W. Kim, T. Atou, O. Fukunaga, H. Hosono, *arXiv:1005.0528v2* **2010**.
  - [18] A. Iandelli, E. Franceschi, *J. Less-Common Metals* **1973**, 30, 211-216.
  - [19] H. Katsuraki, N. Achiwa, *Journal of the Physical Society of Japan* **1966**, 21, 2238.
-

- [20] G. Mu, B. Zeng, X. Zhu, F. Han, P. Cheng, B. Shen, H.-H. Wen, *Phys. Rev. B: Condens. Matter Mater. Phys.* **2009**, 79.
  - [21] G. Wu, H. Chen, T. Wu, Y. L. Xie, Y. J. Yan, R. H. Liu, X. F. Wang, J. J. Ying, X. H. Chen, *J. Phys.: Condens. Matter* **2008**, 20, 422201.
  - [22] A. van Roekeghem, P. Richard, X. Shi, S. Wu, L. Zeng, B. Saparov, Y. Ohtsubo, T. Qian, A. S. Sefat, S. Biermann, *arXiv preprint arXiv:1505.00753* **2015**.
  - [23] K. Gofryk, M. Pan, C. Cantoni, B. Saparov, J. E. Mitchell, A. S. Sefat, *Phys. Rev. Lett.* **2014**, 112, 047005.
-





## 2.3 Properties and High Pressure Synthesis of $\text{Sr}_{0.3}\text{La}_{0.7}\text{Fe}_2\text{As}_2$ and $\text{LaFe}_2\text{As}_2$

### ABSTRACT

Samples of  $\text{Sr}_{1-x}\text{La}_x\text{Fe}_2\text{As}_2$  for  $x = 0.3, 1$  were synthesized under hydrostatic high pressure conditions in a multi anvil setup. At a pressure of 6 GPa we obtained phase pure samples of both compounds.  $\text{LaFe}_2\text{As}_2$  crystallizes in the  $\text{BaZn}_2\text{P}_2$ -type structure (space group  $I4/mmm$ ) with  $a = 3.980(3) \text{ \AA}$  and  $c = 11.280(1) \text{ \AA}$ . Neither compound shows structural transitions at low temperatures. We observe bulk superconductivity at 22 K in  $\text{Sr}_{0.7}\text{La}_{0.3}\text{Fe}_2\text{As}_2$  and complex magnetic ordering at 130 K in  $\text{LaFe}_2\text{As}_2$  resulting in a saturation moment of around  $0.2\mu_B$ .

### 2.3.1 Introduction

After the discovery of superconductivity in hole doped  $\text{BaFe}_2\text{As}_2$  in 2008,<sup>[1]</sup> the family of 122-type iron arsenides has been subject to extensive research over the last few years. In the search for new superconductors many new compounds have been discovered and characterized. In many cases a structural instability at low temperatures has to be suppressed in order to find superconducting properties. This is usually achieved via direct/indirect electron or hole doping, respectively, or in some cases can even be a result of external pressure. The aliovalent doping of  $\text{BaFe}_2\text{As}_2$  with rare earth elements, such as La, turned out to be rather difficult and is mostly done in epitaxial grown films.<sup>[2-4]</sup> This is most likely a result of the substantial size mismatch between rare earth elements and Ba which is why host systems with smaller alkaline earth elements are preferred.

A prominent member of this family of compounds is  $\text{SrFe}_2\text{As}_2$  which undergoes a displacive structural transition from tetragonal to orthorhombic lattice symmetry at 203 K.<sup>[5]</sup> However, when hole doped with K it becomes superconducting at 39 K and the structural transition is fully suppressed.<sup>[6]</sup> Electron doping with Co<sup>[7, 8]</sup> and Ni<sup>[9]</sup> also led to superconductivity albeit at lower critical temperatures of 20 K and 9.8 K, respectively. The application of external pressure of 1.3 GPa could be shown to induce superconductivity with  $T_c = 32 \text{ K}$ .<sup>[10]</sup> DFT calculations suggested that rare earth doped  $\text{SrFe}_2\text{As}_2$  might not exist due to its electronic instability.<sup>[8]</sup>

However, in 2010 *Muraba et al.* reported the synthesis of bulk superconducting  $\text{Sr}_{1-x}\text{La}_x\text{Fe}_2\text{As}_2$  under high pressure conditions with a  $T_c$  of 22 K.<sup>[11]</sup> They concluded that indirect electron doping also induces superconductivity at temperatures close to those of directly doped  $\text{Sr}(\text{Fe},\text{Co})_2\text{As}_2$  but much lower than for the hole doped case. They found samples between  $0.2 \leq x \leq 0.5$  to be superconducting with varying shielding fractions reaching an optimum at  $x = 0.4$ . The critical temperature did not change at different dopant concentrations and a solubility limit of  $x \leq 0.6$  for La was found in this system. Interestingly the phosphide analogue  $\text{LaFe}_2\text{P}_2$ , which behaves like a Pauli-paramagnetic metal, does exist and can be obtained in form of single crystals via Sn-flux synthesis.<sup>[12]</sup> This suggests the possibility that  $\text{LaFe}_2\text{As}_2$  may be obtained by overcoming said solubility limit, which has been shown to be possible under high pressure conditions before (chapter 2.1).

In order to verify the applicability of our multi-anvil setup for the exploration of superconducting systems other than  $(\text{Ca},\text{Pr})\text{Fe}_2\text{As}_2$ , we chose  $(\text{Sr},\text{La})\text{Fe}_2\text{As}_2$  as a model. This should ensure that

superconducting samples can be obtained under these conditions and thus aid in the investigation of the (Ca, Pr)Fe<sub>2</sub>As<sub>2</sub> system. We show that with this method we are not only able to reproduce the findings of *Muraba et al.* but also expand the accessible doping range up to the full substitution of Sr with La. We expand the physical characterization of superconducting Sr<sub>0.7</sub>La<sub>0.3</sub>Fe<sub>2</sub>As<sub>2</sub> by means of low temperature PXR measurements and report on the structural and physical properties of LaFe<sub>2</sub>As<sub>2</sub>, the latest member of the 122-type iron arsenide family.

### 2.3.2 Sample Preparation

The binary starting materials SrAs,<sup>[13]</sup> LaAs<sup>[14]</sup> and Fe<sub>2</sub>As<sup>[15]</sup> were prepared according to the literature from the elements.

Samples were prepared from stoichiometric amounts of the binary starting compounds under hydrostatic high pressure conditions. An 18/11 assembly described in chapter 2.1 was compressed up to 6 GPa at room temperature within 170 min, then the sample space was heated to 1273 K within 60 min, kept at this temperature for 120 min, and cooled to room temperature in 360 min. Subsequently, the pressure was released over a period of 420 min. The sample was isolated and then ground in an agate mortar inside a glove box under purified Ar atmosphere.

### 2.3.3 High Pressure Synthesis of Sr<sub>1-x</sub>La<sub>x</sub>Fe<sub>2</sub>As<sub>2</sub> (x = 0.3, 1)

In order to check the reproducibility of the belt-type high pressure synthesis reported by *Muraba et al.*<sup>[11]</sup> in a multi anvil setup, we started with the synthesis of Sr<sub>0.7</sub>La<sub>0.3</sub>Fe<sub>2</sub>As<sub>2</sub>. This way we wanted to ensure that this method too yields superconducting samples and thus allows for the discovery of new superconductors.

We found that a pressure of 6 GPa and a temperature of 1273 K in fact yield almost phase pure samples (see Figure 2.3-1) which is in contrast to our findings for the Ca-based 122-type compounds. This also contradicts the findings of *Muraba et al.* who reported increasing impurity phase fractions for pressures above 3 GPa as well as Sr<sub>1-x</sub>La<sub>x</sub>Fe<sub>2</sub>As<sub>2</sub> becoming a minority phase at pressures above 4 GPa. This hints at a substantial influence of whether the pressure distribution is hydrostatic or not. LaOFeAs is present in our sample with 6.9 wt%. A small amount of Fe (~1 wt%) can also be identified in the PXR data. The width of the main phase reflections especially for 00l reflections is surprisingly large, which is in accordance with the findings of *Muraba et al.* They explain the broadening as a result from an inhomogeneous distribution of Sr and La leading to a modulation of lattice spacing, i.e. crystallographic strain.

---

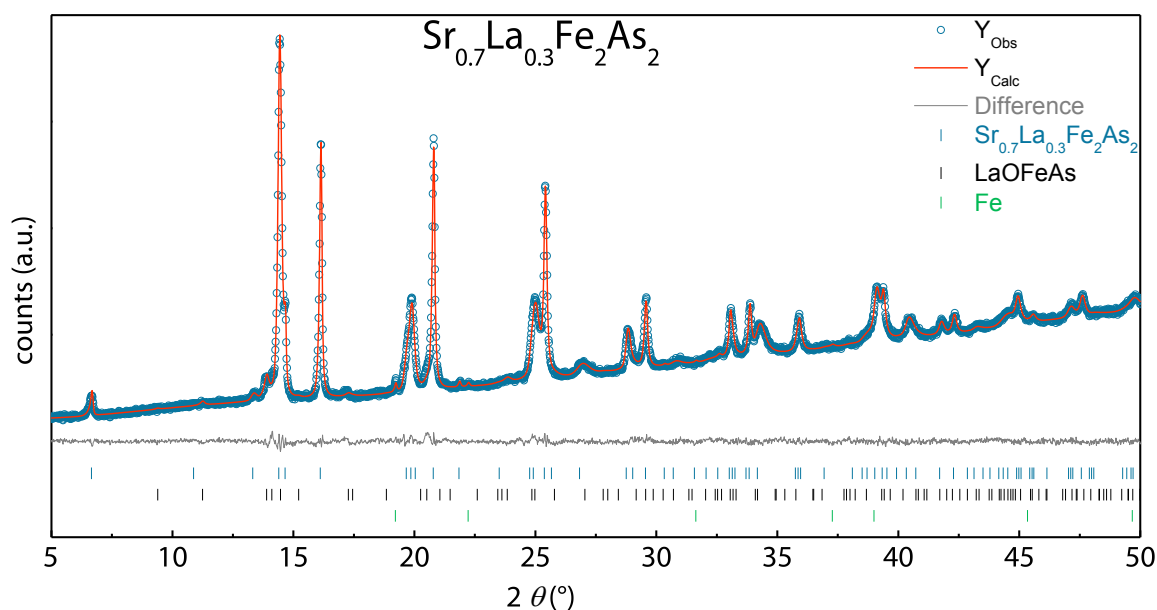


Figure 2.3-1: PXRD data (blue) of  $\text{Sr}_{0.7}\text{La}_{0.3}\text{Fe}_2\text{As}_2$  with Rietveld refinement (red) and difference plot (grey).

Since the synthesis of  $\text{PrFe}_2\text{As}_2$  (see chapter 2.2) was successful, we tried to use the same synthetic conditions to obtain  $\text{LaFe}_2\text{As}_2$ . This yielded an almost phase pure sample with only minor amounts of  $\text{LaOFeAs}$  present (see Figure 2.3-2) which again is in contrast to the findings of *Muraba et al.* who reported a solubility limit of  $x = 0.6$  in this system. We could thus show that the application of high pressures in a multi-anvil setup can not only reproduce the results obtained from a Belt-type setup, but surpass it in the available doping range for rare earth elements in 122-type compounds.

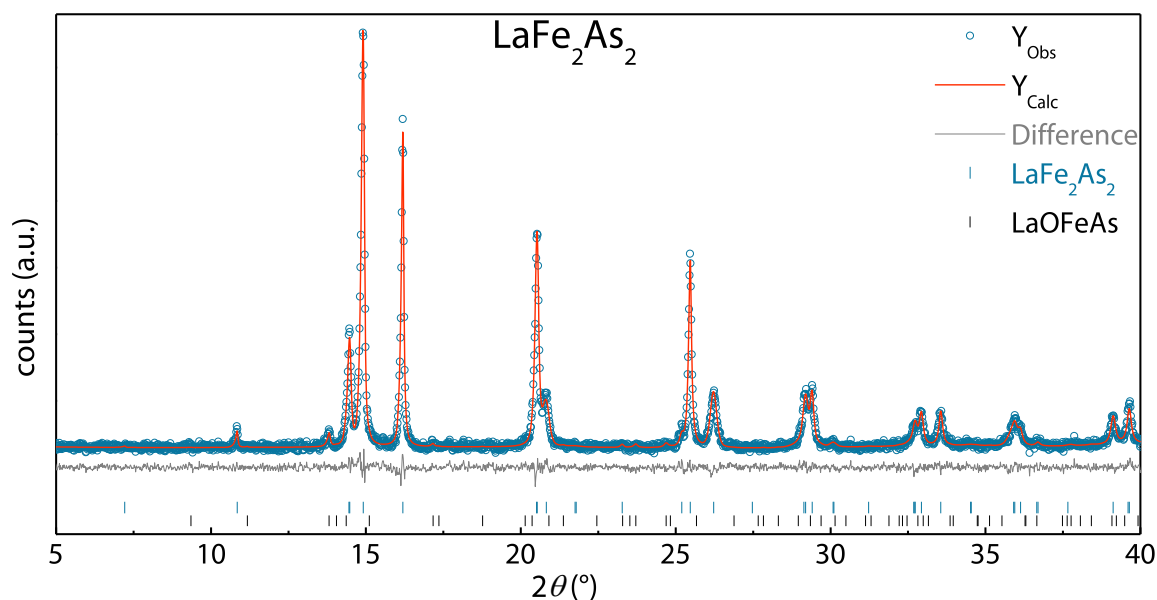


Figure 2.3-2: PXRD data (blue) of  $\text{LaFe}_2\text{As}_2$  with Rietveld refinement (red) and difference plot (grey).

### 2.3.4 Structural and Physical Properties of $\text{LaFe}_2\text{As}_2$

Powder X-ray diffraction (PXRD) measurements and Rietveld refinements yielded the structural parameters summarized in Table 2.3-1. Compared to  $\text{SrFe}_2\text{As}_2$  the general trend in this system seems to be similar to our previous findings for  $(\text{Ca,Pr})\text{Fe}_2\text{As}_2$  since especially  $c$  is substantially

shorter in  $\text{LaFe}_2\text{As}_2$  than in undoped  $\text{SrFe}_2\text{As}_2$ . However, it is still a lot larger than in  $\text{PrFe}_2\text{As}_2$  and the interlayer distance  $d_{\text{As-As}}$ , too does not indicate significant As-As bonding which is why we assign the  $\text{BaZn}_2\text{P}_2$ -type to this new compound. When comparing the decreasing ionic radii<sup>[16]</sup> for six-fold coordinated  $\text{Sr}^{2+}$  ( $r = 1.18 \text{ \AA}$ ),  $\text{La}^{3+}$  ( $r = 1.03 \text{ \AA}$ ) and  $\text{Pr}^{3+}$  ( $r = 0.99 \text{ \AA}$ ), the origin of these structural differences is obvious.

Table 2.3-1: Structural parameters of  $\text{Sr}_{1-x}\text{La}_x\text{Fe}_2\text{As}_2$  ( $x = 0, 0.3, 1$ ) and  $\text{PrFe}_2\text{As}_2$ .

	$\text{SrFe}_2\text{As}_2$ <sup>[17]</sup>	$\text{Sr}_{0.7}\text{La}_{0.3}\text{Fe}_2\text{As}_2$	$\text{LaFe}_2\text{As}_2$	$\text{PrFe}_2\text{As}_2$
<b>Space group</b>	$I4/mmm$	$I4/mmm$	$I4/mmm$	$I4/mmm$
<b>Structure type</b>	$\text{BaZn}_2\text{P}_2$	$\text{BaZn}_2\text{P}_2$	$\text{BaZn}_2\text{P}_2$	$\text{ThCr}_2\text{Si}_2$
<b><math>a</math> (<math>\text{\AA}</math>)</b>	3.927(6)	3.930(1)	3.980(1)	4.000(1)
<b><math>c</math> (<math>\text{\AA}</math>)</b>	12.37(2)	12.23(1)	11.28(1)	10.53(1)
<b><math>V</math> (<math>\text{\AA}^3</math>)</b>	190.76	189.08(6)	178.75(4)	168.55(1)
<b><math>c/a</math></b>	3.14	3.11	2.83	2.63
<b><math>z_{\text{As}}</math></b>	0.37	0.362(1)	0.362(1)	0.362(1)
<b><math>d_{\text{As-As}}</math> (<math>\text{\AA}</math>)</b>	3.462(1)	3.363(1)	3.104(5)	2.893(1)

Since *Muraba et al.* do not report on any structural investigations at low temperatures, we carried out low temperature PXRD measurements on our sample of  $\text{Sr}_{0.7}\text{La}_{0.3}\text{Fe}_2\text{As}_2$  (see Figure 2.3-3). We found the tetragonal to orthorhombic phase transition<sup>[5]</sup> observed in undoped  $\text{SrFe}_2\text{As}_2$  to be suppressed. One would expect this considering the findings for other comparable systems such as rare earth doped  $\text{CaFe}_2\text{As}_2$ . All structural parameters behave continuously. Interestingly lattice parameter  $a$  shows almost no change and only slightly decreases at low temperatures. This is in contrast to many other 122-type compounds where  $a$  usually increases as the cell contracts along  $c$ . Density and volume behave as expected from the behavior of  $a$  and  $c$ .

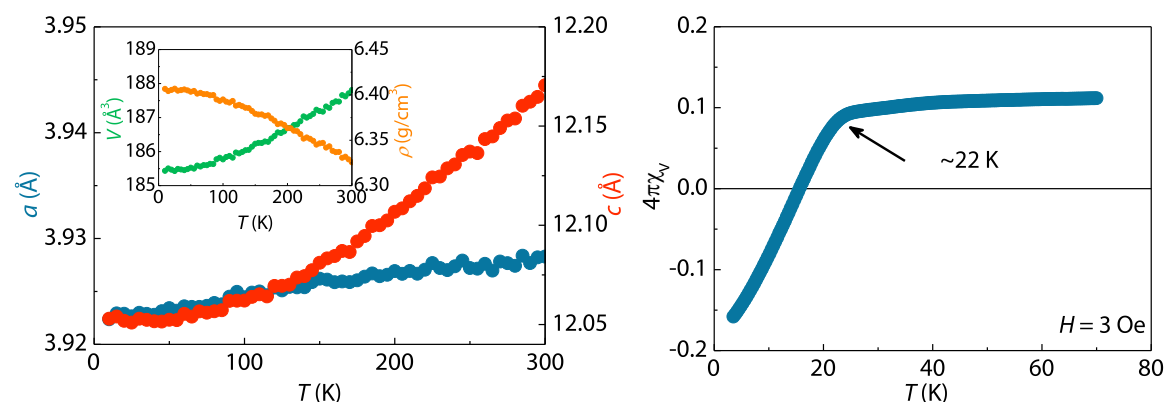


Figure 2.3-3: Left: Development of lattice parameters of  $\text{Sr}_{0.7}\text{La}_{0.3}\text{Fe}_2\text{As}_2$  at low temperatures. Right: Magnetic susceptibility of  $\text{Sr}_{0.7}\text{La}_{0.3}\text{Fe}_2\text{As}_2$  showing superconductivity at 22 K with superconducting volume fraction of about 30%.

Investigations of the magnetic properties showed  $\text{Sr}_{0.7}\text{La}_{0.3}\text{Fe}_2\text{As}_2$  to be superconducting with a  $T_c$  of 22 K and a superconducting volume fraction of about 30% (Figure 2.3-3) which is in good agreement with the findings of *Muraba et al.* A paramagnetic background is visible which results from the presence of Fe in the sample.

Additionally we investigated the structural properties of  $\text{LaFe}_2\text{As}_2$  in a temperature range of 10 K to 300 K (Figure 2.3-4). The lattice parameters behave linearly over the full temperature range. No signs for a structural transition can be observed. Cell volume and phase density behave accordingly.

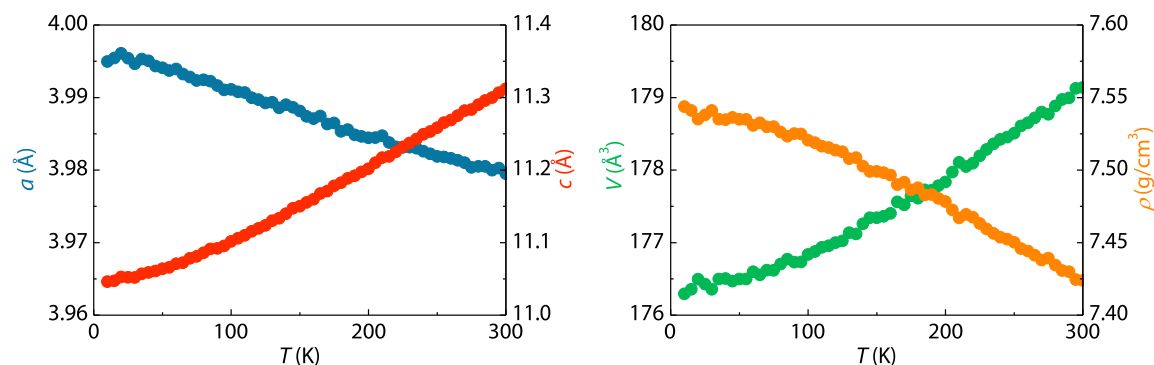


Figure 2.3-4: Left: Development of the lattice parameters of  $\text{LaFe}_2\text{As}_2$  at low temperatures. Right: Behavior of cell volume and density at low temperatures.

Magnetic measurements on  $\text{LaFe}_2\text{As}_2$  revealed a magnetic order at about 130 K that is not fully suppressed by external fields of up to 2 T. Although the curvature of the inverse magnetic susceptibility is rather crass, an extended Curie-Weiss law (Figure 2.3-5) could be realized and suggests a Weiss-constant  $\theta$  of 129.3(1) K along with an effective magnetic moment of 1.261(2)  $\mu_B$  per formula unit. This however is only an approximation, as the curvature of the inverse molar susceptibility is a strong hint at a more complex magnetic behavior, most likely ferrimagnetism. The true nature of this magnetic order will be the subject of future investigations via neutron diffraction.

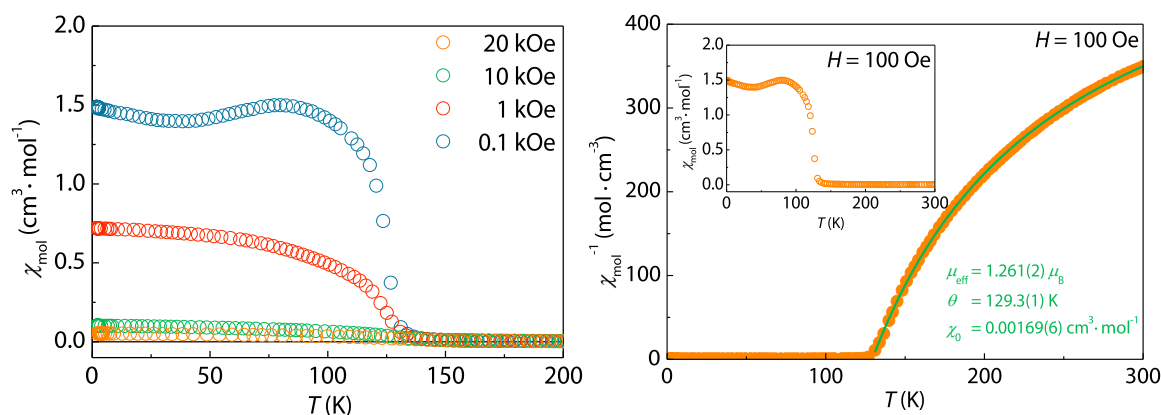


Figure 2.3-5: Left: Molar susceptibility of  $\text{LaFe}_2\text{As}_2$  at different applied fields showing a magnetic order at  $\sim 130$  K. Right: Inverse molar susceptibility of  $\text{LaFe}_2\text{As}_2$  at 100 Oe and extended Curie-Weiss fit.

Taking into account the behavior of the isothermal magnetization (Figure 2.3-6), the overall sample seems to exhibit a small magnetic moment at low temperatures. The zero-field-cooled/field-cooled measurement confirms an ordering temperature of about 130 K. The question whether these signals stem from the bulk sample, a fraction thereof or a minor impurity which is not detectable via PXRD will be subject of future Mössbauer spectroscopy measurements.

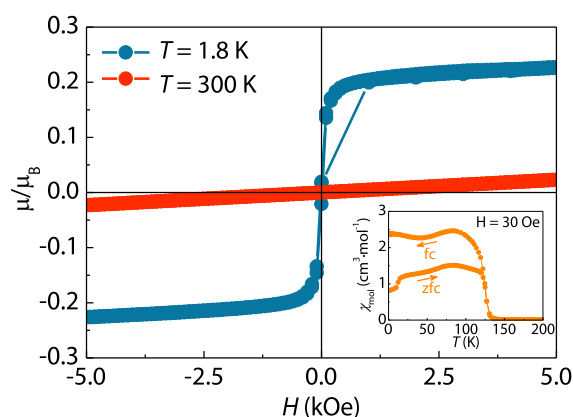


Figure 2.3-6: Magnetization measurements at 1.8 K (blue) and 300 K (red) as well as zero-field cooled/ field-cooled measurements (inset).

### 2.3.5 Conclusions

In summary we successfully applied high pressure synthesis in a multi-anvil setup to obtain almost phase pure samples of  $\text{Sr}_{0.7}\text{La}_{0.3}\text{Fe}_2\text{As}_2$  and the new  $\text{BaZn}_2\text{P}_2$ -type compound  $\text{LaFe}_2\text{As}_2$ . It crystallizes in  $I4/mmm$  with  $a = 3.927(6)$  Å and  $c = 12.37(2)$  Å and forms at 6 GPa and 1273 K from binary starting compounds. Structural and physical characterization revealed a complex magnetic order at  $\sim 130$  K and the absence of structural transitions upon cooling. The origins of this magnetic order will be subject of future investigations.

Characterization of  $\text{Sr}_{0.7}\text{La}_{0.3}\text{Fe}_2\text{As}_2$  reveals no structural transition at low temperatures and bulk superconductivity with a volume fraction of about 20 wt% ( $T_c = 22$  K). This is in very good agreement with the findings of *Muraba et al.* who first discovered superconductivity in La-doped  $\text{SrFe}_2\text{As}_2$  but synthesized their samples in a belt-type high pressure setup at 2 GPa. We could thus show that the multi anvil setup allows for significantly higher pressures during synthesis while the physical properties remain the same, thus allowing for even higher dopant concentrations up to the complete substitution of Sr with La. These findings open the door for future investigations of highly electron doped iron arsenides which are otherwise not accessible and could aid in the search for new iron arsenide superconductors.

### 2.3.6 References

- [1] M. Rotter, M. Tegel, D. Johrendt, *Phys. Rev. Lett.* **2008**, *101*, 107006.
- [2] T. Katase, H. Hiramatsu, T. Kamiya, H. Hosono, *arXiv.org, e-Print Arch., Condens. Matter* **2011**, 1-18, arXiv:1110.0045v1111 [cond-mat.supr-con].
- [3] T. Katase, H. Sato, H. Hiramatsu, T. Kamiya, H. Hosono, *Phys. Rev. B: Condens. Matter Mater. Phys.* **2013**, *88*, 140503.
- [4] T. Katase, H. Hiramatsu, T. Kamiya, H. Hosono, *New J. Phys.* **2013**, *15*, 073019.
- [5] M. Tegel, M. Rotter, V. Weiss, F. Schappacher, R. Pöttgen, D. Johrendt, *J. Phys.: Condens. Matter* **2008**, *20*, 452201.
- [6] K. Sasmal, B. Lv, B. Lorenz, A. Guloy, F. Chen, Y. Xue, C. W. Chu, *Phys. Rev. Lett.* **2008**, *101*, 107007.

- [7] H. Hiramatsu, T. Katase, T. Kamiya, M. Hirano, H. Hosono, *Appl. Phys. Express* **2008**, *1*, 101702.
  - [8] A. Leithe-Jasper, W. Schnelle, C. Geibel, H. Rosner, *Phys. Rev. Lett.* **2008**, *101*, 207004.
  - [9] S. R. Saha, N. P. Butch, K. Kirshenbaum, J. Paglione, *Phys. Rev. B: Condens. Matter Mater. Phys.* **2009**, *79*, 224519.
  - [10] W. O. Uhoja, J. M. Montgomery, G. M. Tsoi, Y. K. Vohra, M. A. McGuire, A. S. Sefat, B. C. Sales, S. T. Weir, *J. Phys.: Condens. Matter* **2011**, *23*, 122201.
  - [11] Y. Muraba, S. Matsuishi, S.-W. Kim, T. Atou, O. Fukunaga, H. Hosono, *Physical Review B* **2010**, *82*, 180512.
  - [12] E. Mörsen, B. D. Mosel, W. Müller-Warmuth, M. Reehuis, W. Jeitschko, *Journal of Physics and Chemistry of Solids* **1988**, *49*, 785-795.
  - [13] A. Iandelli, E. Franceschi, *J. Less-Common Metals* **1973**, *30*, 211-216.
  - [14] G. Mu, B. Zeng, X. Zhu, F. Han, P. Cheng, B. Shen, H.-H. Wen, *Phys. Rev. B: Condens. Matter Mater. Phys.* **2009**, *79*.
  - [15] H. Katsuraki, N. Achiwa, *Journal of the Physical Society of Japan* **1966**, *21*, 2238.
  - [16] R. D. Shannon, *Acta Crystallographica Section A* **1976**, *32*, 751-767.
  - [17] M. Pfisterer, G. Nagorsen, *Z. Naturforsch. B: J. Chem. Sci.* **1980**, *35*, 703.
-





## 2.4 High Pressure Synthesis, Structural and Physical Properties of Rare Earth doped $\alpha$ -CaFe<sub>5</sub>As<sub>3</sub>

Roman Pobel and Dirk Johrendt

*In preparation for publication*

### ABSTRACT

We investigated the solid solution Ca<sub>1-x</sub>Pr<sub>x</sub>Fe<sub>5</sub>As<sub>3</sub> ( $0 \leq x \leq 1$ ) obtained from high pressure synthesis. This led to the discovery of PrFe<sub>5</sub>As<sub>3</sub>, the latest member in the family of interconnected iron arsenides. It is isotypic to CaFe<sub>5</sub>As<sub>3</sub> crystallizing in the space group  $P2_1/m$  with  $a = 7.206(1) \text{ \AA}$ ,  $b = 3.886(1) \text{ \AA}$ ,  $c = 9.765(1) \text{ \AA}$  and  $\beta = 100.5(1)^\circ$ . The lattice parameters of Ca<sub>1-x</sub>Pr<sub>x</sub>Fe<sub>5</sub>As<sub>3</sub> change linearly with  $x$  over the whole range. Low temperature XRD measurements reveal a non-linear structural change in undoped CaFe<sub>5</sub>As<sub>3</sub> around 50 K. This change is enhanced upon moderate Pr-doping but is suppressed at higher dopant concentrations as well as in PrFe<sub>5</sub>As<sub>3</sub>. Magnetic measurements show a magnetic order at around 60 K which is possibly correlated to the structural anomaly. Higher Pr-contents suppress the magnetic order but lead to the emerging of a different order at 75 K most prominent in PrFe<sub>5</sub>As<sub>3</sub>.

### 2.4.1 Introduction

The discovery of superconductivity up to 55 K in layered iron arsenides<sup>[1-4]</sup> has sparked an extensive search for new and possibly superconducting compounds in this class. These new iron arsenides show a remarkable structural diversity and some of them also exhibit exciting magnetic properties. A common structural feature of the iron arsenide superconductors are two dimensional layers of FeAs<sub>4/4</sub> tetrahedra which often show a magnetic instability that has to be suppressed in order to achieve superconductivity.<sup>[5]</sup> In some cases, such as CaFe<sub>2</sub>As<sub>2</sub>, the suppression of a structural instability is also necessary to give rise to superconductivity.<sup>[6, 7]</sup> However, the extensive search for new iron arsenide compounds has led to a variety of interconnected, i.e. “less two dimensional” structures as well. Starting with CaFe<sub>4</sub>As<sub>3</sub> and its substitution variants that have been discovered since 2009, up to the recently characterized Ca<sub>n(n+1)/2</sub>(Fe<sub>1-x</sub>M<sub>x</sub>)<sub>(2+3n)</sub>M'<sub>n(n-1)/2</sub>As<sub>(n+1)(n+2)/2</sub> ( $n = 1-3$ ;  $M = \text{Nb, Pd, Pt}$ ;  $M' = \square, \text{Pd, Pt}$ ) family, the system Ca-Fe-As has proven to be very exciting for solid state chemists and physicists alike.<sup>[8-10]</sup>

CaFe<sub>5</sub>As<sub>3</sub>, which marks the first and structurally simplest member of the interconnected iron arsenides ( $n = 1$ ,  $x = 0$  in the formula above), is only accessible via high pressure synthesis.<sup>[8]</sup> CaFe<sub>4</sub>As<sub>3</sub> which can be viewed as its defect polymorph, can be prepared at ambient pressure.<sup>[8]</sup> Both contain Fe<sup>II</sup>As<sub>4/4</sub> tetrahedra alongside Fe<sup>I</sup>As<sub>5/5</sub> pyramids. In CaFe<sub>4</sub>As<sub>3</sub> these electronic conditions give rise to what might be a spin density wave and incommensurate magnetism<sup>[11]</sup> but CaFe<sub>5</sub>As<sub>3</sub> so far has not been studied with respect to its physical behavior. It crystallizes in space group  $P2_1/m$  with  $a = 7.273(1) \text{ \AA}$ ,  $b = 3.814(1) \text{ \AA}$ ,  $c = 9.757(1) \text{ \AA}$  and  $\beta = 100.7(1)^\circ$  adopting a  $\alpha$ -CaFe<sub>5</sub>As<sub>3</sub>-type structure. The structure (see inset of Figure 2.4-1) comprises a framework consisting of coplanar two-dimensional layers of  $\infty_2[\text{Fe}_4(\text{As}_{4/7})_4]$ , diagonal braces  $\infty_1[\text{Fe}_2(\text{As}_{3/7})_2(\text{As}_{1/7})_2]$  and joints  $\infty_1[\text{Fe}(\text{As}_{2/7})_2\text{As}_{1/7}]$ , which serve as a connection. The channels built

by this framework are populated by Ca. The substitution of Ca in calcium iron arsenides by rare earth elements has led to interesting magnetic behavior as well as superconductivity in several other cases.<sup>[6, 12]</sup> Especially Pr is of interest in this regard since its ionic radius in this coordination is almost exactly the same as that of Ca<sup>[13]</sup> and thus structural distortions due to a size mismatch can be avoided. By investigating the effects of indirect electron doping in CaFe<sub>5</sub>As<sub>3</sub>, we hope to elucidate some of the basic structural and magnetic properties in interconnected iron arsenides and lay the groundwork for the physical investigation of the recently discovered  $\text{Ca}_{n(n+1)/2}(\text{Fe}_{1-x}\text{M}_x)_{(2+3n)}\text{M}'_{n(n-1)/2}\text{As}_{(n+1)(n+2)/2}$  ( $n = 1-3$ ;  $M = \text{Nb, Pd, Pt}$ ;  $M' = \square, \text{Pd, Pt}$ ) family.

### 2.4.2 Sample Preparation

The binary starting materials CaAs,<sup>[14]</sup> PrAs<sup>[15]</sup> and FeAs<sup>[16]</sup> were prepared as described in the literature from the elements.

The 18/11 assembly as described in chapter 2.1, containing a stoichiometric mixture of the starting materials CaAs, PrAs, FeAs and Fe was compressed up to 7 GPa at room temperature within 204 minutes. Then the sample space was heated to 1273 K within 60 minutes, kept at this temperature for 120 minutes, and cooled to room temperature in 360 minutes. Subsequently, the pressure was released over a period of 500 minutes. The sample was isolated and then ground in an agate mortar inside a glove box in a purified Ar atmosphere.

Over the course of our investigations we noticed a direct correlation of the pressure used during the experiment and the phase fraction of the main phase. Yet even at 9 GPa, which is the highest pressure achievable while still yielding reasonable sample sizes, we were unable to obtain phase pure samples. Taking into consideration the abrasion of the assembly materials (especially the tungsten carbide cubes) at these high pressures, we found 7 GPa to be a reasonable compromise between sample purity and setup abrasion.

### 2.4.3 Structural Properties of $\text{Ca}_{1-x}\text{Pr}_x\text{Fe}_5\text{As}_3$ ( $0 \leq x \leq 1$ )

Our experiments towards Pr-doping of CaFe<sub>5</sub>As<sub>3</sub> yielded samples in the full range  $0 \leq x \leq 1$ . The discovery of PrFe<sub>5</sub>As<sub>3</sub> adds a new member to the rapidly growing family of iron arsenides. It is isostructural to the parent compound CaFe<sub>5</sub>As<sub>3</sub> (see inset of Figure 2.4-1). It crystallizes in the space group  $P2_1/m$  with  $a = 7.206(1) \text{ \AA}$ ,  $b = 3.886(1) \text{ \AA}$ ,  $c = 9.765(1) \text{ \AA}$  and  $\beta = 100.5(1)^\circ$  resulting in a unit cell volume of  $268.8(5) \text{ \AA}^3$ . Figure 2.4-1 shows a PXRD pattern and the Rietveld refinement of this compound.

Compared to the parent compound, PrFe<sub>5</sub>As<sub>3</sub> does not show any structural distortions despite being substantially electron doped compared to CaFe<sub>5</sub>As<sub>3</sub>. This situation is remarkably similar to some of our previously reported results (see chapter 2.2) and hints at a substantial electronic flexibility of the system Ca-Fe-As which might also be visible in other members of the family of interconnected iron arsenides.

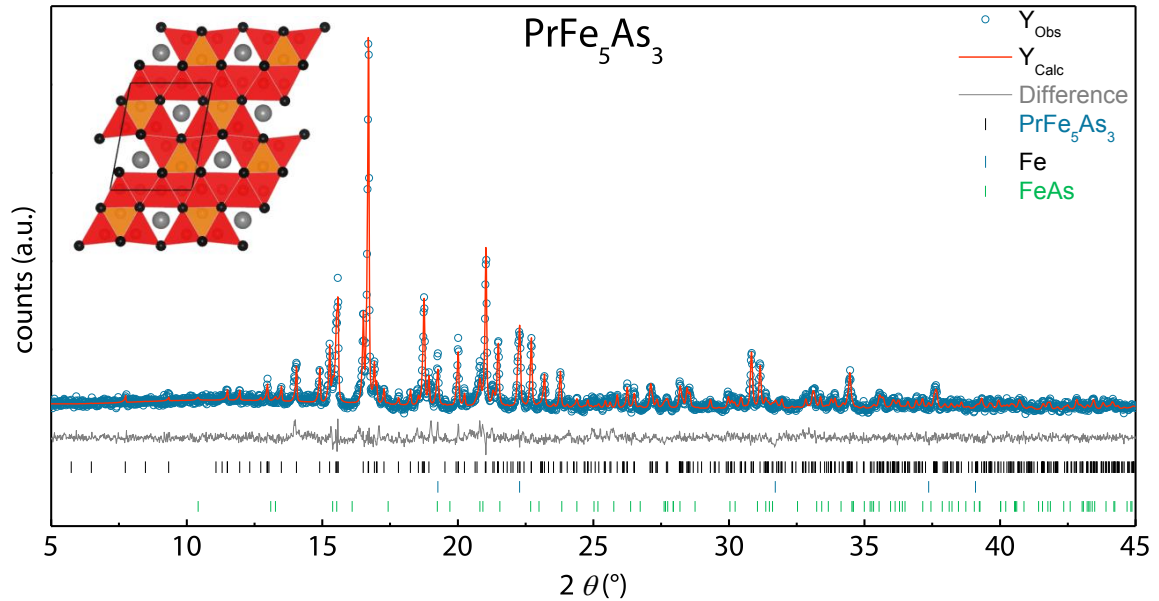


Figure 2.4-1: PXRD data (blue) with Rietveld refinement (red) and difference plot (grey). Inset: Crystal structure of  $\text{PrFe}_5\text{As}_3$  with highlighted pyramidal coordinated Fe-sites (orange polyhedra). Pr atoms are colored grey; Fe atoms are shown in red and As atoms appear black with  $\text{FeAs}_{4/4}$  tetrahedra being highlighted in red.

Starting from  $x = 0$ , all structural parameters show linear behavior with increasing Pr-content (Figure 2.4-3) resulting in a linear increase of volume reminiscent of Vegard's law.<sup>[17]</sup> The linear increase of density (Figure 2.4-2) may at first seem unusual in this context. It is however easily understandable taking into account that the change in volume is very small whereas the mass difference of Pr and Ca is quite substantial.

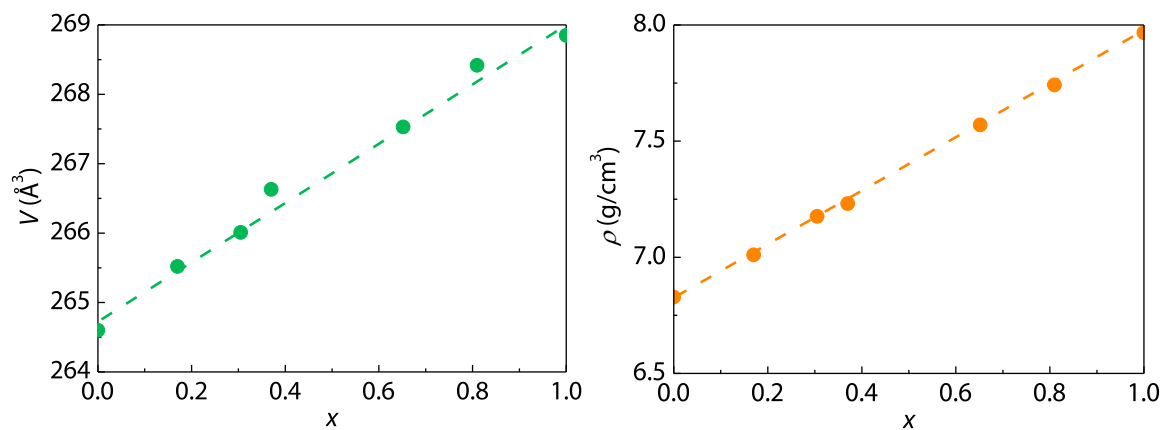
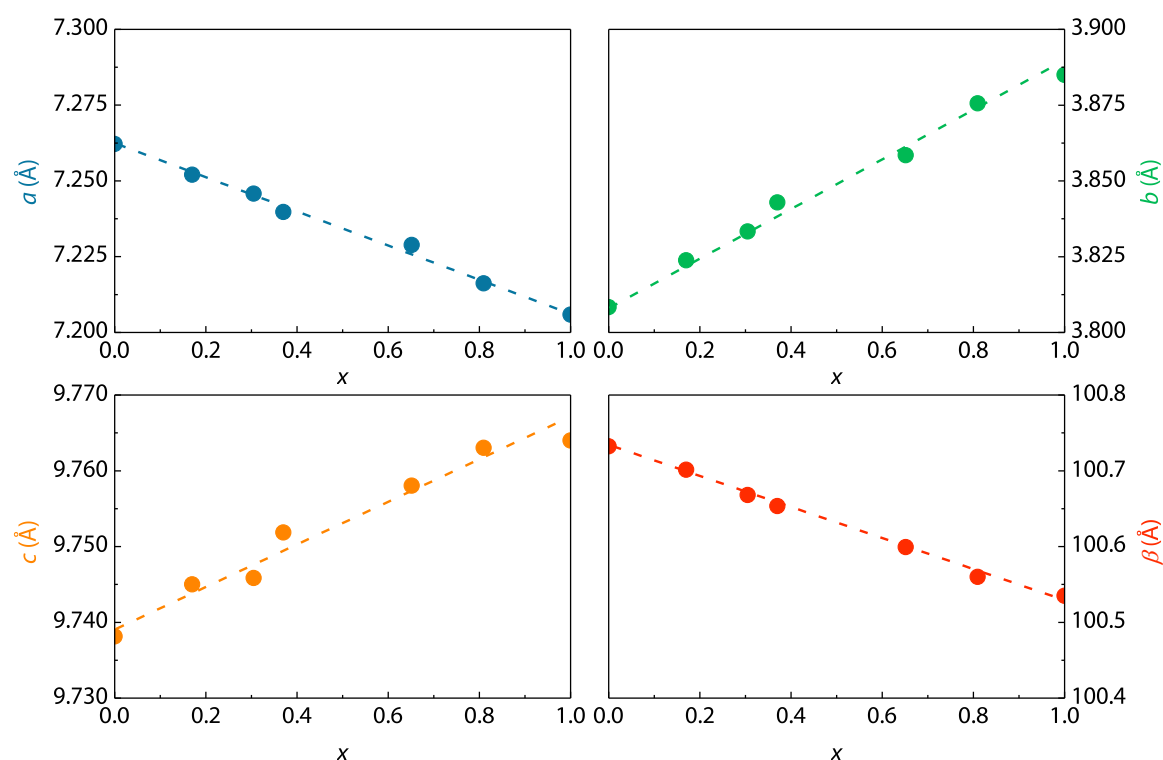


Figure 2.4-2: Volume (left) and density (right) of  $\text{Ca}_{1-x}\text{Pr}_x\text{Fe}_5\text{As}_3$  increase linearly with increasing Pr-content.

The decrease of  $a$  and  $\beta$  together with the slight expansion of  $b$  and  $c$  (see Table 2.4-1) can be interpreted as a very slight compression of the unit cell along  $a$  to which the cell reacts by expanding along the lattice parameters. Considering previous DFT calculations,<sup>[18]</sup> which found a dominance of Fe-states in the DOS around  $E_F$ , this means that doping mostly influences Fe-Fe bonds in the frame. As the frame is a layer of edge-sharing  $\text{FeAs}_{4/4}$  tetrahedra, this situation is very similar to what was found for 122-compounds. However the overall changes in all structural parameters are small with a maximum change of 2% being found in  $b$  (see Figure 2.4-3).

Table 2.4-1: Structural parameters of the solid solution  $\text{Ca}_{1-x}\text{Pr}_x\text{Fe}_5\text{As}_3$ .

$x$	$a$ (Å)	$b$ (Å)	$c$ (Å)	$\beta$ (°)
0	7.262(2)	3.808(4)	9.738(4)	100.73(2)
0.17	7.252(1)	3.823(8)	9.745(1)	100.70(1)
0.30	7.245(7)	3.833(3)	9.745(5)	100.66(8)
0.37	7.239(7)	3.842(9)	9.751(6)	100.65(3)
0.65	7.228(8)	3.858(4)	9.763(2)	100.59(9)
0.81	7.216(2)	3.875(5)	9.758(3)	100.55(9)
1	7.205(9)	3.885(5)	9.764(3)	100.53(5)

Figure 2.4-3: Linear progression of the lattice parameters and the monoclinic angle  $\beta$  with increasing Pr contents in  $\text{Ca}_{1-x}\text{Pr}_x\text{Fe}_5\text{As}_3$ .

#### 2.4.4 Structural Changes in $\text{Ca}_{1-x}\text{Pr}_x\text{Fe}_5\text{As}_3$ ( $0 \leq x \leq 1$ ) at Low Temperatures

Since the family of interconnected iron arsenides is relatively new, the behavior of its members at different conditions is thus mostly unknown. We set out to investigate the behavior the solid solution  $\text{Ca}_{1-x}\text{Pr}_x\text{Fe}_5\text{As}_3$  exhibits upon cooling, which is especially interesting in context with the subsequent physical characterization.

The structural behavior upon cooling differs for varying Pr-contents (Figure 2.4-4). The undoped parent compound  $\text{CaFe}_5\text{As}_3$  shows a linear contraction down to  $\sim 50$  K. A sudden deviation from the linear behavior can then be seen which is particularly well visible in  $a$ . This behavior consequently results in a linear shrinkage of the cell volume with a drop around 50 K. However no hints at a change in symmetry or other major structural distortions upon cooling are visible in the XRD patterns (Figure 2.4-4).

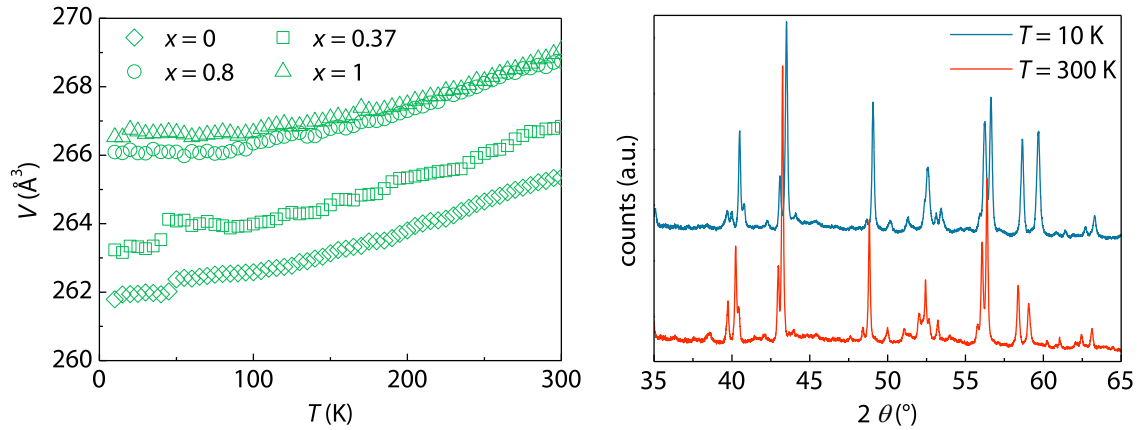


Figure 2.4-4: Left: Shrinkage of the cell volumes of  $(\text{Ca,Pr})\text{Fe}_5\text{As}_3$  upon cooling. Right: Comparison of PXRD patterns of undoped  $\text{CaFe}_5\text{As}_3$  at 10 K (blue) and 300 K (red).

Parameters  $a$  and  $\beta$  show a drop of about 0.2-0.5% while  $b$  and  $c$  show a sudden expansion of the same order of magnitude (Figure 2.4-5). After this nonlinear change, all parameters seem to return to a linear behavior for temperatures lower than about 45 K. This is a stark contrast to  $\alpha\text{-Ca}_3(\text{Fe,Pt})_8\text{PtAs}_6$ , a higher member of the family of interconnected iron arsenides, that shows no significant structural changes at low temperatures at all.<sup>[18]</sup>

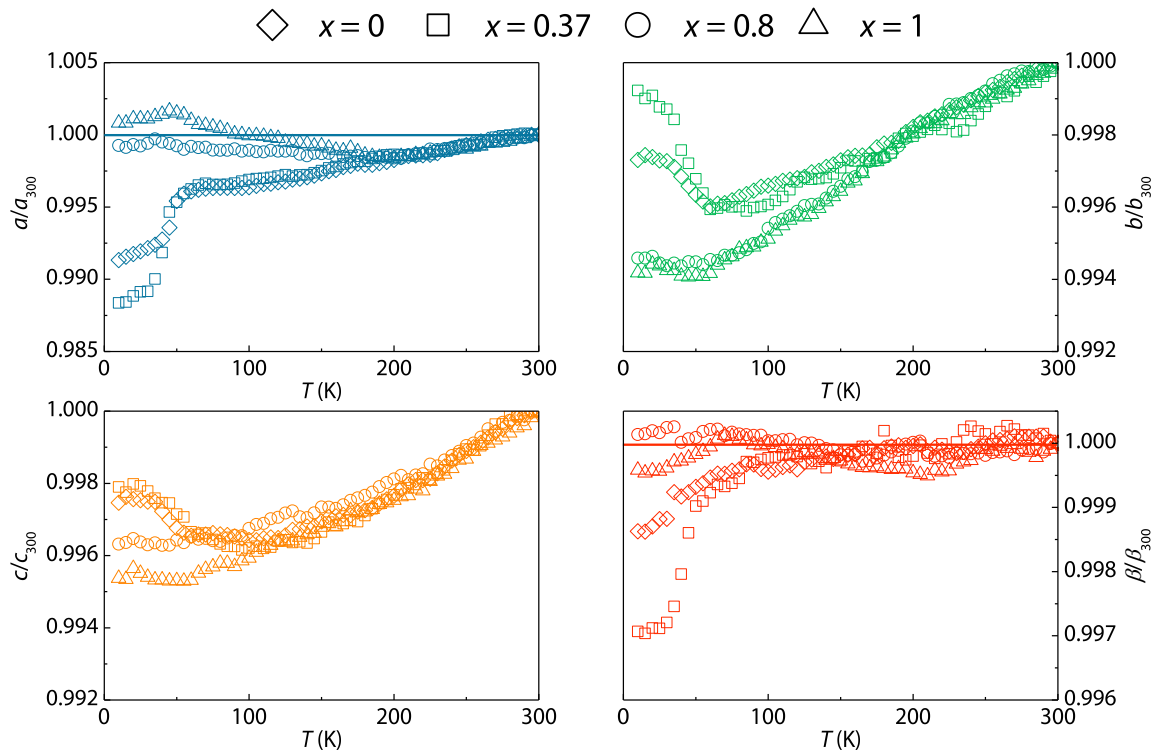


Figure 2.4-5: Comparison of the temperature dependent progression of lattice parameters in  $\text{Ca}_{1-x}\text{Pr}_x\text{Fe}_5\text{As}_3$ . The structural change at  $\sim 50$  K becomes more pronounced as  $x$  increases which is especially visible in parameters  $a$  and  $\beta$  but disappears at higher Pr-contents.

At intermediate Pr-contents, in this case  $x = 0.37$ , the general behavior of all structural features remains the same. However the steepness of the irregularity at 50 K becomes more pronounced in all parameters except  $c$  which shows the same behavior as observed in the undoped sample. At a Pr-content of  $x = 0.8$  this structural change is already completely suppressed. No noticeable

structural anomaly is visible but the structure rather seems to continuously contract along  $b$  and  $c$  while parameters  $a$  and  $\beta$  show no significant change. However, it is noteworthy that their behavior seems to be similar to that of the other samples down to 200 K and only deviates at lower temperatures, which also is mostly visible in  $b$ . In accordance with these findings the cell volume decreases without any apparent anomalies. The structural behavior then remains the same for in  $\text{PrFe}_5\text{As}_3$ .

These findings suggest that substitution of Ca with Pr at first enhances the structural irregularity but suppresses it at higher Pr-contents. This is reminiscent of the 122-type iron arsenides which often exhibit structural changes that require suppression in order to become superconductors.

On a structural level the change is most distinct in the interatomic distance between the iron atoms of the frame. This interatomic distance directly correlates to lattice parameters  $a$  and  $b$ . This means that the structural change is most likely driven by the bonding situation in the structural frame.

#### 2.4.5 Physical Properties of $\text{Ca}_{1-x}\text{Pr}_x\text{Fe}_5\text{As}_3$ ( $0 \leq x \leq 1$ ) at Low Temperatures

Field cooled susceptibility measurements employing fields of  $H \leq 30$  Oe show a magnetic order already present at 300 K and a reordering around 60 K-70 K (Figure 2.4-6). At low Pr-contents this reordering seems relatively weak and occurs over a wide temperature range whereas samples with higher Pr-contents show a more pronounced and narrow signal.

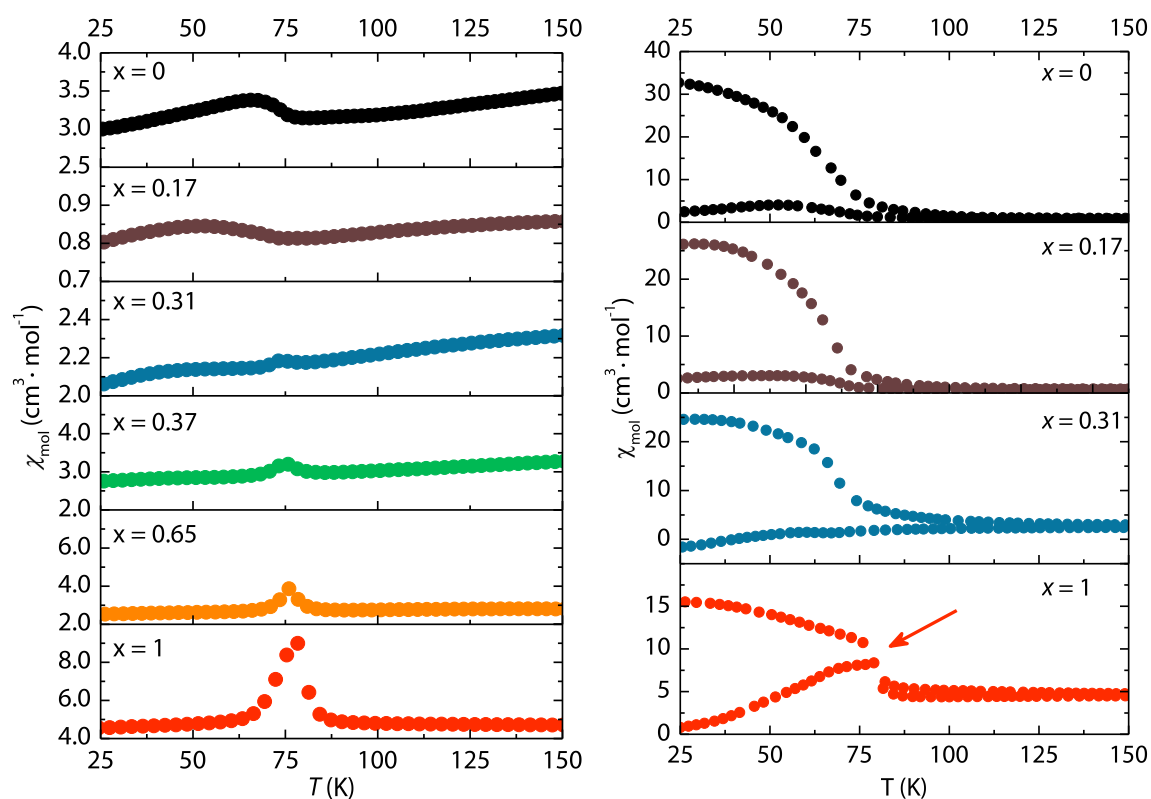


Figure 2.4-6: Left side: AC-Susceptibility measurements of  $\text{Ca}_{1-x}\text{Pr}_x\text{Fe}_5\text{As}_3$  at  $H = 3$  Oe. The emergence of a magnetic order at 75 K for increasing values of  $x$  is clearly visible. Right side: Susceptibility measurements at higher fields ( $H \leq 30$  Oe) show the weakness of the magnetic order as it becomes most distinct for  $x = 1$  (arrow).

To distinguish between the different magnetic orders occurring in a relatively close temperature range, measurements taken at zero-field conditions are compared with field cooled measurements taken with an external field applied. AC-Susceptibility measurements of selected samples at a low field of  $H = 3$  Oe show a possible correlation of the structural features discussed above with the magnetic behavior at low temperatures. All samples show a flat behavior of the susceptibility down to about 80 K. In undoped  $\text{CaFe}_5\text{As}_3$  the magnetic reordering appears around 75 K and stretches down to 25 K with its peak appearing at 60 K. With increasing Pr-content this order is suppressed and shifted to lower temperatures until it disappears completely at around  $x = 0.37$ . At the same time a different magnetic order at 75 K emerges, starting at  $x = 0.31$ , and gains intensity with increasing Pr-content until it reaches its maximum in  $\text{PrFe}_5\text{As}_3$ . This magnetic order is also faintly visible in field cooled DC-measurements as a kink, highlighted in the right plot of Figure 2.4-6. The signal remains unchanged for  $T > 150$  K which is why this temperature range is not depicted. These observations suggest a magnetic ordering of the  $\text{Pr}^{3+}$  moments additional to an ordering of the Fe-moments which yields this complex behavior. However, more detailed measurements on even purer samples will be necessary to elucidate the magnetism of  $(\text{Ca},\text{Pr})\text{Fe}_5\text{As}_3$ . As one would expect, the magnetic behavior of the samples could in no case be described with the Curie-Weiss law.

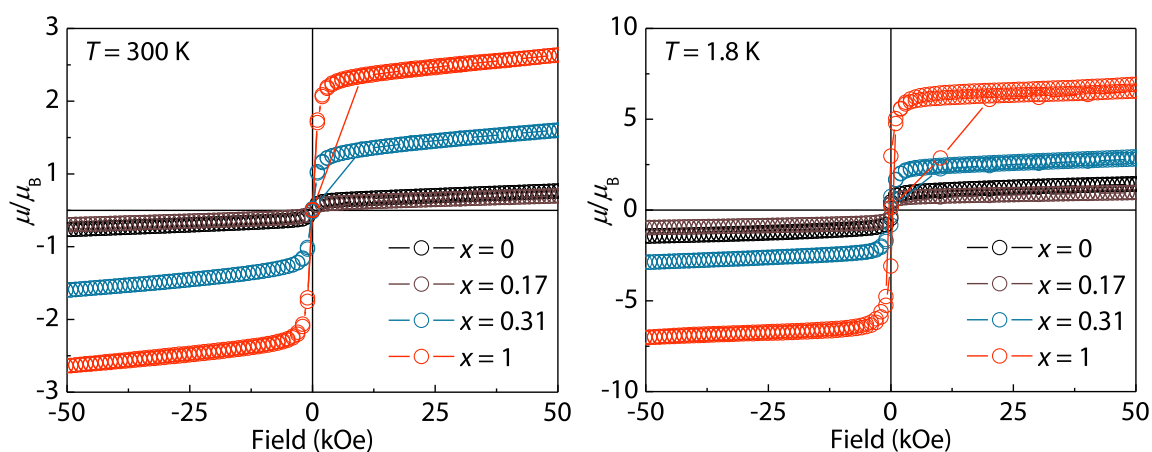


Figure 2.4-7: Isothermal magnetization per formula unit at 300 K (left) and 1.8 K (right).

Isothermal magnetization measurements shown in Figure 2.4-7 also show that at 300 K magnetic ordering is already present. Whether this is due to an impurity phase or a property of the main phase cannot be distinguished. However the high saturation moments which also increase with  $x$  further support the hypothesis that the ordering observed in the susceptibility measurements may be a re-ordering phenomenon.

## 2.4.6 Conclusions

In conclusion we could not only find that rare earth doping of  $\text{CaFe}_5\text{As}_3$  is possible but also achieve complete substitution of  $\text{Ca}^{\text{II}}$  with  $\text{Pr}^{\text{III}}$  resulting in the discovery of  $\text{PrFe}_5\text{As}_3$ . It is isotypic to  $\text{CaFe}_5\text{As}_3$  crystallizing in the space group  $P2_1/m$  with  $a = 7.206(1)$  Å,  $b = 3.886(1)$  Å,  $c = 9.765(1)$  Å and  $\beta = 100.5(1)^\circ$ .

Substitution of  $\text{Ca}^{\text{II}}$  with  $\text{Pr}^{\text{III}}$  in  $\text{CaFe}_5\text{As}_3$  was achieved over the complete range of  $0 \leq x \leq 1$  using high pressure synthesis. This marks the second compound in the system Ca-Fe-As for which this could be achieved and hints at a universal ability of these compounds to incorporate  $\text{Pr}^{\text{III}}$  and likely other rare earth metals for  $\text{Ca}^{\text{II}}$  without undergoing major structural changes. This also highlights the many possibilities high pressure synthesis has to offer for the discovery of new iron arsenide compounds.

The investigation of the solid solution  $\text{Ca}_{1-x}\text{Pr}_x\text{Fe}_5\text{As}_3$  revealed a linear behavior of lattice constants and monoclinic angle with  $x$ . This results in a linear increase in cell volume with increasing Pr content. At low temperatures  $\text{CaFe}_5\text{As}_3$  shows a non-linear structural behavior. Down to about 50 K all structural parameters decrease slightly, with a maximum relative change of 1.5% in  $a$ . Low temperature PXRD measurements also reveal a nonlinear structural change at 50 K in samples of  $\text{Ca}_{1-x}\text{Pr}_x\text{Fe}_5\text{As}_3$  with Pr-contents up to ~40%. This change, albeit only in the order of 0.1-1.5%, happens under symmetry and is visible in all structural parameters but most apparent in  $a$ . At higher Pr-contents up to 100% the structure contracts in an almost linear fashion without any apparent irregularities. The ability of the compound to incorporate aliovalent dopant atoms seems to be strongly correlated to a fitting atomic radius as experiments towards La-doping of  $\text{CaFe}_5\text{As}_3$  did not yield any results.

Measurements of the physical properties reveal an emerging magnetic order at 75 K for increasing Pr-contents. A magnetic order present in undoped  $\text{CaFe}_5\text{As}_3$  and at low Pr-contents is increasingly suppressed. This order albeit very weak could be shown to be an intrinsic property of the compound. Unfortunately detailed investigations such as neutron diffraction experiments or Mössbauer spectrometry are hindered by the presence of magnetically active impurity phases and the sample size limitation. We still found hints at a ferromagnetic nature of this order. Since  $\text{Fe}^{\text{I}}$  and  $\text{Fe}^{\text{II}}$  are both present in the structure, complex magnetic behavior is expected and our findings support this assumption. The correlation of the magnetic order with the structural changes is not clear although very likely, as both appear within the same temperature range. The magnetic order observed in undoped  $\text{CaFe}_5\text{As}_3$  is suppressed in the same way the structural change disappears with increasing Pr-content. The introduction of  $\text{Pr}^{\text{III}}$  into the structure gives rise to a distinct magnetic order at 75 K.

Very pure samples which allow for a detailed analysis by means of neutron diffraction and Mössbauer spectrometry will be needed to further investigate the magnetic interactions. However especially the sample size limitations of the high pressure setup pose a great challenge for future investigations of this system.

It will be interesting to further investigate other possible dopants not only on the Ca- but also the As- and Fe-site. The further investigation of the physical properties of doped and undoped  $\text{CaFe}_5\text{As}_3$  presents a great challenge but the results may lead to a more detailed understanding of the magnetic behavior of iron arsenides as a whole and help in the development of new superconducting materials.

---



## ACKNOWLEDGEMENTS

We would like to thank Wolfgang Schnick for courteously allowing us to use his 1000t press. This work was financially supported by the German Research Foundation (DFG) within the priority program SPP1458, Project No. JO257/6-2.

## 2.4.7 References

- [1] Y. Kamihara, T. Watanabe, M. Hirano, H. Hosono, *J. Am. Chem. Soc.* **2008**, *130*, 3296.
- [2] H. Takahashi, K. Igawa, K. Arii, Y. Kamihara, M. Hirano, H. Hosono, *Nature* **2008**, *453*, 376-378.
- [3] Z.-A. Ren, W. Lu, J. Yang, W. Yi, X.-L. Shen, Z.-C. Li, G.-C. Che, X.-L. Dong, L.-L. Sun, F. Zhou, Z.-X. Zhao, *Chin. Phys. Lett.* **2008**, *25*, 2215.
- [4] D. Johrendt, *Journal of Materials Chemistry* **2011**, *21*, 13726-13736.
- [5] D. C. Johnston, *Advances in Physics* **2010**, *59*, 803-1061.
- [6] S. R. Saha, N. P. Butch, T. Drye, J. Magill, S. Ziemak, K. Kirshenbaum, P. Y. Zavalij, J. W. Lynn, J. Paglione, *Physical Review B* **2012**, *85*, 024525.
- [7] K. Prokes, A. Kreyssig, B. Ouladdiaf, D. K. Pratt, N. Ni, S. L. Bud'ko, P. C. Canfield, R. J. McQueeney, A. I. Goldman, D. N. Argyriou, *J. Phys.: Conf. Ser.* **2011**, *273*, 012102.
- [8] T. Stürzer, C. Hieke, C. Löhnert, F. Nitsche, J. Stahl, C. Maak, R. Pobel, D. Johrendt, *Inorganic Chemistry* **2014**, *53*, 6235-6240.
- [9] I. Todorov, D. Y. Chung, C. D. Malliakas, Q. a. Li, T. Bakas, A. Douvalis, G. Trimarchi, K. Gray, J. F. Mitchell, A. J. Freeman, M. G. Kanatzidis, *Journal of the American Chemical Society* **2009**, *131*, 5405-5407.
- [10] I. Todorov, D. Y. Chung, H. Claus, K. E. Gray, Q. a. Li, J. Schleuter, T. Bakas, A. P. Douvalis, M. Gutmann, M. G. Kanatzidis, *Chemistry of Materials* **2010**, *22*, 4996-5002.
- [11] Y. Nambu, L. L. Zhao, E. Morosan, K. Kim, G. Kotliar, P. Zajdel, M. A. Green, W. Ratcliff, J. A. Rodriguez-Rivera, C. Broholm, *Physical review letters* **2011**, *106*, 037201.
- [12] Z. Gao, Y. Qi, L. Wang, D. Wang, X. Zhang, C. Yao, C. Wang, Y. Ma, *EPL* **2011**, *95*, 67002.
- [13] R. D. Shannon, *Acta Crystallographica Section A* **1976**, *32*, 751-767.
- [14] A. Iandelli, E. Franceschi, *J. Less-Common Metals* **1973**, *30*, 211-216.
- [15] G. Mu, B. Zeng, X. Zhu, F. Han, P. Cheng, B. Shen, H.-H. Wen, *Phys. Rev. B: Condens. Matter Mater. Phys.* **2009**, *79*.
- [16] H. Luo, Z. Wang, H. Yang, P. Cheng, X. Zhu, H.-H. Wen, *Superconductor Science and Technology* **2008**, *21*, 125014.
- [17] L. Vegard, *Zeitschrift für Physik A Hadrons and Nuclei* **1921**, *5*, 17-26.
- [18] T. Stürzer, Dissertation thesis, LMU (München), **2015**.

## 2.5 Details of the High Pressure Synthesis of Pr-doped $\text{CaFe}_2\text{As}_2$ and other Iron Pnictides

### 2.5.1 Introduction

The application of high pressure during synthesis is a fairly unexplored for iron pnictide superconductor research and especially the application of hydrostatic pressure in this context has been reported very rarely. As shown in the previous chapter this technique offers a gateway to hitherto unknown and otherwise unobtainable compounds with exciting properties. At the same time it offers new ways of investigating the properties of known systems via doping. The substitution of Ca in  $\text{CaFe}_2\text{As}_2$  with elements of smaller ionic radii for example is of interest because of the “chemical pressure” arising from the size mismatch that can greatly influence the physical properties of the host.<sup>[1-3]</sup> Furthermore the substitution of  $\text{Ca}^{\text{II}}$  with  $\text{RE}^{\text{III}}$  (rare earth elements) leads to electron doping of the  $\text{FeAs}_{4/4}$  layer thus offering an additional way to influence the physical properties of the host compound.

This chapter is intended to serve as a guideline for someone who wishes to apply high pressure synthesis in a multi-anvil setup for the synthesis of transition metal pnictides and/or chalcogenides.

### 2.5.2 Sample Preparation

The binary starting materials  $\text{CaAs}$ ,<sup>[4]</sup>  $\text{Fe}_2\text{As}$ <sup>[5]</sup> and  $\text{PrAs}$ <sup>[6]</sup> were prepared as described in the literature from the elements.

The 18/11 assembly as described in chapter 2.1 was compressed up to the respective pressure at room temperature, then heated to 1273 K within 60 minutes, kept at this temperature for 120 minutes, and cooled to room temperature in 360 minutes. Subsequently, the pressure was released. The necessary oil pressure  $p_{\text{Oil}}$  in bar was determined using a calibration curve. The compression/release times were calculated according to (1) and (2), respectively.

$$t_{\text{compression}} = \frac{p_{\text{Oil}} \cdot 60\text{min}}{72} \quad (1)$$

$$t_{\text{release}} = 3t_{\text{compression}} \quad (2)$$

The recovered MgO octahedron was cracked open in a glove box, and the sample was carefully isolated from the surrounding BN crucible. When needed, the isolated pellet was then ground in an agate mortar and kept inside the glove box for storage and preparation of physical measurements.

### 2.5.3 Influence of Pressure During Synthesis

In order to determine the most favorable synthesis conditions, the applied pressure was varied within a range of 2-6 GPa. Since *Muraba et al.* reported the successful synthesis of  $(\text{Sr},\text{La})\text{Fe}_2\text{As}_2$  at pressures below 4 GPa<sup>[7]</sup> we were surprised to find that the optimal pressure in a multi anvil setup for  $(\text{Ca},\text{Pr})\text{Fe}_2\text{As}_2$  was found to be 6 GPa. These conditions also yielded almost pure samples of

---

(La,Sr)Fe<sub>2</sub>As<sub>2</sub> which were discussed in chapter 0. The phase compositions of samples from synthesis at 2 GPa suggest that the reaction is incomplete (Figure 2.5-1). Between 3 GPa and 6 GPa there is a significant amount of CaFe<sub>4</sub>As<sub>3</sub> in all samples. At pressures of 6 GPa or above there is no significant change in the main phase fraction (~80 wt%), however the formation of CaFe<sub>4</sub>As<sub>3</sub> is suppressed. Also the phase fraction of (Ca,Pr)Fe<sub>5</sub>As<sub>3</sub> increases at higher pressures which is unfavorable.

Since Pr possesses nearly the same ionic radius as Ca, all Ca-containing impurity phases potentially incorporate some Pr which could be shown via PXRD and Rietveld refinements. This needs to be considered when aiming for a particular doping level in the main phase.

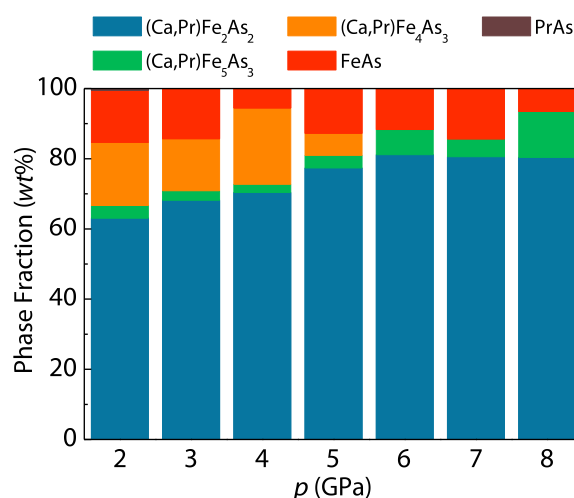


Figure 2.5-1: Pressure dependency of sample composition.

During the experiments, we found that this system seems to be particularly sensitive towards even a small inhomogeneity in pressure. This is why a homogenous and thorough compaction of the starting materials in the *h*-BN crucible is of crucial importance.

#### 2.5.4 Influence of Crucible Treatment

Another important aspect in the high pressure synthesis of iron arsenides is the complete absence of oxygen in the setup. In order to ensure that the *h*-BN crucibles are not contaminated by H<sub>3</sub>BO<sub>3</sub> or other boron-oxygen compounds, the crucibles were refluxed for 8 h in dry, absolute EtOH over molar sieve (Fluka, Molecular sieve UOP Type 3A, pore size 3 Å). These contaminations could otherwise serve as an oxygen source during synthesis. Drying of the EtOH was achieved with the same molar sieve. The crucibles were subsequently dried under vacuum and stored in a glove box.

#### 2.5.5 Conductivity Measurements on Unrefined Samples

It is possible to directly measure the conductivity on sample pellets that have not been ground or otherwise treated after recovery from the MgO octahedron. This may be useful for compounds that undergo a structural transition upon grinding or cannot be pelletized and sintered.

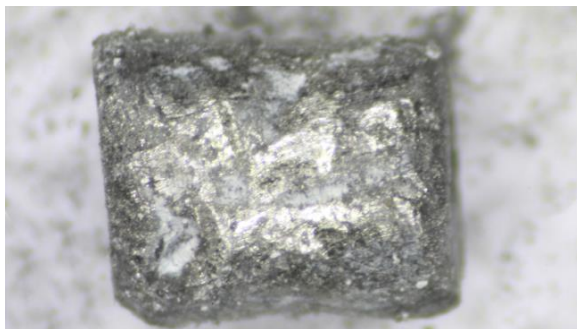


Figure 2.5-2: The pellet needs to be clean and regularly shaped.

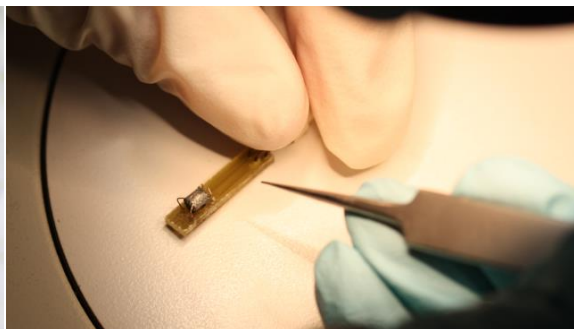


Figure 2.5-3: The pellet is placed on the sample holder and fixed with a small amount of grease.

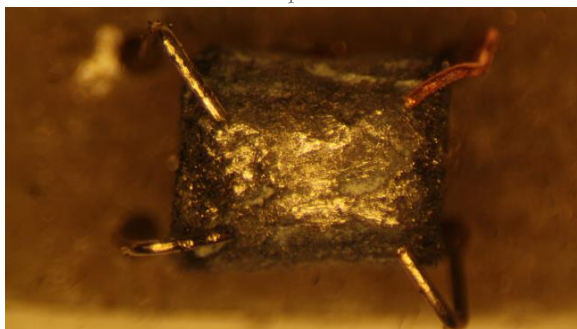


Figure 2.5-4: The connectors of the sample holder are bent into position.

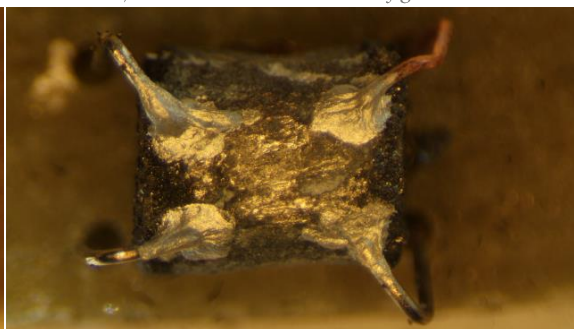


Figure 2.5-5: The connection is finalized with the application of conductive varnish.

The recovered pellet has to be of regular shape (regular cylinder without crooked surfaces or major dents/scratches) and needs to be carefully cleansed from *h*-BN in order to allow for a clean connection of the measuring setup (Figure 2.5-2). It is necessary to use a sample holder that allows for free positioning of the connectors to accommodate the unusual sample shape. In a next step the sample is fixed with a small amount of grease on the sample holder (Figure 2.5-3). The connectors are bent into the desired position (Figure 2.5-4) and connection is completed with the application of conductive varnish (Figure 2.5-5). It is very important to cover the setup in a polymer foil as the pellet can disintegrate into a fine powder should a structural transition take place in the desired temperature range. Furthermore, as the sample shape is not suitable for a meaningful *van-der-Pauw*-measurement, the resulting data should only be evaluated qualitatively.

### 2.5.6 Crystal Growth from FeAs Flux under High Pressure

Some preliminary experiments towards growing larger single crystals from a FeAs-flux under pressure were done in a 25/17 assembly. The starting materials were carefully mixed with the flux material at a ratio of 1:2. A pressure of 4 GPa was applied, the mixture was heated to 1273 K and kept at this temperature for 2 h. The assembly was then slowly cooled to room temperature at a rate of 10 K/h and the pressure released afterwards. The experiment yielded rather large single crystals but the identification of target phase crystals and the separation from the flux were not trivial. Another major problem was the reactivity of the *h*-BN crucible at these long heating times. One needs to find different materials in order to avoid contamination of the sample and loss of starting materials.

### 2.5.7 Conclusions

The multi-anvil setup has proven to be a promising tool in the explorative synthesis aiming at the discovery of new superconductors. This chapter summarizes the smaller aspects of the high pressure synthesis that was employed in the previously described experiments. While they may not seem particularly important at first, they have proven to be crucial to the success of the experiments.

The pressure dependency of the phase composition shows that the response of the system to hydrostatic pressure differs from that of other systems. While higher pressure is generally beneficial for purer samples, there is a maximum of the attainable phase fraction. To achieve optimal sample purity the absence of even trace amounts of oxygen has to be ensured. This was done by refluxing the crucibles in dry ethanol for 8 hours. Conductivity measurements on unrefined samples were shown to be possible in order to qualitatively analyze the properties of compounds that cannot be pelletized and/or sintered once ground. Finally a technique for growing larger single crystals from FeAs-flux under pressure was introduced. While this method still suffers from some problems, it may be a useful tool in the further investigation of the properties of highly electron doped  $\text{CaFe}_2\text{As}_2$ ,  $\text{CaFe}_5\text{As}_3$  and other iron arsenides.

Overall the results presented in this section highlight the range of possible outcomes when straying from the path of more traditional solid state synthesis. The discovery of rare earth iron arsenides  $\text{PrFe}_2\text{As}_2$  and  $\text{LaFe}_2\text{As}_2$  as well as the  $\text{CaFe}_5\text{As}_3$  system give a glance at the possibilities that lie in the application of this synthetic technique. It will be exciting to see what other discoveries will be made involving high pressure synthesis.

### 2.5.8 Reference

- [1] D. Johrendt, *Journal of Materials Chemistry* **2011**, *21*, 13726-13736.
- [2] H. L. Shi, H. X. Yang, H. F. Tian, C. Ma, J. B. Lu, Z. W. Wang, Y. B. Qin, Y. J. Song, J. Q. Li, *J. Phys. Chem. Solids* **2011**, *72*, 420-422.
- [3] F. Ronning, T. Klimczuk, E. D. Bauer, H. Volz, J. D. Thompson, *J. Phys.: Condens. Matter* **2008**, *20*, 322201.
- [4] A. Iandelli, E. Franceschi, *J. Less-Common Metals* **1973**, *30*, 211-216.
- [5] H. Katsuraki, N. Achiwa, *Journal of the Physical Society of Japan* **1966**, *21*, 2238.
- [6] G. Mu, B. Zeng, X. Zhu, F. Han, P. Cheng, B. Shen, H.-H. Wen, *Phys. Rev. B: Condens. Matter Mater. Phys.* **2009**, *79*.
- [7] Y. Muraba, S. Matsuishi, S.-W. Kim, T. Atou, O. Fukunaga, H. Hosono, *Physical Review B* **2010**, *82*, 180512.



## 3 MICROWAVE BASED SYNTHESIS OF TRANSITION METAL Pnictides and Chalcogenides

### 3.1 Introduction

The energy efficiency of manufacturing processes has been getting more and more attention in recent years. Microwave heating may be able to offer a way of significantly reducing the energy consumption, especially for the preparation of materials with high formation temperatures. But despite their advantages, microwave based heating methods are still not widely used among solid state and material chemists. This chapter aims to contribute to the understanding of microwave based synthesis through the exploration of several different classes of materials and their preparation via microwave heating.

#### 3.1.1 The History of Microwaves

Microwave radiation is a form of electromagnetic radiation with wavelengths between one meter and one millimeter, resulting in frequencies between 300 MHz and 300 GHz.<sup>[1]</sup> It is usually generated in a diode with a cylindrical anode, called a magnetron. The magnetron was first discovered in 1921 and developed into the basic technology for radar applications as well as communication by English and American military researchers.<sup>[2-4]</sup> Today it is used in many applications ranging from navigation to Wireless LAN communication but the most familiar one might be the domestic microwave oven (DMO). To avoid interference with telecommunication frequencies, all microwave heating applications are required to use ISM bands (Industrial Scientific and Medical frequencies) which are 27.12 MHz, 915 MHz and 2.45 GHz, the latter of which is the frequency used in DMOs.<sup>[1]</sup>

The heating capabilities of microwaves were supposedly discovered when a chocolate bar in the pocket of *P.L. Spencer*, who was a scientist at a major radar manufacturer, began to melt. Other versions of this legend involve corn kernels popping in his pockets. Still, whether molten chocolate or popcorn, *Spencer* went on to patent the first microwave oven in 1952 and nowadays a DMO is found in nearly every kitchen.<sup>[5]</sup>

Because of their efficiency and speed, microwave conveyors are widely used in gastronomic industry as well.<sup>[6]</sup> The efficiency of microwave heating can be illustrated with a report by the International Energy Agency (IEA). It has found that during its life time, a DMO consumes more energy for the clock that is usually built in, than it does for actually heating food.<sup>[7]</sup> While heating of a meal mostly happens through the excitations of water molecules, microwaves show a wide range of interactions with solids of all kinds. This made it a highly researched method of heat generation for chemical synthesis.

#### 3.1.2 Physical Principles of Microwave Radiation

In order to provide a better understanding of the particularities of microwave heating in solid state synthesis, some basic physical principles behind the interaction of microwaves and matter have to be understood.

---

When an object is subjected to microwave radiation it becomes polarized. Since dipolar polarization  $P_d$  happens on the same timescale as the oscillation of microwaves, the intrinsic properties of a dielectric can be related to the electromagnetic field strength  $E$  as shown in equation 1.

$$P_d = \epsilon_0(\epsilon_r - 1)E = E(\epsilon_0\epsilon_r - \epsilon_0) \quad (1)$$

Here  $\epsilon_0$  is the permittivity of free space, and  $\epsilon_r$  is the relative permittivity of the material. The permittivity of real world materials is a complex quantity which is expressed as  $\epsilon^* = \epsilon' + i\epsilon''$ . It consists of two components,  $\epsilon'$  representing the time independent polarizability of a material and  $\epsilon''$  which accounts for the time dependent efficiency of the conversion of electromagnetic energy into heat. Since all samples discussed in this work are metallic, a discussion of the principles of dielectric heating will be omitted.

In the case of conductive samples like carbon or metals, ohmic heating has to be taken into account. This means adding a term to  $\epsilon^*$  that accounts for the interaction of the charge carriers in these materials with the applied electric field.

$$\epsilon_0\epsilon_r = \epsilon^* = \epsilon' - i\epsilon'' - \left(\frac{i\sigma_i}{\omega\epsilon_0}\right) \quad (2)$$

This so called conduction term is added in the far right side of equation 2 and includes the conductivity  $\sigma_i$  of a material, as well as the frequency  $\omega$  of the microwave field. This term hence has a great influence on the polarizability of a conductive sample and all deducted quantities.

The total power absorbed by a sample  $P$ , can then be written as shown in (2) where  $\sigma$  is the total effective conductivity of the material,  $f$  is the frequency of the microwave field, and  $E$  is the magnitude of the internal electric field.

$$P = \sigma|E|^2 = 2\pi f\epsilon_0\epsilon''|E|^2 \quad (3)$$

This means the heating of a sample in a microwave field depends not only on the power of the field and for how long it is applied. The efficiency of the energy to heat conversion, which can be represented by the conductivity of a sample, plays an important role as well. This is one reason why microwave heating is fundamentally different from other heating methods.

Furthermore for practical applications, the penetration depth  $D_p$  of a given material has to be considered. It represents the distance from the sample surface at which the electric field is damped to  $1/e$  of its surface value.

$$D_p = \frac{\lambda_0\sqrt{\epsilon'}}{2\pi\epsilon''} \quad (4)$$

Here  $\lambda_0$  is the wavelength of the microwave radiation. This means the more efficient the conversion of electromagnetic energy to heat, the smaller  $D_p$  becomes. For conducting starting materials this means that a small particle size is beneficial for an even heat distribution across the



sample because  $D_p$  usually has a magnitude of only several  $\mu\text{m}$  in metals. At the same time this means only crucible materials that are virtually transparent to microwave radiation should be used.

### 3.1.3 Practical aspects of microwave heating

Since microwave heating is fundamentally different from other methods some practical aspects have to be taken into account.

Microwave heating is usually direct heating. This means the material itself interacts with the microwave radiation leading to a volumetric heating of the sample. This leads to a temperature profile that is the inverse of conventional furnace heating, where the surface of a sample becomes hotter than the inside.<sup>[8, 9]</sup> This is the main reason for the significantly lower energy requirements of microwave heating, as the heat is generated precisely where it is wanted.

Another aspect resulting from the direct interaction of microwave radiation with a substance is the extremely rapid rise of temperature. This is the main reason for drastically reduced reaction times but also for evaporation of some compounds. At the same time the end of irradiation means an immediate stop of heating. This quenching of the reaction may or may not be beneficial, depending on whether metastable products can form or are wanted, respectively.

The specificity of microwave heating also makes it vastly different from conventional heating methods. Depending on the sample composition, only specific regions may be heated while others remain unaffected by the radiation. Thus a homogenous sample is usually favorable but the regionally specific heating can also be exploited for certain starting material compositions.

### 3.1.4 Chemical application of microwave heating

The first use of microwaves as a heat source for chemical synthesis was reported in 1971 but it took almost 15 years until the first chemical reaction in a DMO was reported in 1986.<sup>[10, 11]</sup> Since microwave applicators were rather hard to come by and usually targeted towards organic synthesis, this marked a turning point. Now that microwave chemistry was easily accessible for researchers outside the solution based disciplines as well, it started to attract more and more attention.

The use of microwaves in the preparation of organic as well as solution-phase compounds was able to rapidly enhance the reaction rates, often by several orders of magnitude.<sup>[12]</sup> Naturally this led to interest in the industrial application of this technique. Today microwave based synthesis is a well-established technique in the preparation and procession of organic, pharmaceutical and medicinal chemicals.<sup>[13]</sup> The availability of specific laboratory grade microwave applicators further highlights its significance in contemporary organic and solution-phase chemistry.

### 3.1.5 Microwaves and materials chemistry

The situation in materials and solid state chemistry however is somewhat different. Over the course of the 1980's, the potential of microwave based synthesis was investigated by a number of material scientists.<sup>[14, 15]</sup> While exploring new synthetic method for the preparation of ceramic

---

superconductors like  $\text{YBa}_2\text{Cu}_3\text{O}_{7-x}$  or  $\text{Bi}_2\text{Sr}_2\text{CaCu}_2\text{O}_{8-x}$  microwave based synthesis was successfully employed. Protocols not just in laboratory microwave devices but also in DMOs were reported and patented.<sup>[16-21]</sup>

Since then the appeal of being able to prepare samples in a fraction of the time needed with solid state synthesis has led to a plethora of protocols for many different classes of materials. These range from the ceramic superconductors to oxidic Eu-doped<sup>[22-24]</sup> as well as Ce-doped<sup>[25]</sup> phosphors and other ceramics<sup>[26-30]</sup> to thermoelectric materials<sup>[31, 32]</sup> and metallic compounds.<sup>[33-35]</sup> Even some more exotic materials like the chalcogenide glass  $\text{As}_{40}\text{Se}_{60}$  have been prepared in a domestic microwave oven.<sup>[36]</sup>

But despite these numerous successful applications, microwave heating still has little significance in materials and solid state chemistry. There are several reasons contributing to this phenomenon. One particular problem is the lack of commercially available microwave applicators tailored to the needs of solid state synthesis. Reaction temperatures often reach more than 1273 K which requires insulation and several other adjustments compared to solution phase synthesis. Also the monitoring of temperature and other reaction parameters is significantly more complex and often virtually impossible. Another aspect is the lack of understanding of many interactions between microwaves and solid matter. Besides heating there are hypotheses concerning nonthermal interactions that might play a role in microwave based solid state synthesis but are not easily verifiable.<sup>[37, 38]</sup>

Still, since the understanding of these interactions has grown over the last few years, some pilot- and full-scale applications in chemical processing have been established. The advantages of microwave heating in many steps of solid state synthesis along with the growing interest in green chemistry will probably lead to an increase in commercial applications in the next few years.<sup>[39, 40]</sup>

In 1999 *Rao et al.* provided an overview of the state of the art in microwave based solid state synthesis.<sup>[41]</sup> Since then there has been a rapid growth of knowledge which was comprehensively reviewed by *Kitchen et al.* in 2014.<sup>[42]</sup> The reader is kindly encouraged to refer to these resources for a more detailed overview of the many laboratory and industrial applications of microwave heating in solid state chemistry.

### **3.1.6 Microwave based synthesis of pnictides and chalcogenides**

In the synthesis of metal chalcogenides from the elements the selectivity of microwave heating has been shown to be very beneficial.<sup>[43]</sup> Since the metallic components of the starting mixture are preferentially heated, they can react very quickly with the otherwise volatile chalcogen. This way a number of different chalcogenide compounds, for example the *Zintl* phases  $\text{Na}_3\text{SbTe}_3$ ,  $\text{NaSbTe}_2$  and  $\text{K}_3\text{SbTe}_3$ , were obtained in a DMO. The formation of a particular phase could in this case even be directed via power level and irradiation time.<sup>[44]</sup>

---

While many metal nitrides were obtained via microwave heating, this method has only been reported for five other pnictides. One publication details the preparation of  $\text{Li}_3\text{Bi}$  and  $\text{Li}_3\text{Sb}$  in carbon coated quartz ampoules at 900 W in a DMO within 1 min and 2 min, respectively.<sup>[45]</sup>

The other is the only report on the microwave based synthesis of iron pnictide superconductors so far. A DMO was employed in the preparation of  $\text{NdFeAsO}$  and  $\text{NdFe}_{0.9}\text{Co}_{0.1}\text{AsO}$  from the elements and  $\text{Nd}_2\text{O}_3$  as starting materials within 10x5 min intervals.<sup>[46]</sup> The resulting samples were of high purity and became superconducting at  $T_c = 16$  K. Furthermore a patent for the microwave based preparation of the related  $\text{SmFeAsO}_{0.85}\text{F}_{0.15}$  was filed by scientists at the Shanghai Institute for Ceramics in 2012.<sup>[47]</sup>

These reports show that the rapid and energy saving preparation of iron pnictides in a microwave indeed yields promising results. However the lack of knowledge of the microwave based synthesis of pnictides remains an obstacle. In this chapter the findings on basic principles of the microwave based preparation of pnictides and related compounds are presented. Based on these results a time saving technique for the identification of suitable dopants for a given system has been developed and applied to  $\text{Ca}_2\text{Cu}_6\text{P}_5$ . The results may aid in an accelerated further exploration of pnictide superconductors and other compounds.

### 3.1.7 References

- [1] D. Stuerger, in *Microwaves in Organic Synthesis, Vol. 1*, 2 ed. (Ed.: A. Loupy), Wiley-VCH Verlag, Weinheim, **2006**, pp. 1-57.
  - [2] A. W. Hull, *Phys. Rev.* **1921**, *18*, 31-57.
  - [3] A. W. Hull, *American Institute of Electrical Engineers, Journal of the* **1921**, *40*, 715-723.
  - [4] E. H. Hans, *Washington, DC: U.S. Patent and Trademark Office* **1938**, U.S. Patent No. 2,123,728.
  - [5] R. V. Decareau, R. A. Peterson, *Microwave processing and engineering*, VCH, **1986**.
  - [6] G. Meurant, *Advances in food research*, Elsevier Science, **1951**.
  - [7] IEA, in *More Data, Less Energy - Making Network Standby More Efficient in Billions of Connected Devices*, International Energy Agency, France, **2014**, p. 18.
  - [8] D. E. Clark, W. H. Sutton, *Annu. Rev. Mater. Sci.* **1996**, *26*, 299-331.
  - [9] A. a. Metaxas, R. J. Meredith, *Industrial microwave heating*, IET, **1983**.
  - [10] R. Gedye, F. Smith, K. Westaway, H. Ali, L. Baldisera, L. Laberge, J. Rousell, *Tetrahedron Lett.* **1986**, *27*, 279-282.
  - [11] S. W. Liu, J. P. Wightman, *J. Appl. Chem. Biotechnol.* **1971**, *21*, 168-172.
  - [12] R. J. Giguere, T. L. Bray, S. M. Duncan, G. Majetich, *Tetrahedron Lett.* **1986**, *27*, 4945-4948.
  - [13] C. O. Kappe, A. Stadler, D. Dallinger, *Microwaves in Organic and Medicinal Chemistry, Vol. 52*, 2nd ed., Wiley-VCH, Weinheim, **2012**.
-

- [14] D. R. Baghurst, A. M. Chippindale, D. M. P. Mingos, *Nature (London)* **1988**, 332, 311.
- [15] R. Roy, S. Komarneni, L. J. Yang, *J. Am. Ceram. Soc.* **1985**, 68, 392-395.
- [16] K. G. K. Warriar, H. K. Varma, T. V. Mani, A. D. Damodaran, *J. Am. Ceram. Soc.* **1992**, 75, 1990-1992.
- [17] K. Naitoh, T. Takizawa, T. Matsuse, *Jpn. J. Appl. Phys., Part 2* **1999**, 38, 724-726.
- [18] M. Kato, K. Sakakibara, Y. Koike, *Appl. Supercond.* **1998**, 5, 33-39.
- [19] M. Kato, K. Sakakibara, Y. Koike, *Jpn. J. Appl. Phys., Part 1* **1999**, 38, 5867-5868.
- [20] D. Grossin, C. Harnois, S. Marinel, J. G. Noudem, *J. Eur. Ceram. Soc.* **2005**, 25, 2939-2942.
- [21] O. Vasilievna Kharissova, B. Ildusovich Kharissov, F. Mendirichaga Orozco, A. A. Cueva Zambrano, M. Cueva Zambrano, Oxana Vasilievna Kharissova, Mex. . **2014**, p. 20pp.
- [22] T. Ishigaki, H. Mizushina, K. Uematsu, N. Matsushita, M. Yoshimura, K. Toda, M. Sato, *Mater. Sci. Eng., B* **2010**, 173, 109-112.
- [23] H.-Y. Chen, R.-Y. Yang, S.-J. Chang, *Mater. Lett.* **2010**, 64, 2548-2550.
- [24] R.-Y. Yang, H.-Y. Chen, C.-M. Hsiung, S.-J. Chang, *Ceram. Int.* **2011**, 37, 749-752.
- [25] A. Birkel, K. A. Denault, N. C. George, C. E. Doll, B. Hery, A. A. Mikhailovsky, C. S. Birkel, B.-C. Hong, R. Seshadri, *Chem. Mater.* **2012**, 24, 1198-1204.
- [26] P. D. Ramesh, B. Vaidhyanathan, M. Ganguli, K. J. Rao, *J. Mater. Res.* **1994**, 9, 3025-3027.
- [27] P. D. Ramesh, D. Brandon, L. Schachter, *Mater. Sci. Eng., A* **1999**, A266, 211-220.
- [28] W. L. E. Wong, S. Karthik, M. Gupta, *Mater. Sci. Technol.* **2005**, 21, 1063-1070.
- [29] D. K. Agrawal, *Curr. Opin. Solid State Mater. Sci.* **1998**, 3, 480-485.
- [30] Z. Xie, C. Wang, X. Fan, Y. Huang, *Mater. Lett.* **1999**, 38, 190-196.
- [31] C. S. Birkel, W. G. Zeier, J. E. Douglas, B. R. Lettiere, C. E. Mills, G. Seward, A. Birkel, M. L. Snedaker, Y. Zhang, G. J. Snyder, T. M. Pollock, R. Seshadri, G. D. Stucky, *Chemistry of Materials* **2012**, 24, 2558-2565.
- [32] K. Biswas, S. Muir, M. A. Subramanian, *Mater. Res. Bull.* **2011**, 46, 2288-2290.
- [33] J. W. Lekse, T. J. Stagger, J. A. Aitken, *Chemistry of Materials* **2007**, 19, 3601-3603.
- [34] C. Mastrovito, J. W. Lekse, J. A. Aitken, *J. Solid State Chem.* **2007**, 180, 3262-3270.
- [35] A. G. Whittaker, D. M. P. Mingos, *J. Chem. Soc., Dalton Trans.* **1993**, 2541-2543.
- [36] N. Prasad, D. Furniss, H. L. Rowe, C. A. Miller, D. H. Gregory, A. B. Seddon, *J. Non-Cryst. Solids* **2010**, 356, 2134-2145.
-

- [37] D. A. C. Stuerger, P. Gaillard, *Journal of Microwave Power and Electromagnetic Energy* **1996**, 31, 87-100.
- [38] D. A. C. Stuerger, P. Gaillard, *Journal of Microwave Power and Electromagnetic Energy* **1996**, 31, 101-113.
- [39] J. G. P. Binner, B. Vaidhyanathan, *Key Eng. Mater.* **2004**, 264-268, 725-730.
- [40] E. Dudnik, Z. Zaitseva, A. Shevchenko, L. Lopato, *Powder Metallurgy and Metal Ceramics* **1995**, 34, 263-271.
- [41] K. J. Rao, B. Vaidhyanathan, M. Ganguli, P. A. Ramakrishnan, *Chem. Mater.* **1999**, 11, 882-895.
- [42] H. J. Kitchen, S. R. Vallance, J. L. Kennedy, N. Tapia-Ruiz, L. Carassiti, A. Harrison, A. G. Whittaker, T. D. Drysdale, S. W. Kingman, D. H. Gregory, *Chem Rev* **2014**, 114, 1170-1206.
- [43] A. G. Whittaker, D. M. P. Mingos, *J. Chem. Soc., Dalton Trans.* **1992**, 2751-2752.
- [44] G.-T. Zhou, V. G. Pol, O. Palchik, R. Kerner, E. Sominski, Y. Koltypin, A. Gedanken, *Journal of Solid State Chemistry* **2004**, 177, 361-365.
- [45] G.-T. Zhou, O. Palchik, V. G. Pol, E. Sominski, Y. Koltypin, A. Gedanken, *J. Mater. Chem.* **2003**, 13, 2607-2611.
- [46] S. W. Muir, O. D. Rachdi, M. A. Subramanian, *Mater. Res. Bull.* **2012**, 47, 798-800.
- [47] F. Huang, H. Chen, A. Fang, Z. Liu, X. Xie, *Faming Zhuanli Shenqing* **2014**, CN 103771861, 8pp.
-

## 3.2 Materials and Methods

### 3.2.1 Sample preparation

A mixture of the respective starting materials was intimately mixed and filled into a crucible. The crucible material was chosen according to the desired compound (for details see chapter 3.2.3) and sealed in a quartz tube under Ar atmosphere. After the synthesis was completed the quartz tube was cracked open and the contents of the crucible were ground in an agate mortar. The preparation and handling as well as the storage of the powdered samples were done in a glove box (Unilab, MBraun, Garching; O<sub>2</sub> < 1 ppm, H<sub>2</sub>O < 1 ppm) under purified Ar (99.999%, Air Liquide).

#### SOLID STATE SYNTHESIS OF STARTING MATERIALS

CuP<sub>2</sub> was obtained through solid state synthesis from stoichiometric amounts of transition metal powder and red phosphorus lumps which were carefully mixed but not ground. The size of the starting materials turned out to be crucial as neither the use of Cu granules nor of P powder led to formation of the target phase. The mixture was heated to 1073 K at a rate of 20 K/h, kept at this temperature for 24 h and cooled to room temperature within 8 h. Synthesis was carried out in tubular resistance furnaces with Pt/PtRh or NiCr/Ni thermocouples and PID temperature controllers (Eurotherm, model 2408). The heating profiles were customized based on the synthesis of other transition metal pnictides.<sup>[1]</sup> Table 3.2-1 lists all other substances that were used in the following experiments.

Table 3.2-1: Substances used in the experiments.

Substance	Purity	Molar weight (g/mol)	Appearance	Supplier
As	99.95 %	74.9216	Powder	Sigma-Aldrich
Ca	99.99 %	40.078	Dendritic pieces	Sigma-Aldrich
Co	99.9 %	58.933200	Powder	Sigma-Aldrich
Cu	99.99 %	63.546	Powder	Chempur
Cu	99.99 %	63.546	Granules	Chempur
Fe	99.90 %	55.845	Powder	Chempur
Ge	99.999 %	72.64	Powder	Sigma-Aldrich
Mn	99.985 %	54.938	Powder	Alfa Aesar
Ni	99.99 %	58.6934	Powder	Chempur
P	99.999 %	30.9738	Pieces	Chempur
S	99.999 %	32.065	Powder	Sigma-Aldrich
Sb	99.999 %	121.760	Powder	Alfa Aesar
Se	99.999 %	78.96	Powder	Chempur
Si	99.99 9%	28.0855	Powder	Merck

### 3.2.2 Sample characterization

#### X-RAY DIFFRACTION

The sample composition was analyzed via powder X-ray diffraction (PXRD) on a STOE Stadi P diffractometer (Mo K $\alpha$ <sub>1</sub> radiation, Ge[111] monochromator) and a Huber G670 Guinier imaging plate diffractometer (Cu-K $\alpha$ <sub>1</sub> radiation, Ge[111] monochromator), respectively. Low temperature

PXRD was performed using the latter setup but with Ge[111] monochromated Co-K $\alpha_1$  radiation. Temperatures between 300 K and 8 K were achieved using a cryostat (CTI-Cryogenics, Model 22 CP) controlled by a Si-diode sensor (Lakeshore, model 331). Diffractograms over a range of 6.5-100 ° were recorded at temperatures from 10 K to 300 K. Data acquisition in all cases was done using the STOE software (WinX<sup>POW</sup>), data recorded on the Huber G670 diffractometers was corrected using a custom script.<sup>[2]</sup> Rietveld refinements were performed with the TOPAS package.<sup>[3]</sup>

Single Crystal diffractometry was performed on a BRUKER D8 Quest diffractometer using Mo-K $\alpha$  radiation. Structures were solved using the charge flipping method implemented in the JANA2006 program package, structure refinement was done using JANA2006 as well.<sup>[4]</sup>

### **SCANNING ELECTRON MICROSCOPY (SEM) AND ENERGY DISPERSIVE X-RAY ANALYSIS (EDX)**

Verification of the chemical composition and morphological analysis was performed in a Carl Zeiss EVO-MA 10 SEM with SE (secondary electrons), BSE (back scattered electrons) detectors as well as a Bruker Nano EDX (X-Flash 420-M) detector. The samples were fixed on an Al sample holder with an adhesive conducting carbon film. The elements C and Al were hence excluded from the measurement. The composition of a particular crystallite was determined by averaging 10-20 individual spectra taken from different locations.

### **MAGNETIC MEASUREMENTS**

AC-Susceptibility as well as magnetization measurements were carried out using a MPM-XL (Quantum Design) SQUID magnetometer which allowed for measurements at fields between -50 kOe and 50 kOe and temperatures between 1.8 K and 400 K.

Further susceptibility measurements were done on a custom device employing a differential dual-coil setup at an applied field of 3 Oe. Temperatures ranging from 3.5 K to 300 K could be achieved. A detailed description of this setup can be found in the literature.<sup>[5]</sup>

All magnetic measurements were carried out on 20-50 mg of each respective sample which were transferred into a gelatin capsule that was then fixed in a plastic straw. The data were processed using an automated script.<sup>[6,7]</sup>

### **ELECTRICAL RESISTIVITY**

Resistivity measurements were carried out using a custom built setup employing the *van-der-Pauw* method at temperatures between 3.5 K and 300 K. Samples were cold pressed into pellets at 10 kN beforehand (4 mm diameter, ca 0.8 mm thickness) and sintered at 773 K for 10 h.

### **DFT CALCULATIONS**

Self-consistent DFT band structure calculations were performed using the LMTO-method in its scalar relativistic version as implemented in the TB-LMTO-ASA program.<sup>[8-10]</sup> Reciprocal space integrations were performed with the tetrahedron method using 16x16x16 irreducible *k*-points in the tetragonal Brillouin zone. The basis sets were Ca-4s/[4p]/3d, Cu-4s/4p/3d and P-3s/3p/[3d]. Orbitals in brackets were downfolded.

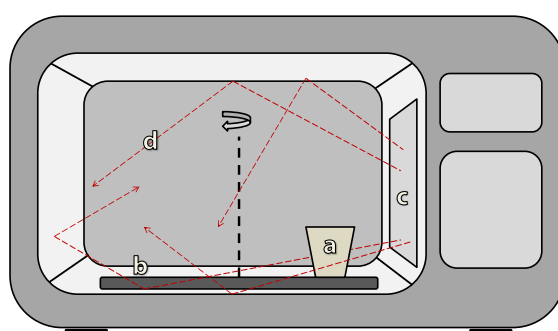
---

### 3.2.3 Microwave based synthesis

The following chapters detail the results of experiments that have been conducted with the goal to obtain several transition metal pnictides and chalcogenides by means of microwave based synthesis. Because this technique is unusual for these types of materials the experimental setup is discussed in detail.

#### EXPERIMENTAL SETUP

The DMO model used in all following experiments was a Panasonic NN-GD462M with a maximum power output of 1000 W and inverter technology. This is important as it ensures a continuous irradiation of the sample space as opposed to the pulsed heating mode in other models. Figure 3.2-1 illustrates the basic setup of the DMO as well as the positioning of the experimental setup.



a – Sample b – Rotor c – Magnetron outlet d – Radiation

Figure 3.2-1: Basic setup of the DMO.

Since the MW field in the sample chamber is not homogeneous one has to find the “sweet spot” before any reproducible experiments are possible. This is the spot that is most evenly irradiated during heating and allows for reproducible heating conditions. This area can be found either by placing activated carbon in a flat container that radially spans the rotator or, alternatively, by placing a sufficiently long piece of thermally active paper (e.g. credit card receipt) in the same way. The sample space is then irradiated at a low or intermediate power level and the spot that first glows (when using carbon) or blackens (when using thermal paper) marks the spot of most continuous irradiation. This spot is marked in a heat resistant manner and marks the position of the setup in all following experiments.

#### ADDITIONAL USAGE OF TUBULAR FURNACES

In many cases the additional usage of a traditional tubular resistance furnace was necessary to complete the reactions and obtain pure samples. Chapter 0 will discuss the details on this step. When needed, the samples were transferred from the DMO setup into a tubular resistance furnace with Pt/PtRh or NiCr/Ni thermocouples and PID temperature controllers (Eurotherm, model 2408) that was already pre-heated to the temperature needed. Since the samples are usually very hot at this stage, this step has to be executed very quickly to avoid temperature drops in the sample that can lead to the formation of impurity phases. Working with two people is advised.



**SECONDARY HEATING MATERIAL / SUSCEPTOR**

As the MW susceptibility of each sample depends on its composition, the heating profile for each compound has to be evaluated individually and on an empirical basis. However the use of activated carbon (Sigma-Aldrich, Norite, type Darko 12x20 from lignite) for secondary heating ensures that the power levels and time frame are somewhat similar even for very different sample compositions.<sup>[11, 12]</sup> This secondary heating material can be any material that is able to convert electromagnetic energy into heat (e.g. graphite/amorphous carbon, SiC, CuO, etc.) and is called a susceptor.<sup>[13]</sup> The use of a susceptor ensures heating even if the sample itself exhibits low microwave susceptibility. It is crucial that the particle size and porosity of the activated carbon is the same in all experiments as these parameters play an important role in the heating behavior.

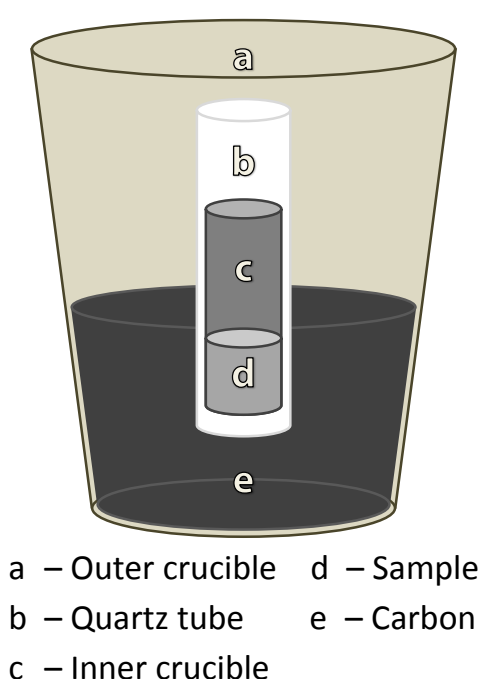


Figure 3.2-2: Left: Schematic setup used in all DMO experiments. Right: Photograph of the actual setup immediately after heating a sample.

Since the carbon is heated in the presence of air, parts of it will combust resulting in the loss of secondary heating material over time. The lost carbon needs to be replaced for each experiment and usually amounts to ~10-12 wt%. Repeated heating of the same batch of carbon will decrease mass loss after about 3-5 uses since humidity and volatile components have been driven out (Figure 3.2-3) which notably changes the MW susceptibility and in turn the heating behavior. To ensure reproducibility one not only has to weigh and replace the secondary heating material before each experiment but also to pay close attention to the mass loss and replace the whole batch once the weight loss per heating reaches ~5%. Before the first use it is also advisable to “break in” a fresh batch of carbon by irradiating it for 6 min at 600 W to get rid of most of initially present moisture (Run #0 in Figure 3.2-3).

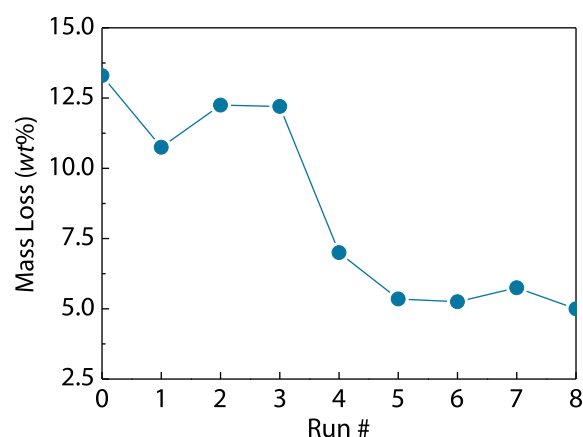


Figure 3.2-3: Mass loss of secondary heating material per run. One run means irradiation of the setup for 6 min at 600 W.

### CRUCIBLE MATERIAL

During the experimental work on this thesis many different crucible materials have been tested. Some of the crucible materials listed in Table 3.2-2 will not be discussed in the following chapters but can and have been used in a microwave setup. The main difference is their susceptibility to microwave radiation.  $\text{Al}_2\text{O}_3$  for example is almost transparent for microwave radiation ( $D_p = 10\text{m}$ ) while Nb as a metal only has a penetration depth of several  $\mu\text{m}$ .<sup>[14]</sup> This is why synthesis in a closed metallic container is complicated and highly dependent on a susceptor as external heat source. The quartz tube surrounding the crucible has to be of constant dimensions to ensure a constant vapor space and was usually 65 mm long at a diameter of 12 mm.

Table 3.2-2: Crucible materials proven to be usable in a MW setup. Given diameters are outside-diameters.

Material	Diameter and height (mm)
$\text{Al}_2\text{O}_3$ (Alumina)	$\varnothing = 10$ $h = 40$
Nb (sealed)	$\varnothing = 10$ $h = 30$
Nb (open)	$\varnothing = 10$ $h = 20$
$\text{Al}_2\text{O}_3$ (Alumina) sealed in Nb	$\varnothing = 8$ $h = 30$ (Alumina) $\varnothing = 10$ $h = 43$ (Nb)
Ta (open)	$\varnothing = 10$ $h = 20$
C (glassy carbon)	$\varnothing = 15$ $h = 20$

### 3.2.4 References

- [1] H. Luo, Z. Wang, H. Yang, P. Cheng, X. Zhu, H.-H. Wen, *Superconductor Science and Technology* **2008**, *21*, 125014.
- [2] M. Tegel, 0.7 ed., unpublished, **2010**.
- [3] A. Coelho, 4.1 ed., Coelho Software, Brisbane, **2007**.
- [4] V. Petricek, M. Dusek, L. Palatinus, *Z. Kristallogr. - Cryst. Mater.* **2014**, *229*, 345-352.
- [5] M. C. Tegel, Dissertation thesis, Ludwig-Maximilians-Universität München (München), **2011**.
- [6] M. Tegel, 0.2 ed., LMU München, **2010**.

- [7] M. Tegel, LMU, München, **2010**.
  - [8] H. L. Skriver, *The LMTO method - muffin tin orbitals and electronic structure*, Springer Verlag, Berlin, **1984**.
  - [9] O. K. Andersen, O. Jepsen, M. Sob, in *Electronic Band Structure and its Applications, Lecture Notes in Physics, Vol. 283* (Ed.: M. Yussouff), Springer Verlag, Berlin, **1987**, pp. 1-57.
  - [10] O. K. Andersen, O. Jepsen, 47c ed., *Tight-Binding LMTO*, Max-Planck-Institut für Festkörperforschung, Stuttgart, **1998**.
  - [11] J. Brgoch, M. Gaultois, M. Kemei, R. Seshadri, *Personal Communication* **2014**.
  - [12] B. Vaidyanathan, P. Raizada, K. J. Rao, *Journal of Materials Science Letters* **1997**, 16, 2022-2025.
  - [13] H. J. Kitchen, S. R. Vallance, J. L. Kennedy, N. Tapia-Ruiz, L. Carassiti, A. Harrison, A. G. Whittaker, T. D. Drysdale, S. W. Kingman, D. H. Gregory, *Chem Rev* **2014**, 114, 1170-1206.
  - [14] K. Rodiger, K. Dreyer, T. Gerdes, M. Willert-Porada, *Int. J. Refract. Met. Hard Mater.* **1998**, 16, 409-416.
-



### 3.3 Superfast Microwave Based Synthesis of Binary Transition Metal Compounds

#### 3.3.1 Introduction

The preparation of iron arsenide superconductors often requires binary starting materials and especially FeAs which is also often used as a flux material in the synthesis of large iron arsenide single crystals.<sup>[1, 2]</sup> For industrial applications such as superconducting wires or tapes these materials not only have to be pure but also obtainable as quick and cost efficient as possible. Microwave based synthesis may significantly reduce the energy consumption for these starting materials which in turn allows for less expensive products. It makes use of the rapid heating of metallic compounds in an oscillating magnetic field to achieve pure samples in significantly less time than solid state synthesis in a furnace would.

The protocol that was established for the synthesis of FeAs turned out to save so much time that protocols for the preparation of other binary iron compounds and intermetallic starting materials were developed as well. FeAs and Fe<sub>2</sub>As were used in some of the experiments leading to the results discussed in chapter 2; CaCu was used for the work presented in chapter 0.

#### 3.3.2 Synthesis of binary iron arsenides FeAs and Fe<sub>2</sub>As

##### INTRODUCTION

The binary arsenides FeAs as well as Fe<sub>2</sub>As can be used as starting materials for the production of Ba<sub>1-x</sub>K<sub>x</sub>Fe<sub>2</sub>As<sub>2</sub> and other iron arsenides (see chapter 2). Hence a cost and time efficient way of obtaining it would be beneficial for their potential commercial application. This is where microwave based synthesis offers a route that fulfills both requirements. At the same time the system Fe-As is well investigated and can serve as a model system for the exploration of basic principles of preparing pnictides and chalcogenides in a DMO.

##### EXPERIMENTAL DETAILS

A stoichiometric amount of Fe was layered on top of the corresponding amount of As with an excess of ~3.5 wt% in an alumina crucible. The total weight of the reaction mixture typically was 500 mg. The crucible was sealed in a quartz tube under Ar which was subsequently placed in the outer crucible and surrounded by 20 g of susceptor material. The setup was irradiated for 10 min at 600 W. An excess amount of As along with the layered arrangement of starting materials is necessary because at these rapid heating rates this element tends to evaporate before a reaction with Fe can take place.

##### RESULTS AND DISCUSSION

Exemplary PXRD patterns of the resulting samples are shown in Figure 3.3-1 along with their respective theoretical patterns generated from single crystal data available in the literature.<sup>[3, 4]</sup> No impurity phase reflections can be detected. Compared to the traditional solid state synthesis the presented protocol reduces the time needed by about 47 h allowing for the rapid production of

large quantities of material without the need for upscaling. This protocol was used multiple times to prepare starting materials for the high pressure experiments described in chapter 2.

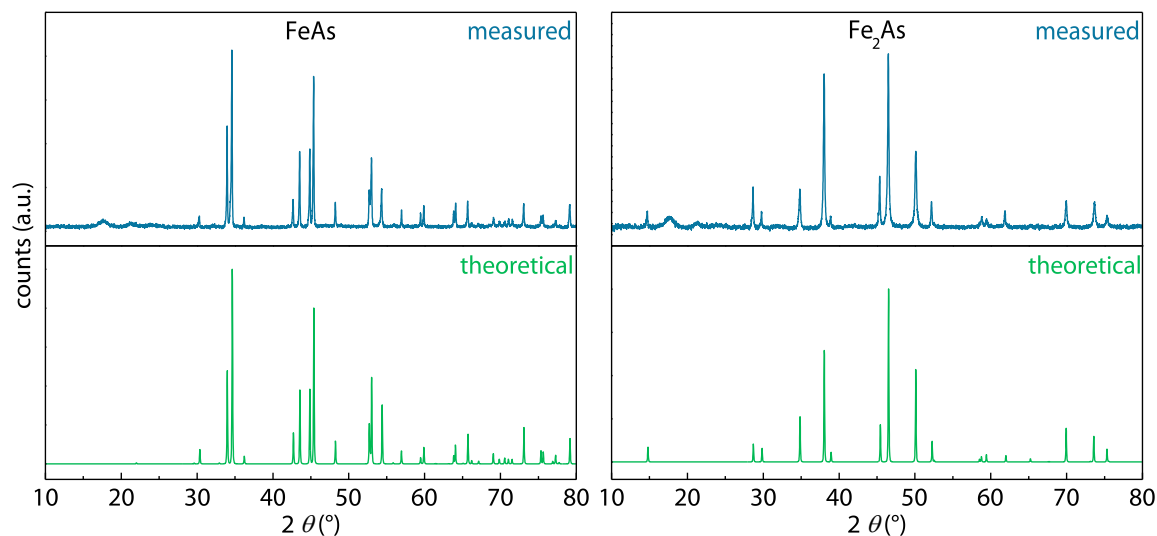


Figure 3.3-1: Resulting PXRD patterns of binary iron arsenides from microwave based synthesis.

The experiments described here mark the first time that arsenides have been successfully prepared via microwave synthesis. Especially in the context of making iron arsenide superconductors available for technical applications such as superconducting wires and tapes, this might present a cost effective way of obtaining the necessary quantities of starting materials.

### 3.3.3 Synthesis of FeSe

#### INTRODUCTION

$\beta$ -FeSe has attracted a lot of interest among superconductivity researchers because it represents the structurally simplest way of arranging the iron centered tetrahedra layers found in the iron pnictide and chalcogenide superconductors. FeSe crystallizes in two polymorphs, one adopting tetragonal symmetry ( $\beta$ -FeSe, *anti*-PbO-type structure, space group  $P4/nmm$ , with  $a = 3.7709(1) \text{ \AA}$  and  $c = 5.5216(1) \text{ \AA}$ ) and the other being of hexagonal symmetry ( $\alpha$ -FeSe, NiAs-type structure, space group  $P6_3/mmc$  with  $a = 3.618 \text{ \AA}$  and  $c = 5.927 \text{ \AA}$ ).<sup>[5]</sup> Tetragonal  $\beta$ -FeSe becomes superconducting at 8-10 K<sup>[6]</sup> and has been subject to extensive research especially regarding the possible intercalation of various atomic and molecular layers.

To aid this research a fast, microwave based synthesis was developed that results in reasonably pure FeSe samples that can be obtained in a very short time frame.

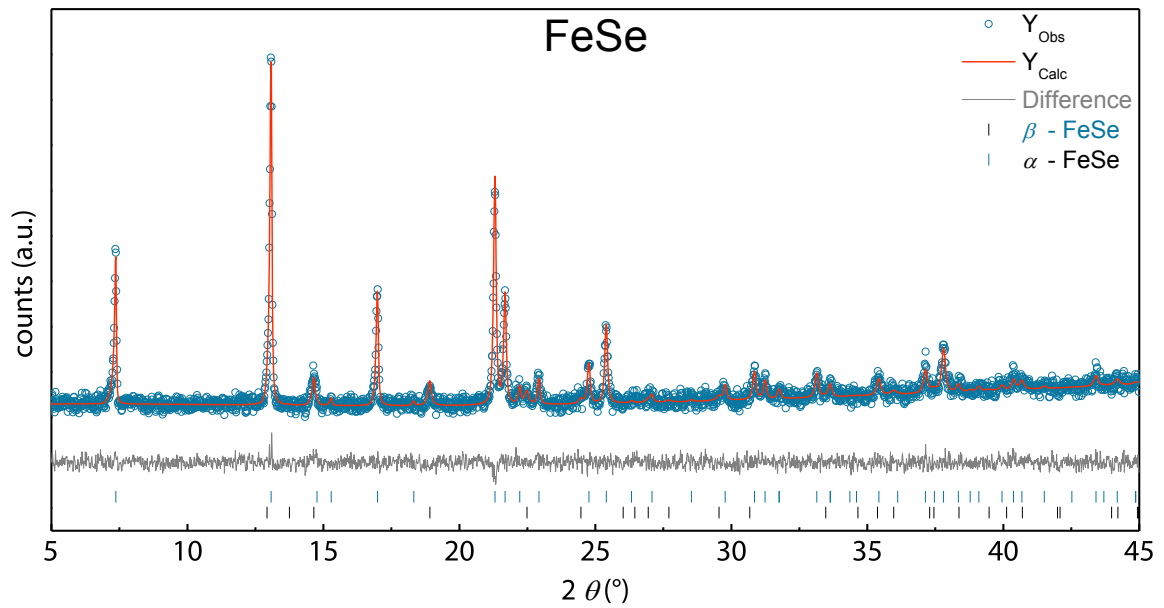


Figure 3.3-2: PXRD data and Rietveld refinement of a sample containing 90 wt%  $\beta$ -FeSe.

### EXPERIMENTAL DETAILS

A stoichiometric mixture of Fe and Se was mixed in an agate mortar and filled into an alumina crucible. The crucible was sealed in an Ar-filled quartz tube which was subsequently placed in 20 g of activated carbon. The setup was irradiated for 20 min at 300 W and the quartz tube was immediately transferred into a pre heated tubular furnace set to 593 K and kept there for 24 h. The reasons for this approach will be discussed in chapter 3.4.2. The quartz tube was then removed from the furnace and quenched in a mixture of salt water and ice ( $\sim 263$  K). The resulting sample contains only the two polymorphs of FeSe with no visible impurity phases, although the background in the magnetic measurements (Figure 3.3-3) hints at trace amounts of iron or another ferromagnetic impurity.

Since the superconducting properties of  $\beta$ -FeSe have been shown to depend on the method of preparation,<sup>[7]</sup> a susceptibility measurement at low temperatures was carried out (Figure 3.3-3). It proves the sample to be bulk superconducting with a superconducting volume fraction that corresponds well to the fraction of  $\beta$ -FeSe determined via Rietveld refinement.

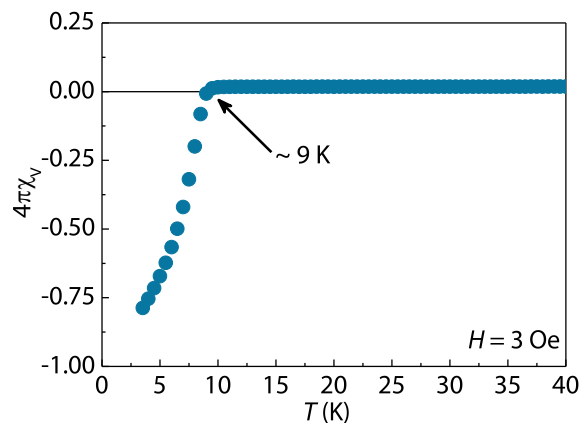


Figure 3.3-3: Low temperature magnetic susceptibility of FeSe from microwave based synthesis.

## RESULTS AND DISCUSSION

The purity of the sample is sufficient for the use as a starting material. The fraction of  $\beta$ -FeSe which is about 90 wt% is remarkably high for such a short sintering time but needs to be increased for detailed physical measurements. This might be achieved by fine tuning the sintering times even though experiments with sintering periods of up to 7 d did not significantly improve the ratio of  $\beta$ -FeSe to  $\alpha$ -FeSe. One problem shared with samples obtained from conventional solid state synthesis is that the presence of  $\alpha$ -FeSe is hard to avoid since  $\beta$ -FeSe is the more favorable polymorph only below 723 K and in a rather narrow temperature range.<sup>[8]</sup> Experiments towards quicker quenching involving different quenching media could improve the results.

The experiments detailed above mark the first ever iron chalcogenide superconductor obtained via microwave based synthesis. They highlight the versatility and quickness of this method as a tool in the investigation of the puzzle of high temperature superconductivity in iron based compounds.

### 3.3.4 Synthesis of CaCu

#### INTRODUCTION

Intermetallic compounds have a wide range of applications from electronics<sup>[9]</sup> to hydrogen storage<sup>[10]</sup> and catalysis.<sup>[11]</sup> In many cases the synthesis is very time consuming and expensive due to the energy demands of furnace or arc melting techniques. The application of microwave based synthesis for the formation of intermetallic compounds has already been successful in several cases and may offer a green route towards this and many other types of materials.<sup>[12]</sup>

The intermetallic compound CaCu was used as a starting material for the synthesis of  $\text{Ca}_2\text{Cu}_6\text{P}_5$  which will be discussed in chapter 0. The stoichiometric alloy appears in two polymorphs:  $\alpha$ -CaCu (space group *Pnma* with  $a = 38.80(1)$  Å,  $b = 4.271(2)$  Å and  $c = 5.8904(9)$ ) and  $\beta$ -CaCu (space group *P2<sub>1</sub>/m* with  $a = 19.47(1)$  Å,  $b = 4.271(2)$  Å,  $c = 5.880(3)$  and  $\beta = 94.3(1)^\circ$ ).<sup>[13]</sup> The high temperature phase  $\alpha$ -CaCu and the low temperature phase  $\beta$ -CaCu show no difference in composition at room temperature which is why a sample only containing these phases is considered “pure” in the following discussion.

Regular furnace synthesis of this compound takes about 48 h as the metals have to be molten at temperatures of about 873 K and cooled down to room temperature afterwards.<sup>[13]</sup> In order to speed up the preparation of this compound for the subsequent experiments and to elucidate the parameters influencing the synthesis of intermetallic substances in a DMO, a quick 5 min synthesis protocol was developed.

#### EXPERIMENTAL DETAILS

A stoichiometric mixture of Ca clippings with an excess of 1 wt% and Cu granules was mixed inside a custom made Nb crucible (see Figure 3.3-4) which was sealed in an Ar-filled quartz tube of 65 mm length. The usual total weight of the reaction mixture was 500 mg. The tube was placed in the reaction setup with 20 g of activated carbon and irradiated at 600 W for 5.5 min. After the

---



DMO program was completed the tube was taken out of the reaction setup in order to quench the reaction mixture in air. The sample was removed by carefully working the Nb-crucible with a hammer.

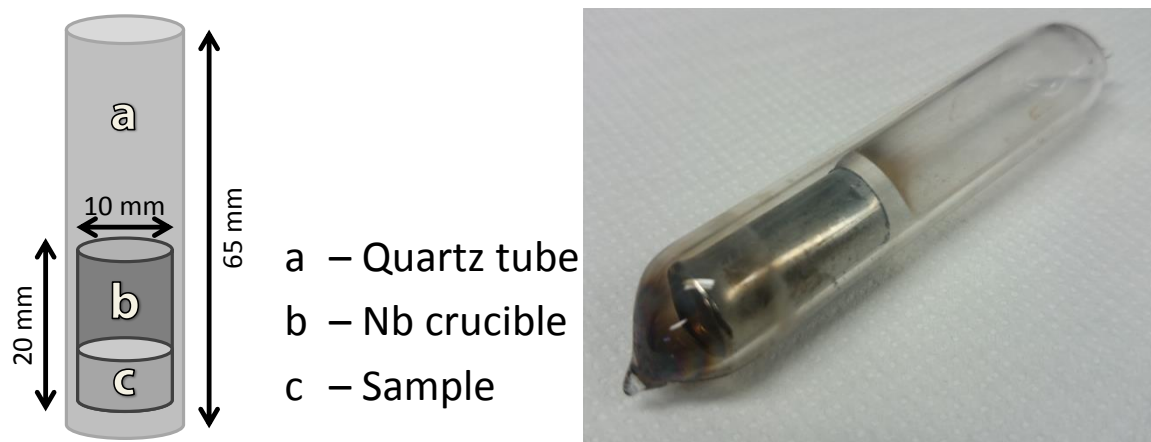


Figure 3.3-4: *Left: Dimensions of the quartz tube and Nb-crucible used in the synthesis. Right: Quartz tube with Nb-crucible after reaction with evaporated Ca visible as a dark condensate.*

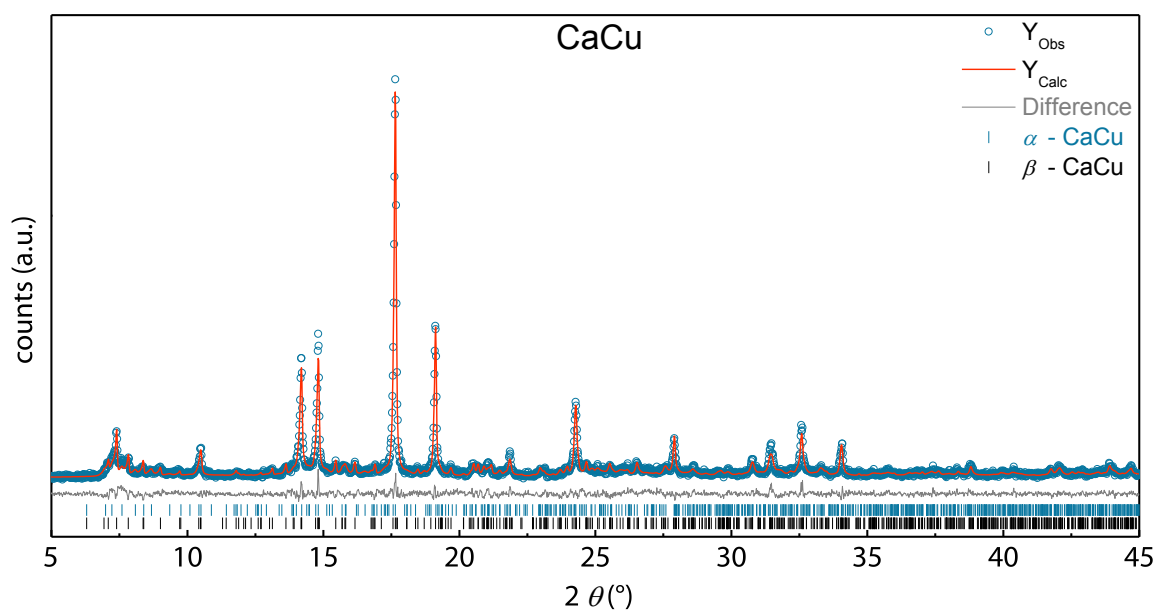


Figure 3.3-5: *A pure sample of CaCu obtained via microwave based synthesis in 5 min.*

## RESULTS AND DISCUSSION

The protocol described above yields pure samples (see Figure 3.3-5) of CaCu with varying ratios of  $\alpha$ -/ $\beta$ -phase due to their respective sensitivity to the cooling rate. Since the samples are usually intended to be used as starting materials this is not an issue.

Because a part of the Ca inevitably evaporates during synthesis (see Figure 3.3-4) using a slight excess of Ca and a constant container volume (i.e. length of the quartz tube) are essential to ensure reproducibility and purity of the samples. The same is true for the choice of crucible material and dimensions. Experiments leading towards this protocol could show that otherwise the formation of impurity phases  $\text{Ca}_2\text{Cu}$  and  $\text{CaCu}_5$  is unavoidable. All other crucible materials that have been

tested did not allow for a clean removal of the sample and thus were not suitable for the preparation of CaCu in a DMO.<sup>[14]</sup>

It should be noted that this technique is theoretically applicable to all intermetallic compounds. One important requirement for the metals used for the reaction however is a relatively low vapor pressure since the rapid heating rates would lead to a substantial loss of reactants. In this case a sealed Nb crucible should be preferred. The crucible material may be replaced by Ta if needed, however the different heating behavior has to be accounted for.

### 3.3.5 Summary

In this chapter synthesis protocols for the preparation of FeAs, Fe<sub>2</sub>As, FeSe and CaCu are discussed. The reaction times have been greatly reduced compared to the respective furnace syntheses and pure samples have been obtained in all cases. Furthermore some general knowledge about the behavior of different materials upon microwave irradiation has been deduced.

The preparation of the binary iron arsenides FeAs and Fe<sub>2</sub>As has been successful for quantities of 500 mg in 5 min at 600 W using a regular alumina crucible with layered reactants. The evaporation of As due to the rapid heating has to be compensated by an excess amount of As in the mixture. This route has been used repeatedly to obtain starting materials for the high pressure synthesis experiments described in chapter 2.

The first microwave based synthesis of the iron based superconductor FeSe has been developed and superconductivity at ~9 K has been verified. Irradiation of a mixture of Fe and Se for 20 min at 440 W with subsequent annealing at 593 K in a tubular furnace and quenching in salt water/ice yielded samples containing ~90 wt% of superconducting  $\beta$ -FeSe. Although these samples contain too much  $\alpha$ -FeSe to allow for detailed physical investigations, the purity is sufficient for a use as starting material in other experiments. Furthermore possibilities for improving the  $\beta$ -FeSe content are presented.

A quick synthesis protocol for the preparation of intermetallic CaCu was developed. Ca clippings and Cu granules are irradiated for 5.5 min at 600 W in a custom Nb crucible that was developed during the experiments leading to the protocol. This protocol can be used as a basis for the preparation of other intermetallic compounds when certain general rules and principles are considered. The evaporation of Ca has to be compensated by using an excess amount in the starting mixture.

During a stay with the *Seshadri* group at the materials research laboratory at UC Santa Barbara (MRL@UCSB) a protocol for the synthesis of CaMo<sub>6</sub>S<sub>8</sub> was also developed but is not detailed in this thesis. It may be used as an electrode material in Ca-S-battery systems and becomes superconducting around 9 K when Ca-deficient.<sup>[15]</sup> This protocol has been used by members of the *Seshadri* group and further exemplifies the versatility of the microwave based synthesis in materials research.<sup>[16]</sup>

---

The synthesis of  $\text{FePd}_{2.2}\text{Te}_2$  within 9 minutes has been successful, starting from the elements. The rapid formation of this phase will aid the investigation of its physical properties by other group members in the future. The details on the synthesis will be published elsewhere.

General aspects that have to be considered in a DMO based synthesis are primarily the loss of reactants due to evaporation and the influence of crucible material/dimensions. The crucible material can serve as a heating source when metallic or reduce the heating rate when it is nonmetallic but susceptible to microwave radiation (e.g. glassy carbon). The irradiation parameters always have to be determined empirically for different crucible types and can usually not be directly transferred. In order to compensate evaporation losses one has to make sure the vapor space is constant and chose an appropriate excess of the reactant in question.

If these aspects are considered the development of new protocols based on the findings presented should be fairly unproblematic.

### 3.3.6 References

- [1] R. Prozorov, M. A. Tanatar, E. C. Blomberg, P. Prommapan, R. T. Gordon, N. Ni, S. L. Bud'ko, P. C. Canfield, *Phys. C (Amsterdam, Neth.)* **2009**, *469*, 667-673.
- [2] Y. Liu, D. L. Sun, J. T. Park, C. T. Lin, *Phys. C (Amsterdam, Neth.)* **2010**, *470*, 513-515.
- [3] A. M. Mills, A. Mar, *J. Alloys Compd.* **2000**, *298*, 82-92.
- [4] J. Nuss, U. Wedig, M. Jansen, *Zeitschrift für Kristallographie* **2006**, *221*, 554-562.
- [5] G. Hägg, A. L. Kindström, *Z. Phys. Chem. B* **1933**, *22*, 453.
- [6] F.-C. Hsu, J.-Y. Luo, K.-W. Yeh, T.-K. Chen, T.-W. Huang, P. M. Wu, Y.-C. Lee, Y.-L. Huang, Y.-Y. Chu, D.-C. Yan, M.-K. Wu, *Proc. Natl. Acad. Sci. U. S. A.* **2008**, *105*, 14262-14264.
- [7] U. Pachmayr, N. Fehn, D. Johrendt, *Chemical Communications* **2015**, *accepted*.
- [8] H. Okamoto, *JPE* **1991**, *12*, 383-389.
- [9] T. Dobrovolska, L. Veleva, I. Krastev, A. Zielonka, *J. Electrochem. Soc.* **2005**, *152*, 137-142.
- [10] R. Kirchheim, T. Muetschele, W. Kieninger, H. Gleiter, R. Birringer, T. D. Koble, *Mater. Sci. Eng.* **1988**, *99*, 457-462.
- [11] A. Roucoux, J. Schulz, H. Patin, *Chem. Rev.* **2002**, *102*, 3757-3778.
- [12] J. W. Lekse, T. J. Stagger, J. A. Aitken, *Chemistry of Materials* **2007**, *19*, 3601-3603.
- [13] F. Merlo, M. L. Fornasini, *Acta Crystallographica Section B* **1981**, *37*, 500-503.
- [14] L. Bulthaupt, R. Pobel, *Forschungsbericht* **2014**.
- [15] C. Geantet, J. Padiou, O. Pena, M. Sergent, R. Horyn, *Solid State Commun.* **1987**, *64*, 1363-1368.
- [16] K. See, Dissertation thesis, UCSB (Santa Barbara), **2014**.



### 3.4 Development and Application of a Fast Microwave Based Dopant Screening Procedure for $\text{Ca}_2\text{Cu}_6\text{P}_5$ and the Physical and Structural Properties of $\text{Ca}_2\text{Cu}_6\text{P}_{5-x}\text{As}_x$ ( $0 \leq x < 2$ )

#### 3.4.1 Introduction

The search for new superconducting compounds has focused mainly on compounds exhibiting the common structural motif of  $\text{TMPn}_{4/4}$  tetrahedra. In order to investigate the effect of introducing magnetic atoms into an otherwise nonmagnetic host system as well as a model system for a general dopant screening  $\text{Ca}_2\text{Cu}_6\text{P}_5$  was chosen.

$\text{Ca}_2\text{Cu}_6\text{P}_5$  crystallizes in the tetragonal space group  $I4/mmm$  with lattice parameters  $a = 4.015 \text{ \AA}$  and  $c = 24.657 \text{ \AA}$ , adopting an unique structure type.<sup>[1]</sup> The 265-type structure can be understood as a hybrid between the  $\text{ThCr}_2\text{Si}_2$ -type (122-type) structure found in many Cu pnictides like  $\text{CaCu}_{1.75}\text{P}_2$  and the  $\text{BaMg}_4\text{Si}_3$ -type (143-type) which is found e.g. in  $\text{LaCu}_4\text{P}_3$ .<sup>[2, 3]</sup> Note that the 143-type structure that is discussed in this chapter is different from the 143-type structure of  $\text{CaFe}_4\text{As}_3$  mentioned in chapter 2.

The 265-type structure thus consists of layers of edge sharing  $\text{CuP}_{4/4}$  tetrahedra and layers of condensed double layers of  $\text{CuP}_{4/4}$  tetrahedra separated by layers of P-coordinated Ca. Another point of view is offered by *Pilchowski et al.* who derive the 265-type structure by omitting every third Ca-P-layer from a  $1 \times 1 \times 3$  supercell of  $\text{CaCu}_2\text{P}_2$  thus explaining the similar lattice parameters as well as interatomic distances found in  $\text{CaCu}_{1.75}\text{P}_2$  and  $\text{Ca}_2\text{Cu}_6\text{P}_5$ . They also point out that this compound interestingly shows no Cu-deficiency like the 122-type Cu pnictides do.<sup>[1, 4]</sup>

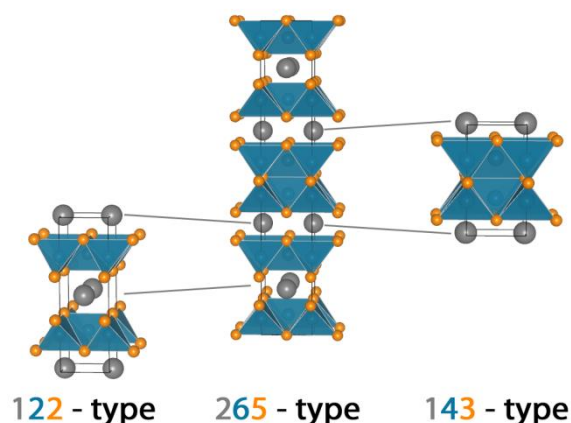


Figure 3.4-1: Illustration of the structural relationship of  $\text{Ca}_2\text{Cu}_6\text{P}_5$  to the 122-type and 143-type structures. The unit cells have been slightly shifted from the standard projection for illustrative purposes.

Even though the first description of  $\text{Ca}_2\text{Cu}_6\text{P}_5$  dates back to 1990 and the structural similarity to the 122-type superconductors is striking, almost no investigations of the physical properties or the ability of the compound to act as a host for dopants have been reported. One of the two publications that exist besides the original paper by *Pilchowski et al.* describes  $\text{Sr}_2\text{Cu}_6\text{P}_5$  and  $\text{Eu}_2\text{Cu}_6\text{P}_5$  as well as their physical properties.<sup>[2]</sup> The other, which has not undergone peer review at the time of writing this work, examines the metallic behavior of the parent compound. Because

this publication may be changed before publication, general aspects will be mentioned but the paper will not be discussed in detail.<sup>[5]</sup>

For the solid state synthesis of  $\text{Ca}_2\text{Cu}_6\text{P}_5$  two rather similar protocols are suggested in the literature. The first protocol by *Pilchowski et al.* starts from the elements and uses a three step synthesis in an alumina crucible at 1173 K and 1373 K respectively which involves grinding of the sample after each step. The total time needed for this approach amounts to 160 h without accounting for opening, grinding and resealing.<sup>[1]</sup> The other approach by *Charkin et al.* uses a slower heating rate with several intermediate holding steps. These are also followed by two regrinding and annealing steps. The total reaction time amounts to 208 h, again without accounting for the time needed to handle the sample between the different heating steps.<sup>[2]</sup>

While these long reaction times are certainly not atypical for solid state synthesis, they still pose a problem when an explorative approach to a new system is wanted. To find a suitable dopant for a certain system usually involves quite a number of experiments. If each experiment takes more than a week, explorative synthesis of such a system becomes time consuming to a point where it almost becomes nonsensical. Still, since doping is an important tool in materials chemistry a fast preparation method is needed to overcome this issue. This is where microwave based synthesis offers an elegant solution.

### 3.4.2 Synthesis optimization

In order to develop a strategy for the broad screening of possible dopants for  $\text{Ca}_2\text{Cu}_6\text{P}_5$  a reliable synthesis protocol is necessary. This section gives an overview over the experiments that led to the protocol employed in the preparation of the samples which will be discussed later in this chapter. The discussion deliberately mentions failed approaches in an effort to illustrate some issues with microwave based synthesis in the hope to facilitate future experiments.

Using the elements as starting materials in a way akin to the solid state synthesis employed by *Charkin et al.* for microwave synthesis suffers from various problems. Besides the material losses of Ca and P due to evaporation, the short timeframe of the synthesis turned out to hinder a homogenous formation of the target phase. Using irradiation times of 5-20 min at power levels of 440 W, 600 W and 1000 W, respectively, did not allow for a phase fraction of more than approximately 30 wt% and yielded mostly binary Cu and Ca phosphides.

#### USING BINARY STARTING MATERIALS TO ENHANCE SAMPLE QUALITY

To improve sample quality, CaCu was chosen as a Ca source because elemental Ca cannot be ground into a powder which would allow for a more even distribution in the sample. CaCu is brittle enough to allow grinding while its melting point of 840 K ensures reactivity.<sup>[6]</sup> This improved the sample quality under the same reactive conditions and led to samples with  $\text{Ca}_2\text{Cu}_6\text{P}_5$  as main phase. Still, this approach did not yield target phase fractions of more than 45 wt% with  $\text{CaCu}_{1.75}\text{P}_2$  and  $\text{CaCu}_{3.8}\text{P}_2$  being the impurity phases.

---

To further increase the homogeneity of the starting mixture,  $\text{CuP}_2$  was chosen as a P-source. As powdered red P tends to be very sticky, losses during handling of the mixture are nearly unavoidable. Using  $\text{CuP}_2$  also turned out to significantly reduce the evaporation losses of elemental P during synthesis. By using this binary phosphide the phase fractions of  $\sim 50\text{-}60\text{ wt}\%$   $\text{Ca}_2\text{Cu}_6\text{P}_5$  could be obtained.

Both approaches illustrate one particularly problematic aspect of microwave based synthesis. Since the reaction times are very short, the reaction may be subject to kinetic effects. If the target phases are binary compounds, as shown in chapter 0, this is usually unproblematic but for ternary or even quaternary compounds this can significantly hinder the formation of a target phase. To circumvent this limitation the additional use of an electrical resistance tubular furnace was tested in an effort to combine “the best of both worlds”.

#### ADDITIONAL USE OF A TUBULAR FURNACE

The very rapid heating of materials in a microwave field is one of the main advantages of this type of synthesis but at the same time the short reaction times also mean very rapid cooling rates. These can be problematic when a target phase is thermodynamically stable but the formation is kinetically hindered and more time at elevated temperatures is needed for the system to move towards such a phase. In solid state synthesis this is usually the case and also the reason for reaction times that can last up to several weeks or even months. A hybrid approach was introduced to compensate the lack of reaction time while at the same time maintaining the quickness of a microwave based synthesis.

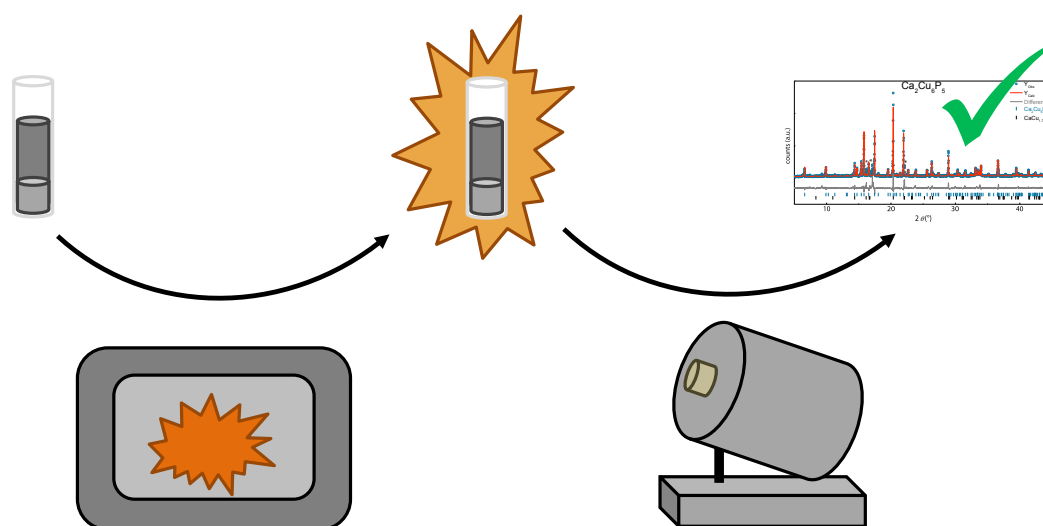


Figure 3.4-2: Schematic representation of the newly developed hybrid microwave synthesis. The sample (far left) is irradiated in the DMO and immediately transferred into a pre-heated furnace. The extended reaction time yields the target phase in good quality.

By placing the sample in a pre-heated tubular furnace right after the completion of microwave irradiation (Figure 3.4-2), a rapid cooling of the system can be avoided and the formation of the target phase can be enhanced. Simultaneously an arbitrarily prolonged reaction time can be realized and sample purity can thus be significantly improved. Another benefit is a controlled

cooling rate which improves the crystallinity of the sample. This hybrid approach was never before reported and may enable the preparation of many more compounds than by purely microwave based synthesis alone.

Systematic investigations showed that the post reaction time plays a significant role. Its effect usually reaches a maximum at 4h for  $\text{Ca}_2\text{Cu}_6\text{P}_5$  and diminishes at longer holding times. On the other hand the nearly phase pure formation of  $\beta\text{-FeSe}$  for example needs up to 24 h (see chapter 0) which indicates that this effect is individual for each compound.

### MICROWAVE BASED SYNTHESIS OF THE HOST COMPOUND

After some optimization a reliable synthesis protocol was established and used for the synthesis of all samples discussed in this chapter.

$\text{Ca}_2\text{Cu}_6\text{P}_5$  was obtained by heating a mixture of  $\text{CaCu}$ ,  $\text{CuP}_2$  and  $\text{Cu}$  powders in the microwave setup described in chapter 3.2.3 using an alumina crucible. An excess amount of 1.6 wt% of  $\text{CuP}_2$  was used to compensate evaporation losses of P. The setup was irradiated for 12 min at 600 W and transferred into a tubular furnace. The furnace was pre-heated to 1173 K and programmed to hold this temperature for 4 h while subsequently cooling to room-temperature at a rate of 100 K/h. The samples contained > 90 wt% of  $\text{Ca}_2\text{Cu}_6\text{P}_5$  with  $\text{CaCu}_{1.75}\text{P}_2$  being the only identifiable impurity phase. Despite extensive research and numerous tries to isolate single crystals, the unidentified impurity phase responsible for the peaks marked with an asterisk in Figure 3.4-3 could not be identified.

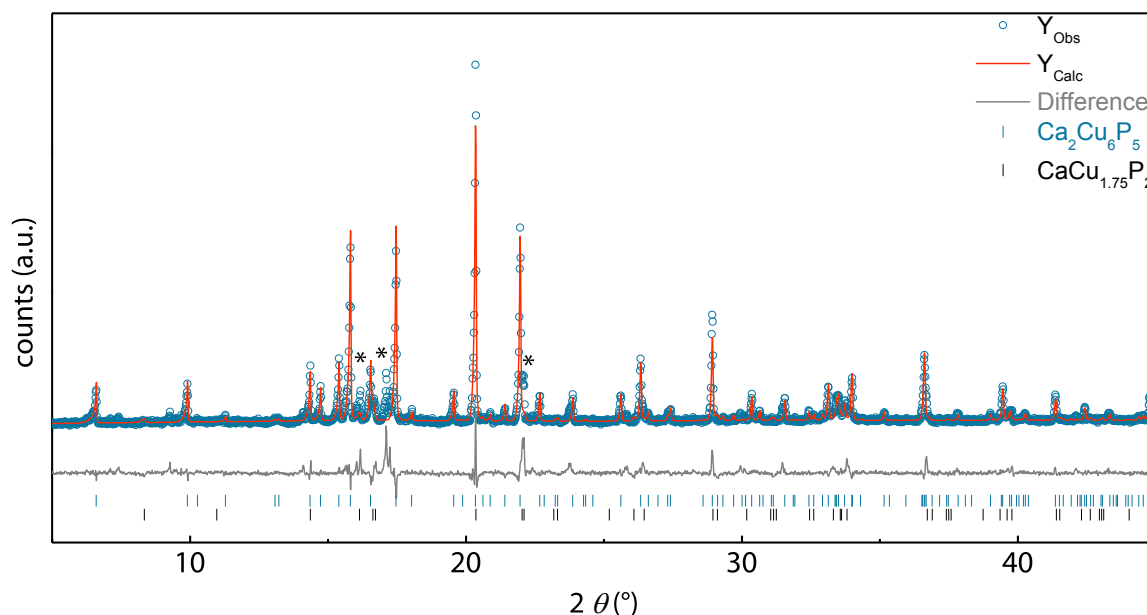


Figure 3.4-3: PXRD data (blue) and Rietveld refinement (red) of a typical sample. Unidentified impurity phase reflections are marked with an asterisk. The phase fraction of the target phase is > 90 wt%.

The reasons why a higher purity could not be achieved are not easy to pinpoint since there is no experience with the microwave based synthesis of ternary and higher pnictides. One major factor could be the use of a DMO as opposed to a laboratory grade microwave device. This would allow finer control of the irradiation power but also provide a homogenous field in the reaction



chamber. More control over the reaction parameters could thus allow for a better understanding on their specific effects on the sample. However, since the focus of this work was on the dopant screening of  $\text{Ca}_2\text{Cu}_6\text{P}_5$  as a potential host system, this small discrepancy can be accepted.

### 3.4.3 Screening for potential transition metal dopants

Since the host compound contains no element that would allow for the expectation of magnetic properties, the primary goal of the experiments in this chapter was to see if any other transition metal elements could serve as a dopant. This way, one might be able to induce magnetic properties or even specifically dope one of the two metal phosphide layers.

The strategy that was established in order to screen the target compound for its ability to incorporate a specific dopant was relatively straight forward. A small amount of the possible dopant was added to a stoichiometric mixture of the starting compounds detailed in chapter 3.4.1 and the heating profile was applied as usual. If the target compound is able to incorporate the doping candidate, it will be visible in the PXRD data by a shift of the lattice parameters even if the occupancy cannot be refined. Once a suitable candidate is found the synthetic conditions can be adjusted to allow for a reasonable sample quality. If higher purities are needed, e.g. for detailed physical measurements, a traditional furnace based synthesis can be employed.

This way the time consuming trial-and-error method of finding suitable dopants for target phases with long preparation times can be significantly accelerated while the higher sample quality of furnace based synthesis may then be employed where needed.

#### NICKEL AS A POSSIBLE DOPANT

When comparing the radii of close neighbors of Cu in the periodic table in the same coordination spheres, it becomes apparent that Ni is the prime candidate for doping  $\text{Ca}_2\text{Cu}_6\text{P}_5$  because it has a magnetic moment while at the same time having a very similar radius to Cu. In 4-fold coordination  $r_{\text{Ni}} = 0.55 \text{ \AA}$  [7] is very close to that of Cu ( $r_{\text{Cu}} = 0.57 \text{ \AA}$ ) [7] and the electronic configuration of  $\text{Ni}^{2+}$  ( $[\text{Ar}]3d^8$ ) in a tetrahedral environment suggests that its incorporation into the host phase may induce new magnetic properties.

To thoroughly test the screening strategy, three different Ni concentrations corresponding to the hypothetical formula  $\text{Ca}_2\text{Cu}_{6-x}\text{Ni}_x\text{P}_5$  ( $x = 0.05, 0.25, 0.5$ ) were chosen. The possible dopant was added as powder to the mixture of starting materials. This way it should be ensured that possible solution limits are circumvented while at the same time providing enough dopant to compensate losses by the formation of impurity phases.

However none of the experiments showed an incorporation of Ni into  $\text{Ca}_2\text{Cu}_6\text{P}_5$  at even a small amount. At a nominal Ni content of  $x = 0.05$  the target phase was present but did not show any changes in lattice parameters. Any further increase in Ni content led to samples that did not contain any fraction of the target phase at all. This is surprising as one would expect it to at least form in this setting even if the substitution of Cu by Ni in the target phase may not be possible.

It seems like the presence of Ni in the reaction mixture completely suppresses  $\text{Ca}_2\text{Cu}_6\text{P}_5$  and the formation of the structurally related phases  $\text{CaCu}_{1.75}\text{P}_2$  and  $\text{Ca}_2\text{Cu}_{3.8}\text{P}_2$  is favored. The presence of elemental Cu in samples with higher Ni contents even suggests a preference of these compounds to incorporate Ni over Cu.

Since the PXRD and EDX data could show that Ni was indeed incorporated into these phases, mainly into the 122-type  $\text{CaCu}_{1.75}\text{P}_2$ , a structural barrier such as a size mismatch can be excluded. The reason may lie in a catalytic influence of Ni that leads to  $\text{Ca}_2\text{Cu}_6\text{P}_5$  not being the thermodynamically stable phase in this system. Experiments at lower temperatures during post reaction furnace heating did also not lead to the formation of even small amounts of the target phase.

### SCREENING FOR OTHER TRANSITION METAL DOPANTS

In order to make use of the versatility of the screening method other transition metals were also investigated. Because a size mismatch may lead to an ordered substitution due to the preference of one Cu-position over the other, larger elements were also included. However, the experiments with Mn, Fe and Co yielded the same results as those with Ni. Again the presence of Cu in the samples suggests a preferential incorporation of these elements into the present phases (mainly  $\text{CaCu}_{1.75}\text{P}_2$ ) and rules out size mismatch as a reason for the total absence of the target phase.

#### 3.4.4 Screening for potential pnictogen/chalcogen dopants

Since doping of  $\text{Ca}_2\text{Cu}_6\text{P}_5$  with transition metals of similar radius did not yield any results, doping of the P-position was investigated. Aliovalent as well as isovalent doping can lead to new electronic properties in 122-type compounds<sup>[8-11]</sup> (e.g. P-doping of  $\text{BaFe}_2\text{As}_2$ ) which is why different pnictogen and chalcogen elements (As, Ge, S, Sb, Se, Si) were chosen.

An amount of  $\sim 3 \text{ wt}\%$  of the respective dopant candidate was added to the mixture of reactants. This way the ability of the system to incorporate a specific element can be tested and the starting composition may be adjusted once a candidate is identified.

In all cases except As, which will be discussed in more detail below, no incorporation of the dopant into the host compound could be observed. The respective dopant could be detected in elemental form (e.g. Ge) or in binary impurity phases (e.g. CaS) in all samples along with  $\text{Ca}_2\text{Cu}_6\text{P}_5$  exhibiting unchanged lattice parameters. The phase fractions of these impurity phases also matched the added amount of dopant. Interestingly the addition of As did in fact lead to a change in lattice parameters and why its influence on the structure and physical properties of  $\text{Ca}_2\text{Cu}_6\text{P}_5$  was investigated in more detail.

#### 3.4.5 The physical and structural properties of $\text{Ca}_2\text{Cu}_6\text{P}_{5-x}\text{As}_x$ ( $0 \leq x < 2$ )

Since the dopant screening showed positive results for As, samples with As contents of up to  $x = 1.8$  were prepared yielding samples with about 80 wt% main phase. The sample quality however diminished rapidly when As contents surpassed  $x = \sim 1.5$  (see Figure 3.4-4). Beyond  $x = 1.7$  the fraction of the main phase becomes too low to allow for a sensible discussion of the

---

resulting data. At  $x = 2$  the target phase is not detectable via PXRD measurements, suggesting a solution limit for this method of preparation.

EDX measurements verify the composition obtained from Rietveld refinements as shown in Figure 3.4-4 but also illustrate the complicated analysis of samples with higher As content as the standard deviation becomes substantial.

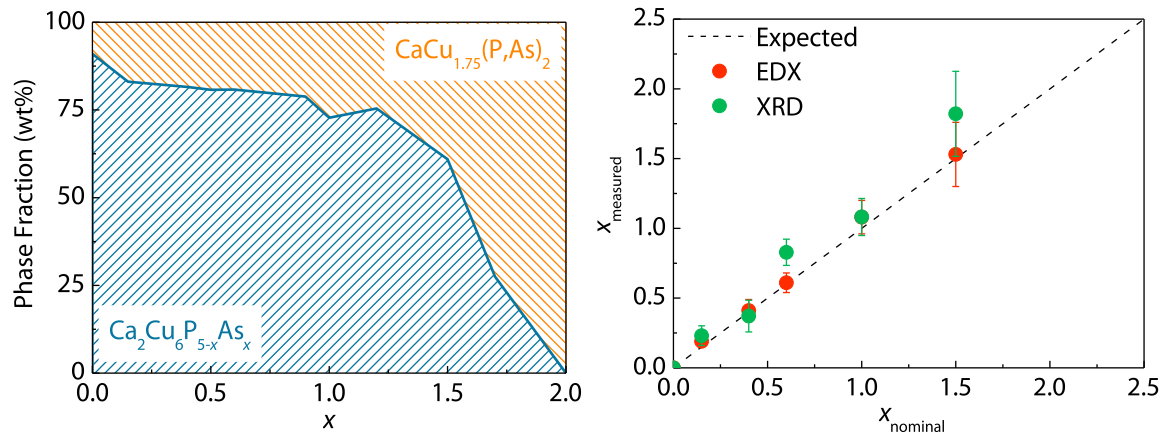


Figure 3.4-4 Left: Development of the sample composition with increasing As-content. Right: Comparison of the As content obtained via Rietveld refinements (XRD) and EDX measurements.

### STRUCTURAL PROPERTIES

Increasing the As content in  $\text{Ca}_2\text{Cu}_6\text{P}_{5-x}\text{As}_x$  results in an increase in both lattice parameters (Figure 3.4-5) which is in agreement with the larger radius of As compared to P.<sup>[7]</sup> While the increase is relatively large along  $c$ , parameter  $a$  only increases very slightly. The increase in the interlayer distance corresponds well to the overall increase of the lattice parameter  $c$  while the two fold angles  $\epsilon$  of the different tetrahedral layers remain almost constant.

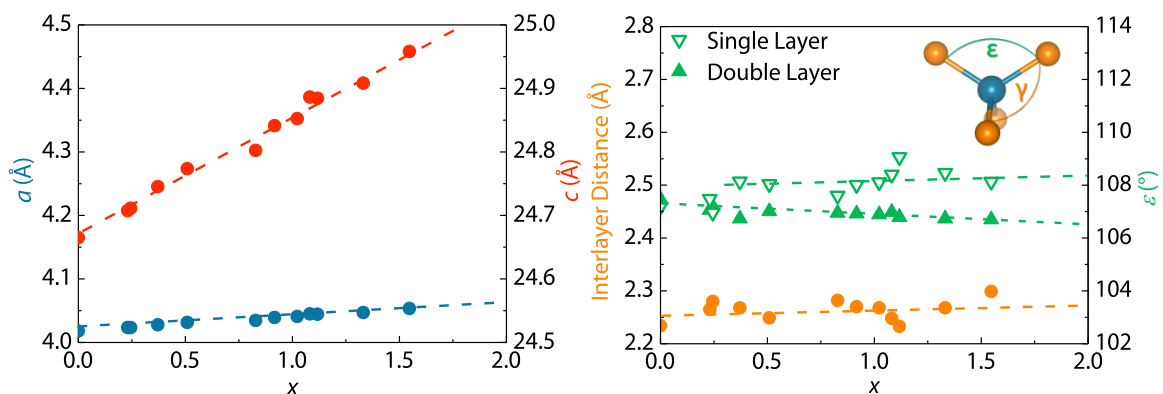


Figure 3.4-5 Left: Progression of the lattice parameters with increasing As content in  $\text{Ca}_2\text{Cu}_6\text{P}_{5-x}\text{As}_x$ . Right: Structural details of the solid solution  $\text{Ca}_2\text{Cu}_6\text{P}_{5-x}\text{As}_x$ .

A closer look reveals that the behavior of these angles differs for the different layers above  $x = 1$ . This corresponds well with the behavior of site occupancies for the P-sites in the mono and double layer. Within the margin of error there seems to be a saturation of As doping in the double layer while the As content of the single layer further increases linearly. This might give a hint at the reason why the system approaches a solubility limit at  $x = 2$  and why the phase fraction of

$\text{CaCu}_{1.75}(\text{P,As})_2$  increases dramatically above  $x = 1.7$  until the formation of  $\text{Ca}_2\text{Cu}_6(\text{P,As})_5$  is suppressed completely. Since the double layer seems to be unable to incorporate any more As,  $\text{CaCu}_{1.75}(\text{P,As})_2$  becomes more favorable as it consists solely of single layers.

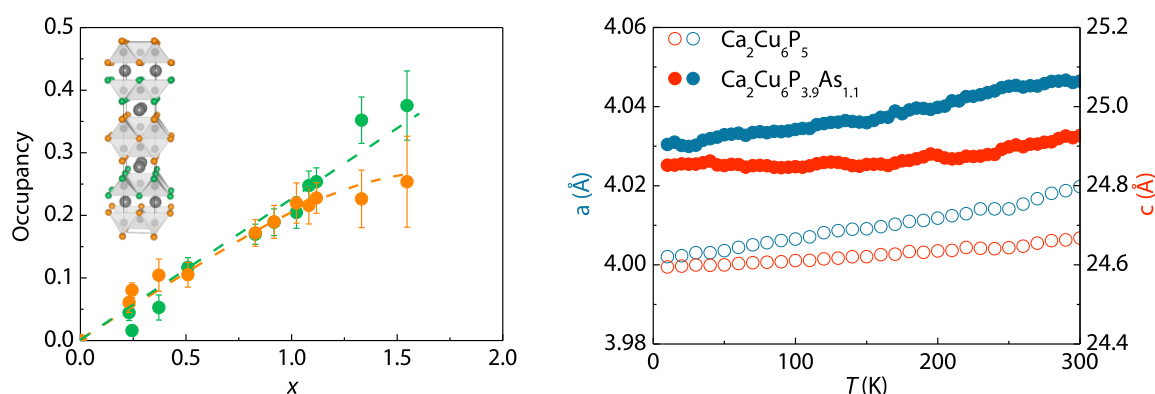


Figure 3.4-6 Left: Occupancy of the different P-positions in the structure. Right: Behavior of the lattice parameters of  $\text{Ca}_2\text{Cu}_6\text{P}_5$  (hollow circles) and  $\text{Ca}_2\text{Cu}_6\text{P}_{3.9}\text{As}_{1.1}$  (full circles) at low temperatures.

Low temperature PXRD measurements (Figure 3.4-6) have been performed as well but indicate no structural transition in  $\text{Ca}_2\text{Cu}_6\text{P}_5$  or  $\text{Ca}_2\text{Cu}_6\text{P}_{3.9}\text{As}_{1.1}$  and show a linear compression of the unit cell along all axes.

To investigate whether there is a preferential and ordered occupancy of P sites in As-doped  $\text{Ca}_2\text{Cu}_6\text{P}_5$  a single crystal was isolated from a powder sample of  $\text{Ca}_2\text{Cu}_6\text{P}_{3.9}\text{As}_{1.1}$  and analyzed via X-ray diffraction (Table 3.4-1). The composition was in good agreement with the data obtained from Rietveld refinement and the data did not show any signs of ordering or a superstructure.

Table 3.4-1: Crystallographic data of  $\text{Ca}_2\text{Cu}_6\text{P}_{3.94}\text{As}_{1.06}$ .

Crystal system, space group	Tetragonal, $I4/mmm$ , No. 139
$a, c$ (Å)	4.0446(3), 24.8721(18)
Cell volume (Å <sup>3</sup> )	406.88(4)
Calculated density (g/cm <sup>3</sup> ), $Z$	5.13, 2
Radiation type, $\lambda$ (Å)	Mo- $K_{\alpha}$ , 0.71069
$\theta$ range (°)	3.28 – 33.67
Reflections (total, independent, $I > 3\sigma(I)$ )	4797, 296, 235
$R_{\text{int}}, R_{\sigma}$	0.0313, 0.0116
GooF (all), GooF ( $I > 3\sigma(I)$ )	1.50, 1.60
Refined parameters, refinement	21, $F^2$
$R_1, wR2$ ( $I > 3\sigma(I)$ )	0.0209, 0.0470
$R_1, wR2$ (all)	0.0314, 0.0499
Largest residual peak, hole $e/\text{Å}^3$	1.23, -0.69

## PHYSICAL PROPERTIES

In order to investigate the influence of As doping, several samples underwent physical characterization. Figure 3.4-7 shows a comparison of the temperature dependent susceptibility measurements and isothermal magnetization measurements at 1.8 K (inset) of undoped  $\text{Ca}_2\text{Cu}_6\text{P}_5$  and heavily As doped  $\text{Ca}_2\text{Cu}_6\text{P}_{3.7}\text{As}_{1.3}$ . It is clearly visible that the reaction to an external field is

very small. Susceptibility measurements at fields up to 2 T confirmed that the undoped sample shows a very weak and nearly temperature independent diamagnetic response while the As-doped sample shows Pauli-paramagnetic behavior. This is in good agreement with the magnetization curves. As-doping of  $\text{Ca}_2\text{Cu}_6\text{P}_5$  thus is able to induce a clearly different behavior than that of other related Cu-pnictides like  $\text{CaCu}_{1.75}\text{As}_2$  or  $\text{ACu}_2\text{Pn}_2$  ( $A = \text{Ba, Sr}$ ;  $\text{Pn} = \text{As}$ ) which all show the nearly temperature independent diamagnetism observed in undoped  $\text{Ca}_2\text{Cu}_6\text{P}_5$ .<sup>[12-14]</sup>

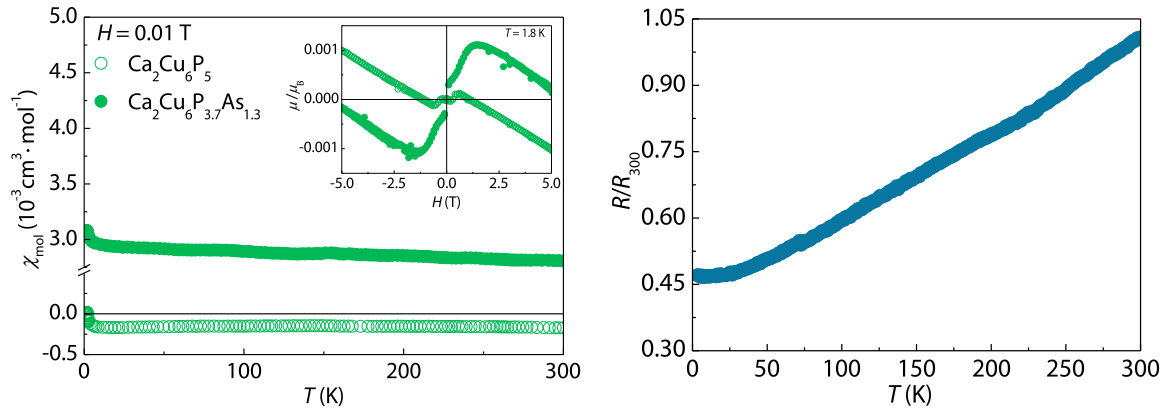


Figure 3.4-7 Left: Comparison of the magnetic measurements of As-doped (full circles) and undoped (open circles)  $\text{Ca}_2\text{Cu}_6\text{P}_5$ . Right: Low temperature resistivity of As-doped  $\text{Ca}_2\text{Cu}_6\text{P}_{3.7}\text{As}_{1.3}$ .

The investigation of the electrical conductivity of  $\text{Ca}_2\text{Cu}_6\text{P}_{3.7}\text{As}_{1.3}$  revealed metallic behavior without any signs of anomalies or transitions. It is a poor metal with a room temperature resistivity  $\rho$  of  $5.48 \pm 3 \mu\Omega\cdot\text{m}$ . *Li et al.* report a significantly lower resistivity which indicates that As-doping of  $\text{Ca}_2\text{Cu}_6\text{P}_5$  indeed influences its electronic properties even though no anomalies like in  $\text{EuCa}_2\text{Cu}_6\text{P}_5$  can be observed.<sup>[2]</sup> As one would expect the isovalent substitution of P by As does not have a major effect on  $\text{Ca}_2\text{Cu}_6\text{P}_5$  regarding its magnetic and electronic properties.

### DFT CALCULATIONS

In order to gain a better understanding of the physical properties self-consistent DFT calculations were performed. The resulting band structure is depicted in Figure 3.4-8 along with the DOS and the Brillouin zone.

The band structure clearly shows a metallic compound and no strong anisotropy, which one might expect given the layered structure and the short metal bonds within these layers. However the interlayer P-P bonds most likely allow for a more isotropic movement of the electrons.

The DOS of  $\text{Ca}_2\text{Cu}_6\text{P}_5$  shows some striking similarities to that of other Cu pnictides.<sup>[15]</sup> As in  $\text{ACu}_2\text{Pn}_2$  ( $A = \text{Ba, Sr}$ ;  $\text{Pn} = \text{As, Sb}$ ) the Cu states are largely localized into a band between -3 eV and -5 eV. Also clearly visible is the low energy pnictogen band between -15 eV and -10 eV which is also found in the iron pnictides.<sup>[16]</sup>

The electronic structure explains why As doping does not seem to change the properties of  $\text{Ca}_2\text{Cu}_6\text{P}_5$  as the DOS around the Fermi level is very low compared to other transition metal pnictides. Furthermore without the presence of metal states no influence on the magnetic properties can be expected upon doping with nonmagnetic elements.

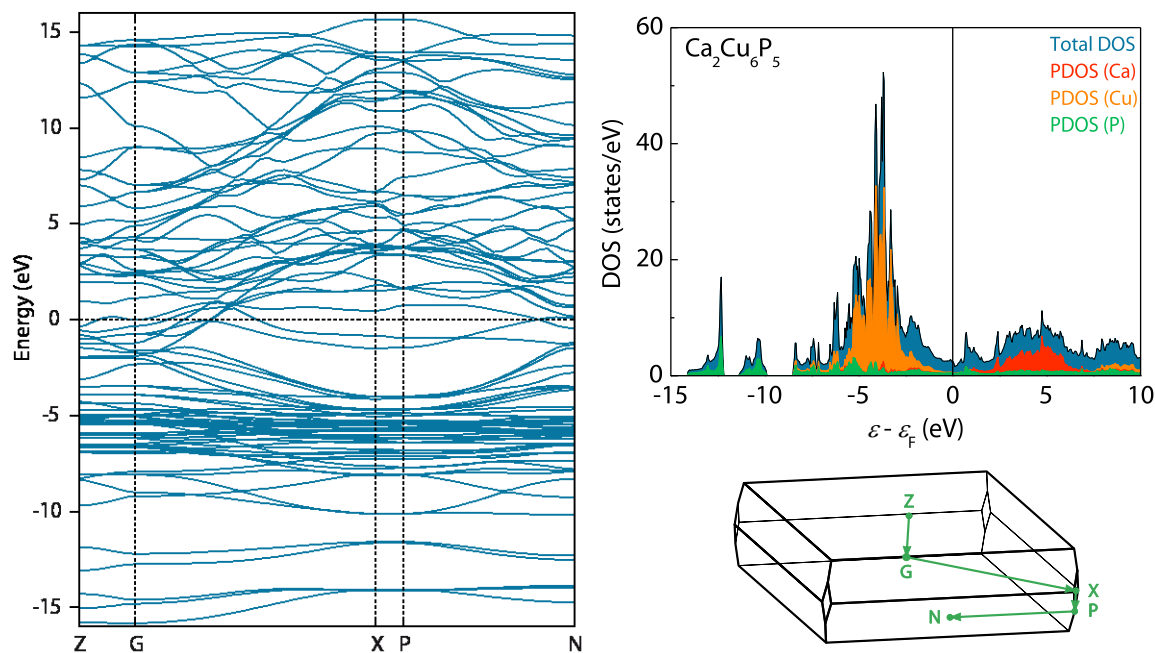


Figure 3.4-8: Band structure (left) and DOS (right) of  $\text{Ca}_2\text{Cu}_6\text{P}_5$  with the PDOS of Ca (red), Cu (yellow) and P (green). The Brillouin zone is depicted in the lower right corner.

### 3.4.6 Summary

In this chapter the development of a microwave based synthesis protocol for  $\text{Ca}_2\text{Cu}_6\text{P}_5$  was discussed. The quickness of this approach was harnessed in an extensive dopant screening using  $\text{Ca}_2\text{Cu}_6\text{P}_5$  as a host system. As is a suitable dopant and the investigation of the solid solution  $\text{Ca}_2\text{Cu}_6\text{P}_{5-x}\text{As}_x$  ( $0 \leq x < 2$ ) which is the first pnictogen doped variant of this compound.

In a first step the microwave based synthesis of  $\text{Ca}_2\text{Cu}_6\text{P}_5$  was optimized. The use of binary starting materials and an electrical tubular furnace for the extension of reaction time and controlled cooling rates yielded phase fractions of over 90 wt%. This hybrid approach was never before reported and may significantly increase the range of compounds accessible via microwave based synthesis.

The screening of transition metals with ionic radii similar to Cu could rule out the elements Mn, Fe, Co and Ni as possible dopants. Screening for possible doping of the pnictide position ruled out Ge, S, Sb, Se and Si as suitable candidates but revealed As as a suitable dopant.

The systematic investigation of  $\text{Ca}_2\text{Cu}_6\text{P}_{5-x}\text{As}_x$  was also done via microwave based synthesis. A maximum dopant content of  $x < 2$  was found. The occupancy of the P sites in the double layer with As reaches a maximum at  $\sim 0.25$  while the occupancy of the single layer P-sites commences linearly with no apparent maximum. This offers a possible explanation for the solubility limit, since the main phase in samples with As contents of more than  $x = 1.5$  is  $\text{CaCu}_{1.75}(\text{P},\text{As})_2$  which essentially consists only of the tetrahedral single layers. Both lattice parameters expand linearly with  $x$  and the expansion along  $c$  matches the sum of the expansions of the interlayer distances in the unit cell while the tetrahedral angle  $\epsilon$  is almost unaffected. Single Crystal diffraction showed no ordered occupation of the P-sites by As and hence suggest statistical substitution.

Low temperature XRD measurements showed no indication of a structural transition. Resistivity measurements showed As-doped  $\text{Ca}_2\text{Cu}_6\text{P}_5$  to exhibit metallic behavior down to 3.5 K while being less conductive than its undoped variant. Magnetic measurements revealed undoped  $\text{Ca}_2\text{Cu}_6\text{P}_5$  to exhibit nearly temperature independent diamagnetism which is also found in related 122-type compounds like  $\text{CaCu}_{1.75}\text{P}_2$  while  $\text{Ca}_2\text{Cu}_6\text{P}_{3.7}\text{As}_{1.3}$  shows Pauli-paramagnetic behavior.

The results presented in this chapter highlight the versatility of microwave based synthesis and show the potential of the combination with other synthetic approaches. A screening of similar dimensions would have taken several months with traditional solid state synthesis while the samples discussed here can be prepared within several weeks. Once a synthesis protocol is established, which can be time consuming in some cases, microwave based synthesis can severely reduce the amount of time needed for the synthetic exploration of a given system. In combination with traditional solid state synthesis, which allows for very high quality samples once a suitable candidate is found, this approach enables a very quick discovery and thorough investigation of new materials.

### 3.4.7 References

- [1] I. Pilchowski, A. Mewis, *Z. Anorg. Allg. Chem.* **1990**, 581, 173-182.
- [2] D. O. Charkin, A. V. Urmanov, S. M. Kazakov, D. Batuk, A. M. Abakumov, S. Knöner, E. Gati, B. Wolf, M. Lang, A. V. Shevelkov, G. V. Tendeloo, E. V. Antipov, *Inorganic Chemistry* **2012**, 51, 8948-8955.
- [3] J. Wang, K. Lee, K. Kovnir, *Inorg Chem* **2015**, 54, 890-897.
- [4] A. Mewis, *Z. Naturforsch. B: J. Chem. Sci.* **1980**, 35, 141.
- [5] L. Li, D. Parker, M. Chi, G. M. Tsoi, Y. K. Vohra, A. S. Sefat, *arXiv preprint arXiv:1509.02508* **2015**.
- [6] D. J. Chakrabarti, D. E. Laughlin, *Bulletin of Alloy Phase Diagrams* **1984**, 5, 570-576.
- [7] R. D. Shannon, *Acta Crystallographica Section A* **1976**, 32, 751-767.
- [8] H. L. Shi, H. X. Yang, H. F. Tian, J. B. Lu, Z. W. Wang, Y. B. Qin, Y. J. Song, J. Q. Li, *Journal of Physics: Condensed Matter* **2010**, 22, 125702.
- [9] A. Leithe-Jasper, W. Schnelle, C. Geibel, H. Rosner, *Phys. Rev. Lett.* **2008**, 101, 207004.
- [10] Z. Ren, Q. Tao, S. Jiang, C. Feng, C. Wang, J. Dai, G. Cao, Z. a. Xu, *Phys. Rev. Lett.* **2009**, 102, 137002.
- [11] S. Jiang, H. Xing, G. Xuan, C. Wang, Z. Ren, C. Feng, J. Dai, Z. a. Xu, G. Cao, *J. Phys.: Condens. Matter* **2009**, 21, 382203.
- [12] V. K. Anand, P. K. Perera, A. Pandey, R. J. Goetsch, A. Kreyssig, D. C. Johnston, *Physical Review B* **2012**, 85, 214523.
- [13] V. K. Anand, D. C. Johnston, *Physical Review B* **2012**, 86, 214501.

- [14] B. Saparov, A. S. Sefat, *Journal of Solid State Chemistry* **2012**, *191*, 213-219.
- [15] J. A. McLeod, E. Z. Kurmaev, I. Perez, V. K. Anand, P. K. Perera, D. C. Johnston, A. Moewes, *Phys. Rev. B: Condens. Matter Mater. Phys.* **2013**, *88*, 014508.
- [16] E. Z. Kurmaev, J. A. McLeod, A. Buling, N. A. Skorikov, A. Moewes, M. Neumann, M. A. Korotin, Y. A. Izyumov, N. Ni, P. C. Canfield, *Phys. Rev. B: Condens. Matter Mater. Phys.* **2009**, *80*, 054508.



## 4 SUMMARY

This work explored high pressure/high temperature as well as microwave based synthesis and their use for explorative synthesis of transition metal pnictides and chalcogenides. This resulted in the discovery of several novel compounds and their substitution variants all of which were physically characterized.

### 4.1 High Pressure Synthesis of Iron Pnictides

High quality polycrystalline samples of  $\text{Ca}_{1-x}\text{Pr}_x\text{Fe}_2\text{As}_2$  with Pr contents of  $0 \leq x \leq 1$  were prepared via high pressure synthesis.  $\text{PrFe}_2\text{As}_2$  is the first 122-type iron arsenide with a trivalent cation. It crystallizes in the  $\text{ThCr}_2\text{Si}_2$ -type structure (space group  $I4/mmm$ ) with  $a = 4.000(1) \text{ \AA}$  and  $c = 10.531(1) \text{ \AA}$ . At lower Pr contents the compounds form a previously unknown metastable high pressure phase representing an intermediate between the collapsed tetragonal ( $cT$ ) phase of  $\text{CaFe}_2\text{As}_2$  and the ambient pressure phase. The relaxation of the metastable form can be observed at temperatures above 573 K and the transition temperature  $T_r$  increases linearly with the Pr-content  $x$ . Samples with Pr contents above  $x = 0.6$  decompose upon heating to these temperatures. No indication for superconductivity could be observed in any of the samples thus proving that members of this system are not intrinsic superconductors.

La-doped  $\text{SrFe}_2\text{As}_2$  becomes superconducting at  $T_c = 22 \text{ K}$  and proves the applicability of a multi anvil setup for the preparation of 122-type superconductors.  $\text{LaFe}_2\text{As}_2$  crystallizes in the space group  $I4/mmm$  adopting a  $\text{BaZn}_2\text{P}_2$ -type structure with  $a = 3.980(3) \text{ \AA}$  and  $c = 11.280(1) \text{ \AA}$ . It shows a possibly ferrimagnetic ordering at 130 K and will be subject to detailed investigations via neutron diffraction in the future.

The new iron arsenides  $\text{CaFe}_5\text{As}_3$  and  $\text{PrFe}_5\text{As}_3$  as well as the substitution variants  $\text{Ca}_{1-x}\text{Pr}_x\text{Fe}_5\text{As}_3$  were discovered via high pressure synthesis as well.  $\alpha\text{-CaFe}_5\text{As}_3$  crystallizes in a new structure type (space group  $P2_1/m$ ) with  $a = 7.273(1) \text{ \AA}$ ,  $b = 3.814(1) \text{ \AA}$ ,  $c = 9.757(1) \text{ \AA}$  and  $\beta = 100.7(1)^\circ$ ,  $\text{PrFe}_5\text{As}_3$  is isotypic with  $a = 7.206(1) \text{ \AA}$ ,  $b = 3.886(1) \text{ \AA}$ ,  $c = 9.765(1) \text{ \AA}$  and  $\beta = 100.5(1)^\circ$ . A nonlinear structural change with symmetry retention was found around 50 K in undoped and lowly doped samples. It correlates with a magnetic reordering at low Pr-contents. At high Pr-contents the magnetic reordering and the structural change are suppressed, but a different magnetic reordering emerges, gaining intensity with increasing  $x$ . Since the compound contains Fe in different oxidation states between +I and +II, the nature of the magnetic order is likely very complex.

### 4.2 Microwave Based Synthesis of Transition Metal Pnictides

Synthesis protocols for the microwave based preparation of several binary transition metal compounds in a domestic microwave oven (DMO) were established. This has never before been reported for these materials. All binary compounds were used as starting materials in other experiments.

The binary iron arsenides FeAs and Fe<sub>2</sub>As could be obtained by irradiating the elements for 5 min at 500 W. Evaporation losses of As have to be compensated by using an excess amount of 3.5 wt% and layering Fe on top of As in an alumina crucible. Sample sizes of 500 mg were obtained phase pure.

Samples of pure FeSe containing 90 wt% of the tetragonal  $\beta$  phase could be reproducibly prepared within 20 min at 300 W with subsequent transfer into a pre-heated tubular furnace for post-treatment at 593 K. Superconductivity was confirmed at 9 K with a superconducting volume fraction of about 90 wt%.

The intermetallic compound CaCu could be obtained phase pure in 5.5 min at 600 W from the elements. A customized Nb-crucible was developed for this protocol.

A microwave based synthesis protocol for CaMo<sub>6</sub>S<sub>8</sub> has been developed during a stay with the Seshadri group at UCSB but was not discussed in this thesis.

Based on the experience with these binary compounds a fast, microwave based dopant screening method for higher transition metal pnictides was developed. It was employed in the investigation of Ca<sub>2</sub>Cu<sub>6</sub>P<sub>5</sub> as a host system. Using microwave heating, the duration of the synthesis could be reduced from ~200 h to about 13 h while still maintaining reasonable sample quality.

Ca<sub>2</sub>Cu<sub>6</sub>P<sub>5</sub> could be obtained in phase fractions greater than 90 wt% within 12 min at 600 W with an immediate transfer into a tubular furnace, pre-heated to 1173 K. The temperature was then kept for 4 h for post-heat treatment before cooling to room temperature.

Mn, Fe, Co and Ni were screened as possible dopants but could not be incorporated into the host structure. The presence of even small amounts of these metals completely suppressed the formation of the target phase.

The pnictogens/chalcogens As, Ge, S, Sb Se and Si were tested for their ability to substitute P in the host phase by the same method. Only As could be incorporated.

A systematic investigation of the solid solution Ca<sub>2</sub>Cu<sub>6</sub>P<sub>5-x</sub>As<sub>x</sub> ( $0 \leq x < 2$ ) was done using microwave based synthesis. A solution limit for this method of preparation seems to exist for values of  $x$  approaching 2 as the fraction of the main phase rapidly diminishes beyond  $x = 1.5$  and samples with a theoretical value of  $x = 2$  did not contain the target phase at all.

The lattice parameters of Ca<sub>2</sub>Cu<sub>6</sub>P<sub>5-x</sub>As<sub>x</sub> ( $0 \leq x < 2$ ) expand linearly with  $x$  without major changes inside the CuP<sub>4/4</sub> tetrahedra layers. Single-crystal X-ray diffraction did not show any signs of an order of As on the P-sites. The substitution of P-sites inside the double tetrahedral layer seems to show a maximum around 0.25 for  $x \geq 1$  while the occupancy of P-sites in the single layer behaves linearly.

Ca<sub>2</sub>Cu<sub>6</sub>(P, As)<sub>5</sub> does not show any structural transitions at low temperatures. Undoped Ca<sub>2</sub>Cu<sub>6</sub>P<sub>5</sub> exhibits nearly temperature independent diamagnetism similar to other Cu pnictides. As-doped

---

$\text{Ca}_2\text{Cu}_6\text{P}_5$  shows Pauli-paramagnetic behavior and conductivity measurements revealed metallicity. Results from DFT calculations were in agreement with these findings.

### **4.3 Final remarks**

The findings presented in this work show that material scientists can learn a lot when straying from the path of traditional solid state synthesis. It further highlights that explorative synthesis remains one of the most rewarding tools for the discovery of new materials. While all of the techniques used are more or less well known they have never before been systematically applied to the transition metal pnictides. This means that using the foundation provided here may lead to exciting discoveries in the future and some of them might aid in solving the puzzle of high temperature superconductivity in iron arsenides.

---

## SCIENTIFIC CONTRIBUTIONS

### Full List of Publications

Framework structures of interconnected layers in calcium iron arsenides

T. Stürzer, C. Hieke, C. Löhnert, F. Nitsche, J. Stahl, C. Maak, R. Pobel, D. Johrendt

*Inorganic Chemistry* **2014**, 53, 6235

Ferromagnetism and the formation of interlayer As<sub>2</sub>-dimers in Ca(Fe<sub>1-x</sub>Ni<sub>x</sub>)<sub>2</sub>As<sub>2</sub>

R. Pobel, R. Frankovsky and D. Johrendt

*Zeitschrift für Naturforschung B* **2013**, 68b, 581

Synthesis of LaO<sub>1-x</sub>F<sub>x</sub>FeAs ( $x = 0-0.15$ ) via solid state metathesis reaction

R. Frankovsky, A. Marchuk, R. Pobel and D. Johrendt

*Solid State Communications* **2012**, 152, 632

### Conference Contributions

#### Talks

Hochdrucksynthese seltenerdsubstituierter Eisenarsenide

R. Pobel and D. Johrendt

*Hirschegg seminar on solid state chemistry*, Hirschegg, Austria **2013**

Strukturelle und magnetische Eigenschaften von Ca(Fe<sub>1-x</sub>Ni<sub>x</sub>)<sub>2</sub>As<sub>2</sub>

R. Pobel and D. Johrendt

*Hirschegg seminar on solid state chemistry*, Hirschegg, Austria **2012**

#### Posters

Absence of superconductivity in metastable Ca<sub>1-x</sub>Pr<sub>x</sub>Fe<sub>2</sub>As<sub>2</sub> ( $x = 0-1$ ) synthesized under high pressure conditions

R. Pobel, K. Strobl, C. Maak and D. Johrendt

*15<sup>th</sup> European Conference of Solid State Chemistry (ECSSC 2015)*, Vienna, Austria **2015**

Metal-metal-bonding, ferromagnetism and the formation of interlayer As<sub>2</sub>-dimers in Ca(Fe<sub>1-x</sub>Ni<sub>x</sub>)<sub>2</sub>As<sub>2</sub>

R. Pobel, R. Frankovsky and D. Johrendt

*Summer school on iron-pnictides*, Achatswies, Germany **2012**

---

## CURRICULUM VITAE

### Personal Details

Full Name: Roman Rupert Pobel

Date Of Birth: 03.01.1986

Place Of Birth: Dachau, Germany

### Education

Since April 2012 PhD thesis with the group of Prof. Dr. Dirk Johrendt  
LMU Munich  
Title: “*High pressure and Microwave Based Synthesis of Transition Metal Pnictides*”

Sept. 2011 – Feb. 2012 Master’s thesis with the group of Prof. Dr. Dirk Johrendt  
LMU Munich  
Title: “*Untersuchungen zur direkten und indirekten Substitution von  $\text{CaFe}_2\text{As}_2$* ”

Apr. 2010 – Apr. 2012 Master studies in Chemistry  
LMU Munich

Oct. 2006 – Apr. 2010 Bachelor studies in Chemistry and Biochemistry  
LMU Munich

Nov. 2005 – Jul. 2006 Civil service  
Landschulheim Schloss Grunertshofen

Jun. 2005 Allgemeine Hochschulreife  
Wernher-von-Braun-Gymnasium Friedberg

Sept. 1996 – Jun 2005 Secondary education  
Wernher-von-Braun-Gymnasium Friedberg

Sept 1992 – Jul 1996 Primary education  
Grundschule Ried

---